USAAMRDL-TR- 75-39B

DESIGN CRITERIA FOR ELASTOMERIC BEARINGS

Volume II - Design Manual

Thiokol/Wasatch Division
A Division of Thiokol Corporation
Brigham City, Utah 84302

March 1976

Final Report

Approved for public release;
distribution unlimited.

Prepared for

EUSTIS DIRECTORATE
U. S. ARMY AIR MOBILITY RESEARCH AND DEVELOPMENT LABORATORY
Fort Eustis, Va. 23604

EUSTIS DIRECTORATE POSITION STATEMENT

The data contained in this report are the results of an effort designed to improve the state of the art of elastomeric bearing design for helicopter rotor head applications. The products of this effort are a design manual and a computer program based on finite-element techniques. The results of this program are contained in the following four volumes:

Volume I - Final Report
Volume II - Design Manual
Volume III - Program User's Manual
Volume IV - Programmer's Manual

Volume I contains the development and background information used in producing the design manual.

Volume II presents design considerations and procedures, bearing applications, methods of analysis, and techniques for predicting bearing performance.

Volumes III and IV contain the computer code and examples of problems showing sample inputs and outputs.

The products of this effort provide a good foundation for building a comprehensive manual and computer code for the design and analysis of elastomeric bearings for helicopter rotor head applications. It was recognized at the onset of this program that both the manual and the code would be first editions. The results of this effort were expected to define areas requiring further development. Further investigations coupled with feedback from users and/or evaluators are expected to provide material for upgrading the content and format of the manual and codes.

Mr. John Sobczak of the Military Operations Technology Division served as project engineer for this effort.

(9) Final rept.

UNCLASSIFIED

SECURITY CLASSIFICATION OF THIS PAGE (When Data Entered)

REPORT DOCUMENTATION PAGE	READ INSTRUCTIONS BEFORE COMPLETING FORM
1. REPORT NUMBER: USAAMRDL-TR-75-39B	2. GOVT ACCESSION NO. / 3. RECIPIENT'S CATALOG NUMBER
4. TITLE (and Subtitle): DESIGN CRITERIA FOR ELASTOMERIC BEARINGS, Volume II - Design Manual	5. TYPE OF REPORT & PERIOD COVERED: Design Manual
	6. PERFORMING ORG. REPORT NUMBER
7. AUTHOR(s): Suresh B. Kulkarni	8. CONTRACT OR GRANT NUMBER(s): DAAJ02-73-C-0091
9. PERFORMING ORGANIZATION NAME AND ADDRESS: Thiokol/Wasatch Division, A Division of Thiokol Corporation, Brigham City, Utah 84302	10. PROGRAM ELEMENT, PROJECT, TASK AREA & WORK UNIT NUMBERS: 62206A / 1F162205A11901, 013 EK
11. CONTROLLING OFFICE NAME AND ADDRESS: Eustis Directorate, U.S. Army Air Mobility Research and Development Laboratory, Fort Eustis, Virginia 23604	12. REPORT DATE: March 1976; 13. NUMBER OF PAGES: 186
14. MONITORING AGENCY NAME & ADDRESS (if different from Controlling Office): (12) 188 p.	15. SECURITY CLASS. (of this report): Unclassified; 15a. DECLASSIFICATION/DOWNGRADING SCHEDULE

16. DISTRIBUTION STATEMENT (of this Report)

Approved for public release; distribution unlimited.

(16) DA-1-F-162205-A-119

17. DISTRIBUTION STATEMENT (of the abstract entered in Block 20, if different from Report)

18. SUPPLEMENTARY NOTES

Volume II of a four-volume report.

19. KEY WORDS (Continue on reverse side if necessary and identify by block number)

Elastomeric Bearings
Helicopter Rotor
Natural Rubber
Finite Element Analysis
Stability
Service Life

20. ABSTRACT (Continue on reverse side if necessary and identify by block number)

This design manual contains the recommended analytical approaches and engineerings procedures to be followed by designers of elastomeric bearings for rotor head applications in helicopters. Three bearing configurations, namely, axially laminated cylindrical (Type I), radially laminated cylindrical (Type II), and spherical laminated (Type III) bearings are considered.

Several levels of design analysis are presented: closed-form operations, computer-developed design curves, and finite-element computer analysis. The

DD FORM 1 JAN 73 1473 EDITION OF 1 NOV 65 IS OBSOLETE

UNCLASSIFIED

SECURITY CLASSIFICATION OF THIS PAGE (When Data Entered)

20.
design restraints determined by stability and service life are also considered.

The material properties required for the design and the suggested experimental methods for their determination are also discussed.

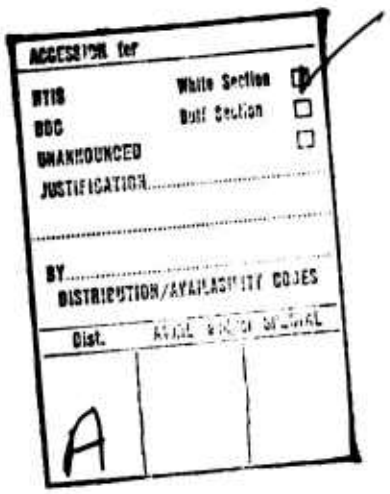

SUMMARY

The application of elastomeric bearings in helicopter systems is of current interest. This manual presents the results of the contract on Design Criteria for Elastomeric Bearings conducted for the Eustis Directorate, U. S. Army Air Mobility Research and Development Laboratory, Fort Eustis, Virginia. The products of this effort are a design manual and a computer program based on finite-element techniques. These developments are an extension of prior solid rocket motor thrust vector control elastomeric bearing and elastomer mechanics technology.

The program scope includes bearing configurations with potential application in rotor heads. Type I (flat laminate) bearings react the main thrust or CF loads and provide for lateral and torsional motion. Type II (radial or cylindrically laminated) bearings react radial loads and provide for torsional motion with some axial motion in the case of cylindrical shims and out-of-plane rotation in the case of spherical shims. Type III (spherically laminated) bearings react axial or CF loads while providing for three degrees of rotational motion.

Several levels of design analysis are presented: closed-form equations, computer-developed design curves, and finite-element computer analyses. The material properties to make these calculations are determined for a selected representative elastomer. Test specimens and methods are included in this discussion.

The design procedures are verified to show the accuracy of these results. The limits or regions of applicability are pointed out.

The design restraints determined by stability and service life are also developed.

The results of this contract are presented in four volumes:

Volume I	Final Report	Volume III	Program User's Manual
Volume II	Design Manual	Volume IV	Programmer's Manual

PREFACE

This manual contains the results of testing and analysis performed by Thiokol/Wasatch Division under Eustis Directorate, U.S. Army Air Mobility Research and Development Laboratory (USAAMRDL), Contract DAAJ02-73-C-0091.

The contracted work was conducted under the technical cognizance of Mr. John Sobczak of the Eustis Directorate.

The work was performed under the direction of Principal Investigators C. W. Vogt and A. R. Thompson with the support of B. W. Law of the Program Management Directorate.

The principal contributors were:

Dr. G. Anderson--Material Properties and Service Life

Dr. S. Kulkarni--Analysis and Stability

W. E. Berndt--Type I Bearing Verification

L. E. Jensen--Type II Bearing Verification

G. J. Bakken--Type III Bearing Verification

D. R. Trauntvein--Fabrication

D. H. Lee--Programming

CONTENTS

CONTENTS (Cont)

CONTENTS (Cont)

LIST OF ILLUSTRATIONS

LIST OF ILLUSTRATIONS (Cont)

LIST OF ILLUSTRATIONS (Cont)

LIST OF ILLUSTRATIONS (Cont)

LIST OF TABLES

1.0 INTRODUCTION

The primary objectives of this contract were the development of this manual and the development of a computer code for the design and analysis of elastomeric bearings for helicopter rotor head applications. It was recognized that the manual and code would be first edition. That is, the results of the analytical and experimental phases would provide definition of technology requiring further development. Also, the feedback from users and evaluators would further define requirements for highly applicable and user-oriented design tools.

1.1 APPROACH USED

The program approach was to utilize the analytical, experimental, design, and process expertise developed for the design of solid rocket motor propellant grains and thrust vector control (TVC) systems. Solid propellant is a nonlinear, viscoelastic material with physical properties and response characteristics of an elastomer. Elastomeric bearings for TVC are spherical (Type III) with core (elastomeric pad and reinforcing shim composite) geometries proportional to that required for rotor head application.

The program effort was planned to have a work scope consisting of the following tasks:

1. Evaluation and selection of a representative material,
2. Evaluation and selection of appropriate test methods,
3. Generation of requisite data,
4. Development of a finite-element computer code,
5. Design and analysis of representative bearings,
6. Fabrication and test of verification bearings,
7. Development of a design manual.

The development and results of this effort are presented in Volume I. The computer code is contained in Volumes III and IV, which are, respectively, the Program User's Manual and the Programmer's Manual.

1.2 ELASTOMERIC BEARING TYPES CONSIDERED

For the purposes of this manual, elastomeric bearings for rotor head applications have been classified into four types. The Type I axial bearing, shown in Figure 1-1, is constructed by laminating flat annulars of elastomeric pads and reinforcing shims between end rings. The primary load and motion for a Type I bearing are the reaction of axial load (F_z) and torsional displacement (θ_z). The bearing will allow some compliance to the asymmetric motions and loads in the x-y plane or about the x and y axes. However, these asymmetric loads and motions will severely compromise the service life and stability of the design.

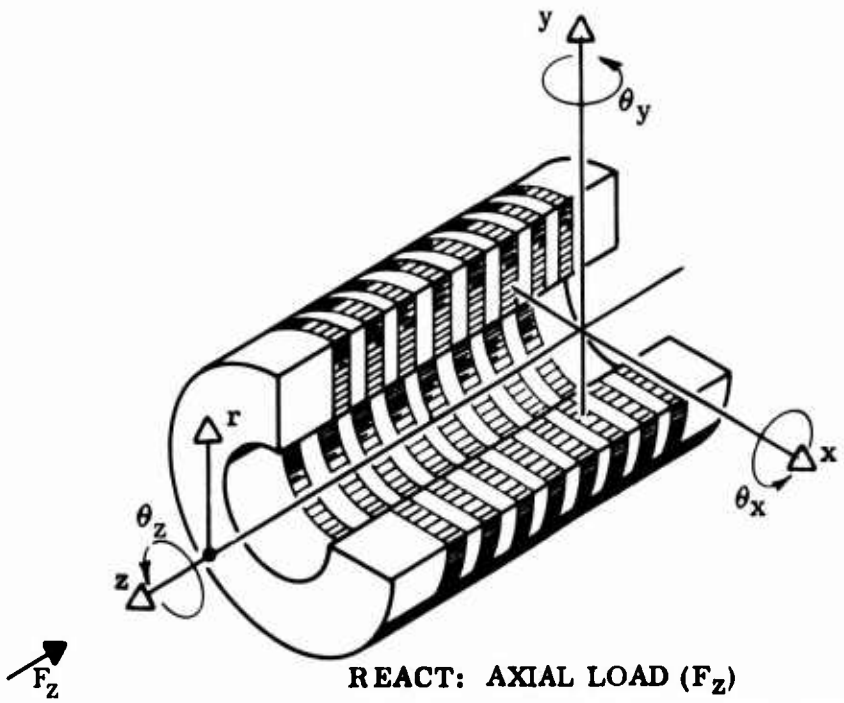

REACT: AXIAL LOAD (F_z)
PROVIDE: TORSIONAL DISPLACEMENT (θ_z)
MINIMAL ASYMMETRIC
COMPLIANCE: θ_y, θ_x, M_y, M_x, u_y, u_x, F_y, F_x

Figure 1-1. Type I axial bearing

The Type II radial bearing, shown in Figure 1-2, is constructed of cylindrical laminates of elastomer and reinforcement. This bearing is difficult to fabricate when residual cure and thermal-induced tensile stresses must be minimized. The primary loads and motions are the reaction of the radial forces (F_r) in the x-y plane and torsional displacement (θ_z) about the z axis. The bearing will also react moments about the x and y axes and will provide minimal compliance in the axial or z direction.

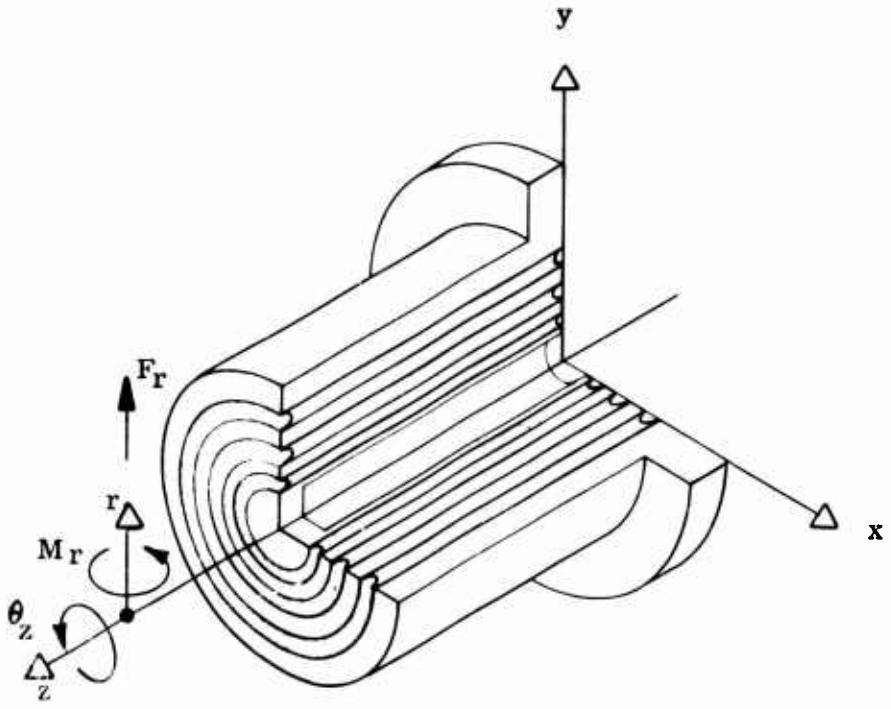

REACT: ASYMMETRIC RADIAL LOAD (F_r) AND ASYMMETRIC RADIAL MOMENT (M_r)

PROVIDE: TORSIONAL DISPLACEMENT (θ_z)

MINIMAL COMPLIANCE: u_z, F_z

Figure 1-2. Type II radial bearing

The Type III spherical bearing, shown in Figure 1-3, is constructed of spherical segments of elastomer and reinforcement between end rings. Compression, transfer, and injection molding techniques are applicable. This bearing provides for rotational motion about all axes while reacting axial and lateral loads.

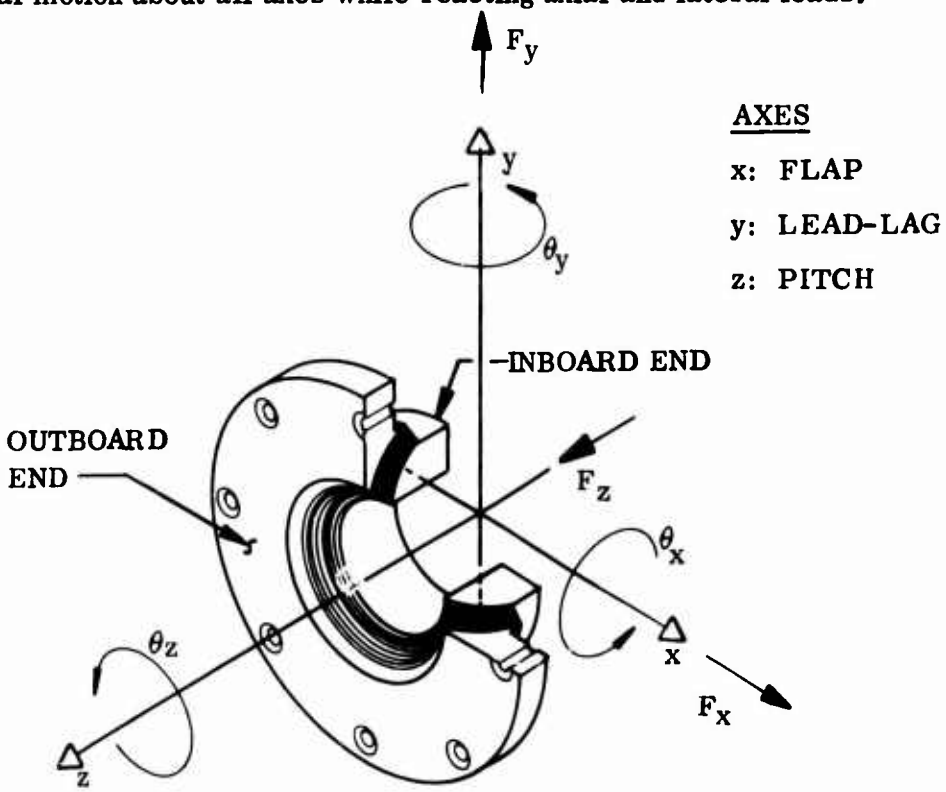

REACT: AXIAL LOAD (F_z); LATERAL LOADS (F_x, F_y)

PROVIDE: DISPLACEMENTS (θ_z, θ_x, θ_y)

Figure 1-3. Type III spherical bearing

The Type IV conical bearing, shown in Figure 1-4, is constructed by laminating conical segments of elastomer and reinforcement between end rings. This bearing primarily provides for torsional displacement about the z axis, while reacting axial and lateral loads. Some compliance to rotation and moments about the x and y axes is provided.

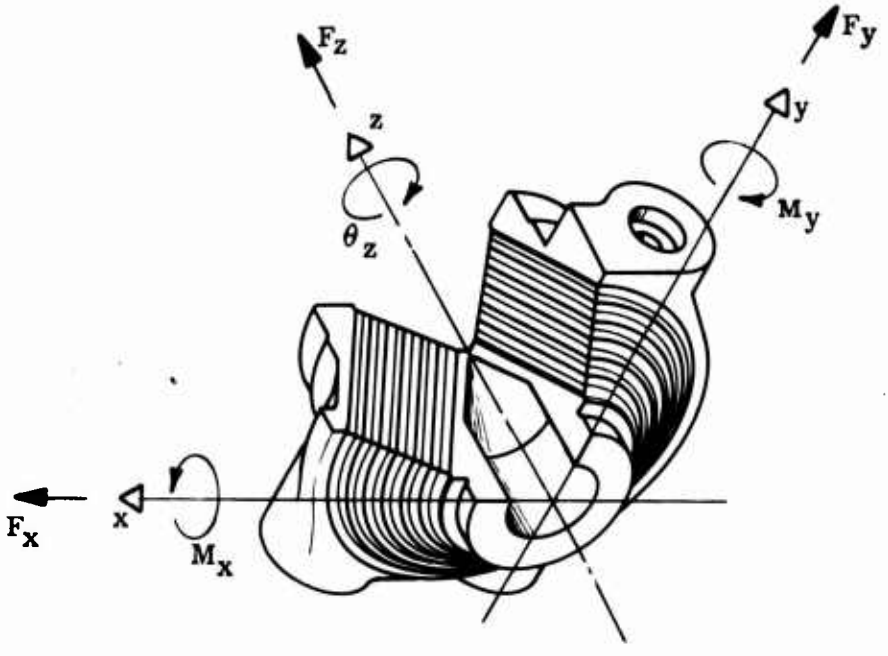

REACT: AXIAL LOAD (F_z); LATERAL LOADS (F_x, F_y, M_x, M_y)

PROVIDE: TORSIONAL DISPLACEMENT (θ_z)

Figure 1-4. Type IV conical bearing

The design of Type I, II and III bearings is presented in this manual. The computer code presented in Volumes III and IV can be used to design the Type IV bearings, and the basic design procedures can be extended to this bearing.

1.3 DESIGN METHODS AND THEIR USAGE

This manual has been organized to reflect a typical design process involving the following:

1. Evaluation of application and experience,
2. Definition of requirements,
3. Selection of material and development of data,

4. Initial design or sizing,

5. Detailed analyses for stress, stability, and service life.

Figure 1-5 presents a generalized design flow diagram that can be applied as a guide to the use of this manual. It illustrates the three levels of design: (1) basic sizing utilizing guidelines in approximate formulations; (2) design refinement using parametric data in closed-form formulations; and (3) detailed design analysis utilizing finite-element computer techniques.

Currently, the number of applications and flight test data are very limited. Four types of general classifications of bearings have been defined, each of which has been subjected to bench testing and some limited flight testing. Future development will be of particular value in establishing the correspondence between flight and ground test qualification requirements.

The materials section presents the general considerations for selecting an elastomer formulation and design data for the elastomer used in the contract. Because of the multitude of potential formulations and sensitivity to constituent variations, the applicability of test methods and the presentation and utilization of data have been emphasized.

The sections on initial design of Type I, II, and III bearings present techniques utilizing equations and parametric data in the basic design or sizing. Resulting designs are of value for rotor head envelope definition and will minimize the iterations in detailed analysis.

The detailed analysis section discusses utilization of modeling techniques for the finite-element computer code presented in Volumes III and IV of this manual. The significance, application, and limitations of bearing stability and service life predictive techniques are presented in independent sections.

In combination, the application of this manual and the computer code will result in rotor head bearing designs that will meet specified requirements. However, as it is typical of a developmental program, additional areas of technological deficiencies are identified. The last section discusses those technological areas requiring further development.

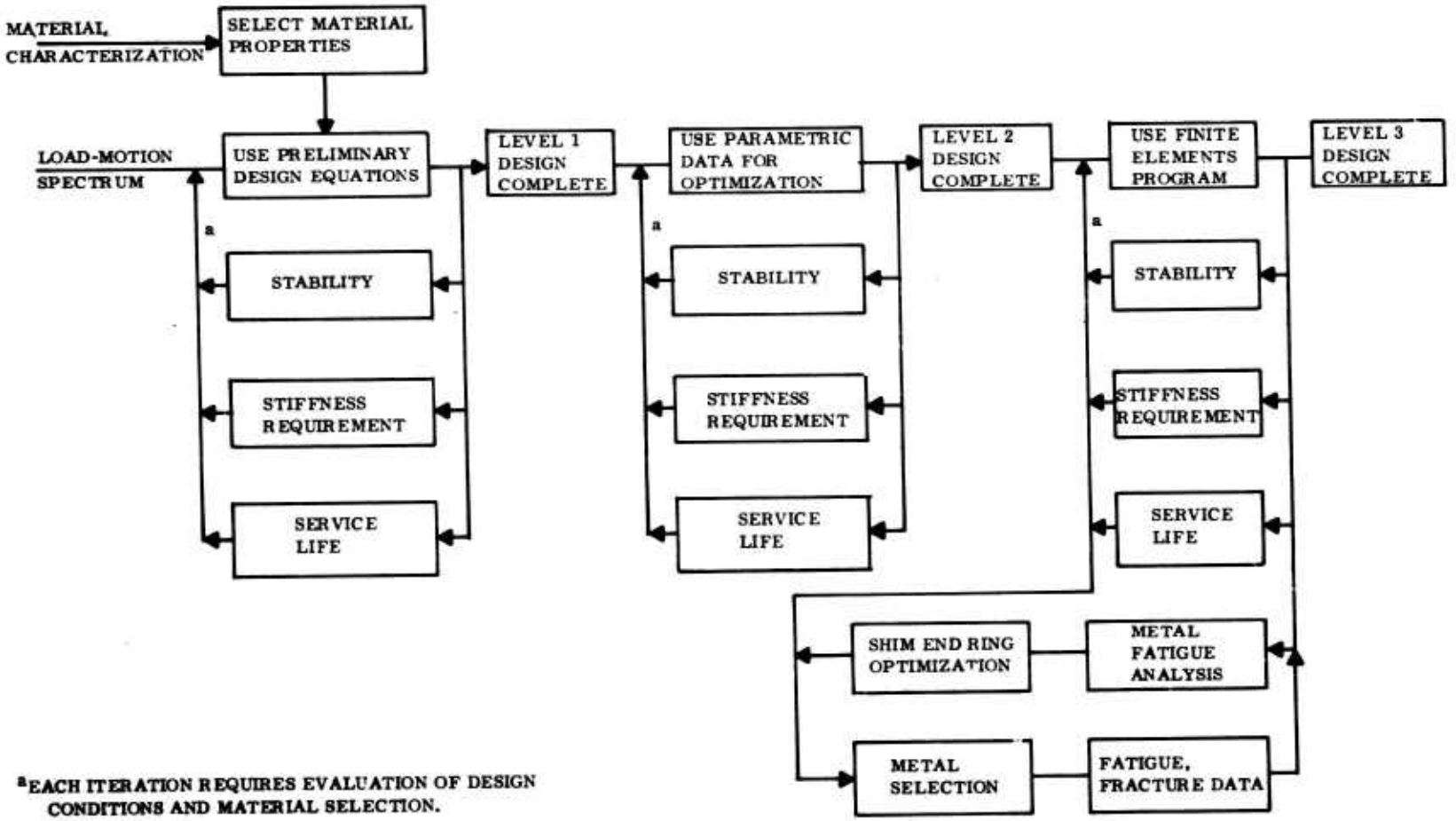

Figure 1-5. Design procedure flow

2.0 APPLICATIONS AND REQUIREMENTS

2.1 APPLICATIONS

The application of elastomeric bearings in rotor head systems should be considered in the early phases of development and demonstration. Current results have verified the potentials and advantages of the elastomeric rotor head. While most bearing comparisons are made on the elastomeric to mechanical component level, the most significant advantages for the elastomeric system are found in such systems considerations as:

1. Freedom from maintenance,
2. Reductions in spares provisioning,
3. Simplicity and flexibility in rotor head system design,
4. Potential for reductions in rotor head volume, weight, and cost.

This manual, while providing design and analysis procedures, also provides an assessment of the state of the art for elastomeric bearing design. To develop the full potential of elastomeric bearings, further development in service life prediction techniques, bench test requirements, and the interaction of design and process variables is required.

Four major flight test programs have been initiated. These rotor head designs indicate the many applications of the particular types of bearings and the multiplicity of rotor head design possibilities.

2.1.1 Bell 540 Rotor System for Cobra

The Cobra is a two-blade aircraft which is ideally suited to the adaptation of Type II radial bearings with cylindrical shims on the teetering hinge or flapping axis as shown in Figure 2-1. The bearing is shown in Figure 2-2. In this application, the critical design loads and motions are a 40-cycle-per-hour radial load and

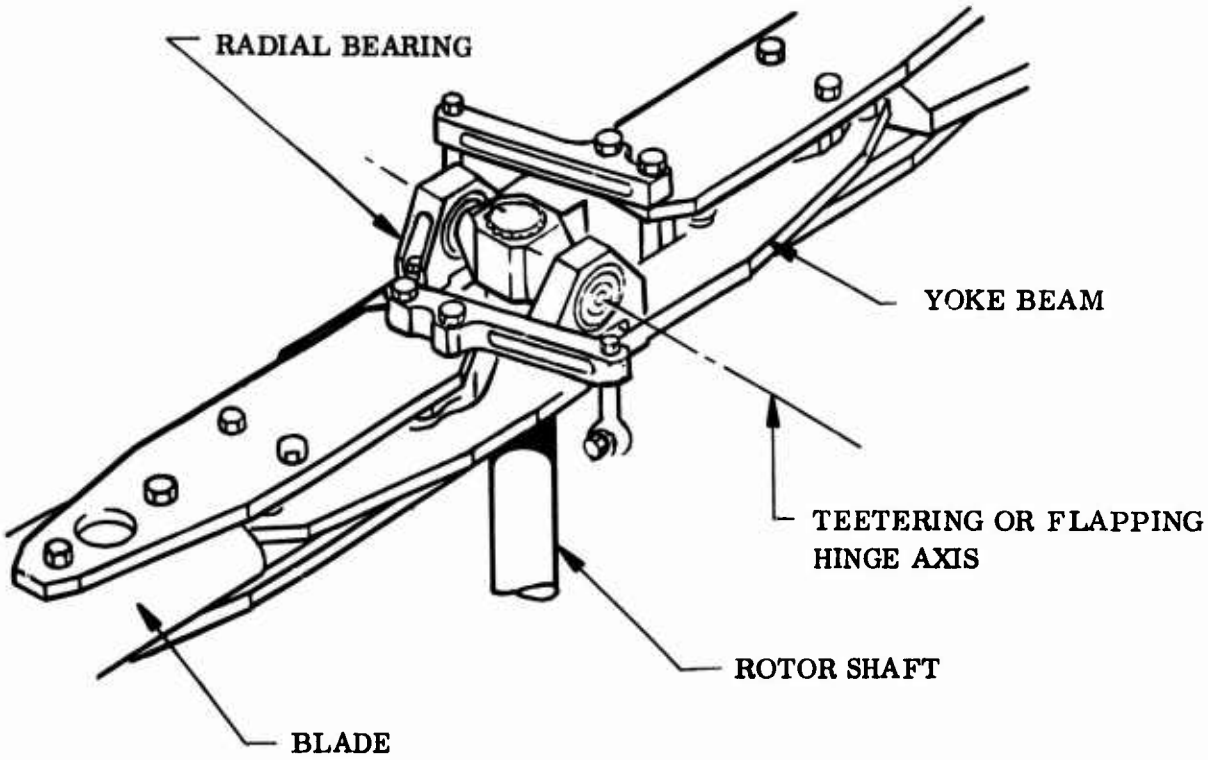

Figure 2-1. Type II (radial) bearing in teetering or flapping hinge on Bell 540 rotor

flap oscillations at 325 cycles per minute. The bearings have met bench life test requirements of 250 hours and some have been tested to 364 hours at test termination. A similar bearing has been flight tested for over 4,000 hours.

The Cobra system has also evaluated the use of Type IV (conical) bearings on the pitch axis. Two bearings are used in each blade grip to provide for pitch motion and to react the blade bending moments. The system is shown in Figure 2-3.

2.1.2 Sikorsky H-53

The H-53 retrofit program has evaluated the use of large Type III (spherical) bearings in conjunction with centering or rod end type bearings. The spherical

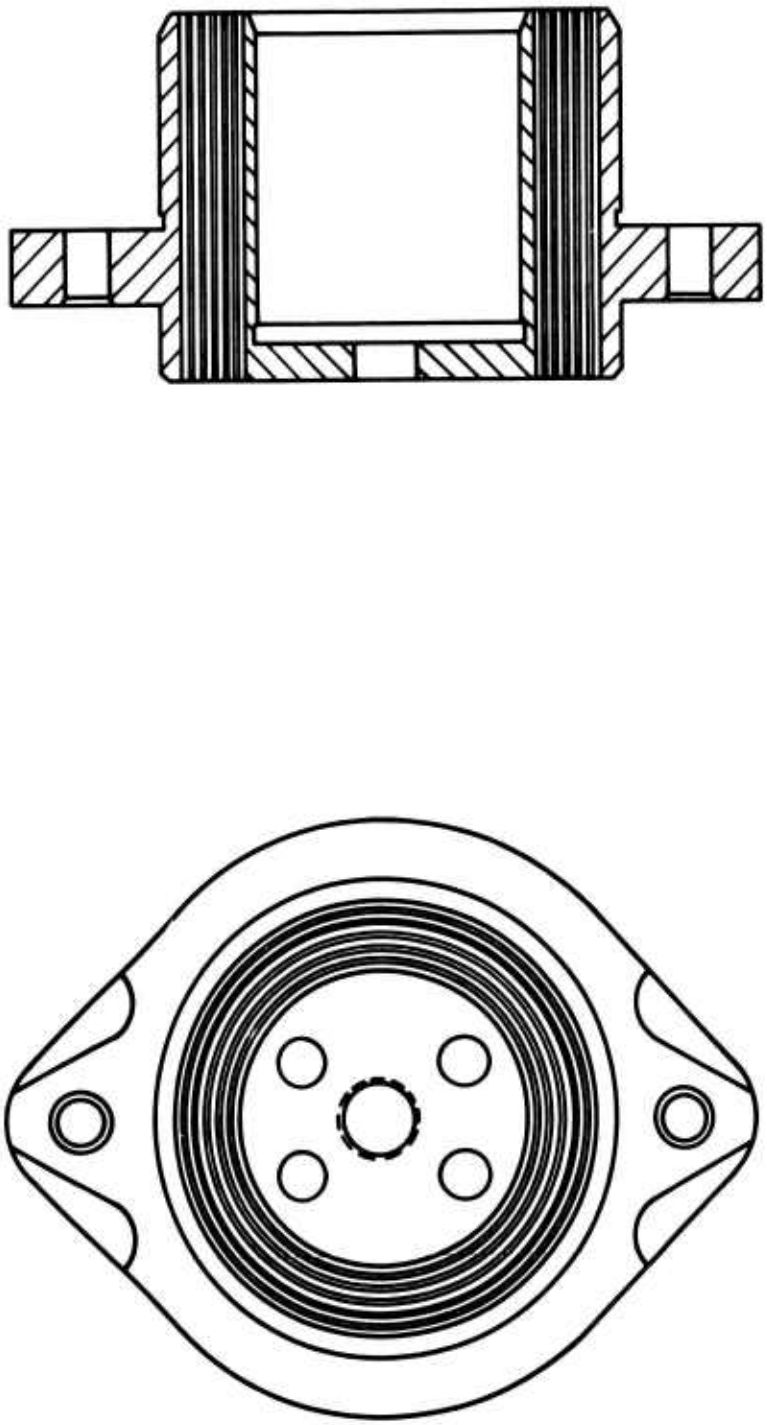

Figure 2-2. Bell 540 rotor flapping bearing

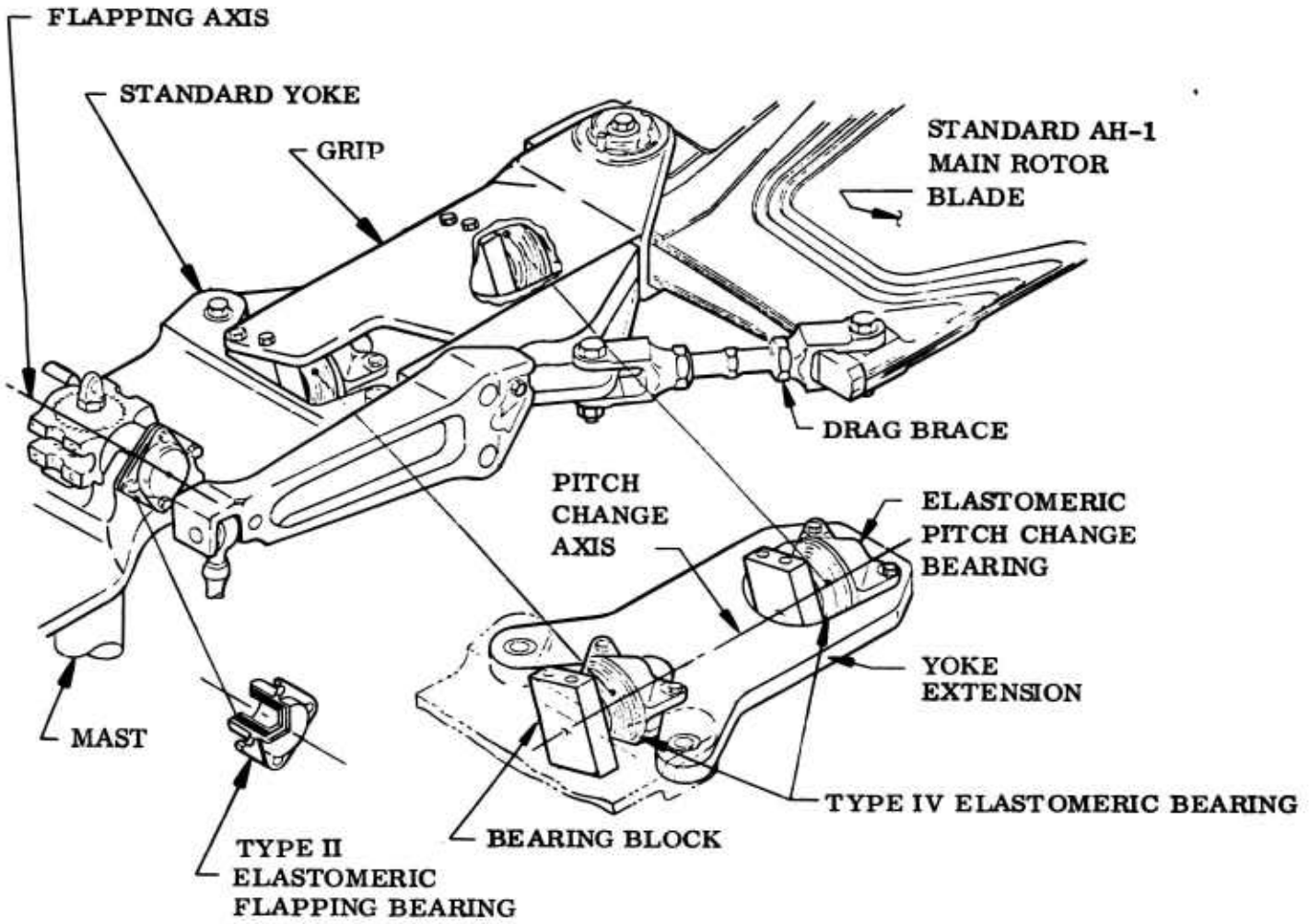

Figure 2-3. Type II and IV bearings for teetering and feathering of Bell 540 rotor

bearing reacts centrifugal force while allowing pitch, flap and lag oscillatory motions. The centering bearing, which uses a Type II (radial) bearing with spherical shims, constrains the pivot point relative to the hub attachment trunnion as shown in Figure 2-4. A rod end or Type II (radial) bearing with spherical shims was also evaluated as a lag damper system. The centering and rod end bearings were fabricated using split shims and split outer races which introduced severe stress singularity in the elastomer and resulted in very low service life.

2.1.3 Sikorsky UTTAS

The UTTAS is a four-blade aircraft that uses a combination of Type I (axial) and Type III (spherical) bearings to react the centrifugal force and allow pitch and flap motions. This system has been flight and bench tested.

2.1.4 Boeing HLH

The HLH elastomeric rotor head system is shown in Figure 2-5. This application of the spherical bearing is quite similar to that for the H-53 retrofit program. The original bearing design proved to be unstable and buckled under static loads.

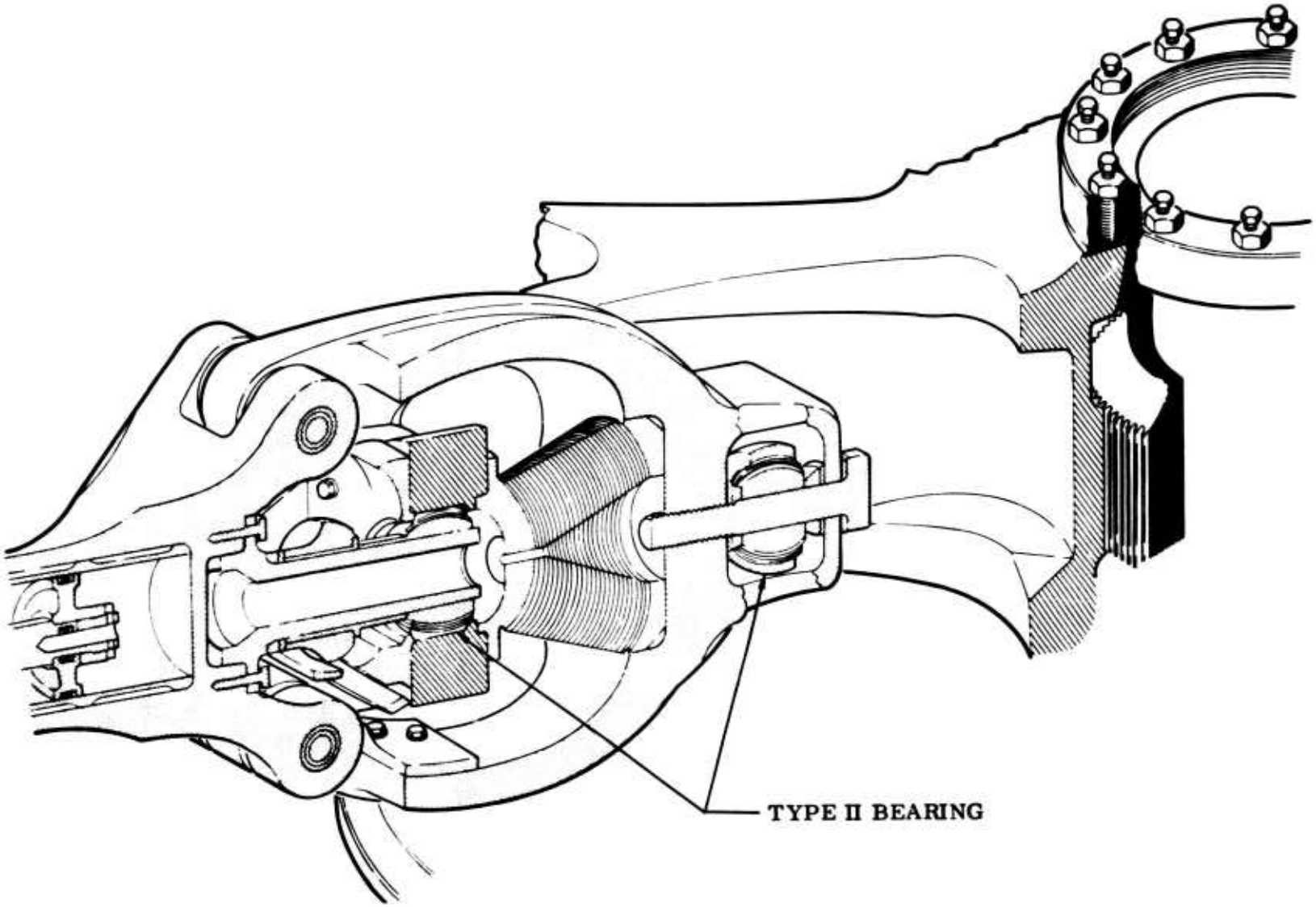

Figure 2-4. Type II (radial) bearing with spherical shims on Sikorsky H-53

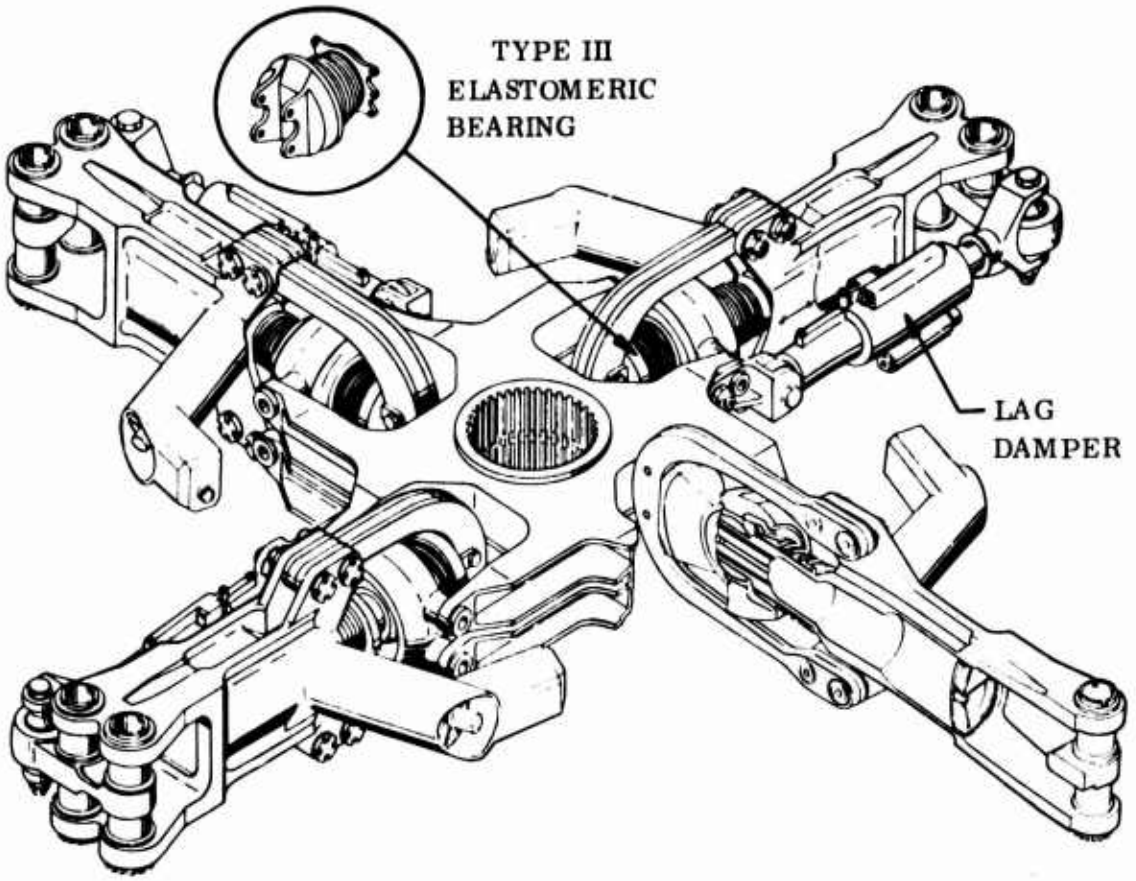

Figure 2-5. Type III (spherical) bearing on Boeing HLH rotor

2.1.5 Future Applications

As indicated by the current demonstration program, elastomeric bearings can afford considerable flexibility in rotor head system design. These bearings provide well defined hinge points which aid in the definition of or tuning of system dynamic characteristics. All four bearing types can be incorporated in designs to provide for the pitch or feathering motions. The Type I, II, and III bearings can react significant axial or centrifugal forces. Type II and III bearings can be designed to provide hinge points for flap or lead-lag motions. Obviously, the Type III (spherical) bearing is ideally suited to fully articulated rotor head systems; while the Type I, II, and IV bearings would be most applicable to the more rigid rotor concepts requiring primarily pitch or feathering motions.

2.2 REQUIREMENTS

Requirements or constraints are necessary to initiate design at the component or detail part level. These constraints must come from the rotor head optimization or trade-off study process which considers service life, spring rate, envelope, and interfaces as dependent variables. This approach presumes a specified load-motion spectrum. Environmental conditions and design factors (structural design criteria) must also be provided.

The service life requirement is generally stated as an objective or goal. Recent indications are that 2,000 flight hours or approximately 30×10^6 cycles will be typical values.

Load-motion requirements will, in general, be defined in terms of the block type endurance test matrix. A typical format of the endurance bench test matrix for a Type III (spherical) bearing is presented in Figure 2-6. Accelerated fatigue and static load-motion test conditions might also be specified for the purpose of early design verification. Current data indicates that bench test conditions are a very severe test relative to practical flight history. That is, the temperature-time dependence of the reversion or elastomer degradation process is not considered.

Environmental requirements are generally standardized by military specifications. Only elastomer formulations that are relatively insensitive to attack by ozone, oxygen, fungus, and other active compounds should be considered in bearing design. The most significant environmental requirement will be the operational temperature extremes. As will be discussed, low-temperature crystallization and thermally induced stresses in elastomer reversion are critical bearing design considerations. However, the initial temperature in the temperature-time problem was not within the scope of the current effort. This manual is, therefore, based on ambient initial condition but indicates the implications of and evaluation procedures for temperature extremes.

ENDURANCE LOADS AND MOTIONS FOR MAIN ROTOR BLADE ELASTOMERIC BEARING

Condition No.	Percent Time	Frequency (cpm)	Cone θ_x (deg)	Flap $\pm\theta_x$ (deg)	Lag θ_y (deg)	Hunt $\pm\theta_y$ (deg)	Pitch		Loads					
									Axial Z (lb)		In Plane X (lb)		Out of Plane Y (lb)	
							θ_z	$\pm\theta_z$	F_z	$\pm F_z$	F_x	$\pm F_x$	F_y	$\pm F_y$

Figure 2-6. Typical endurance loads and motions matrix

While design factors or structural design criteria are certainly significant design requirements, a universal approach within the helicopter industry does not appear to exist. Therefore, this manual currently considers nominal or average conditions to which the designer must apply the specified design factors.

The definition of constraints is very critical to the bearing design process and, thus, to the rotor system design. If service life were the only constraint, the designer could design to that service life while minimizing bearing envelope, weight, and cost and accepting the resulting stiffness or spring rates. If envelope were the predominant constraint, he could maximize service life while accepting resulting spring rate, cost, and weight implications or he could design to a service life while maximizing spring rate or minimizing cost.

3.0 MATERIALS

The design of an elastomeric bearing requires that the designer be familiar with the properties of materials that will be used in the manufacture of that bearing. The purpose of this section is to provide him with information on some of the important properties that are required to carry out a meaningful analysis. Since the bearing is comprised of two materials (namely, elastomer and reinforcements), they will be discussed separately in this section.

3.1 ELASTOMER PAD MATERIALS

The primary objective of this program was to develop reliable analytical techniques to assist in the design of laminated elastomeric bearings. A rubber formulation that is representative of those used in the helicopter industry for elastomeric bearing applications was selected as the pad material. An elastomer formulation development program would have greatly expanded the scope of this study and required considerable research in the area of rubber compounding for different specifications.

3.1.1 Formulation Selection

A typical rubber formulation contains two important ingredients in addition to the basic stock. The first ingredient, usually sulfur, is used for vulcanizing and stabilizing the basic stock. The second ingredient, usually carbon black, is a reinforcing agent that improves the hardness and modulus of the basic stock. The manner in which these ingredients affect the properties of the formulation is discussed in Volume I. The engineer should realize that properties are also affected by (1) variations in the raw rubber and the compounding ingredients, (2) small differences in the mixing procedure, and (3) the time and temperature of vulcanization. In order to achieve the best correlations between design and performance, it is mandatory that the properties of the formulation actually being used to fabricate the bearings be specifically characterized.

The rubber formulation selected for preparation of the test specimens and for fabrication of the three types of bearings that were built under the present contract is of the Efficient Vulcanization (EV) type (References 3-1 through 3-4). The formulation has been given the Thiokol designation TR-3012; its composition is given in Table 3-1.

TABLE 3-1

TR-3012 RUBBER FORMULATION

Ingredients	Parts by Weight
Raw Latex:	
SMR5-CV[a]	100
Filler Agents:	
SRF[b] Black	30
Zinc Oxide[c]	5
Cure Agent:	
Sulfur	0.6
Cure Accelerators:	
Zinc 2 - Ethyl Hexanoate	2
Santocure MOR[d]	1.44
Butyl Tuads[e]	0.6
Antioxidant:	
Flectol H[f]	2

[a] Standard Malayasian Rubber Grade No. 5, Constant Viscosity
[b] Semireinforcement Furnace
[c] Also a Cure Agent
[d] 2 - Morpholinothio Benzothiazole
[e] Tetrabutylphiuram Disulphide
[f] Poly-2, 2, 4 - Trimethyl 1-1, 2 - Dihydroquinoline

The material property data presented in the remaining portion of this section apply to the TR-3012 formulation. Other formulations can markedly affect these properties. It should be pointed out here that rubber compound formulation cannot be done by rules but requires experience, judgment, and skill. The design engineer should coordinate his efforts with those of a rubber specialist.

3.1.2 Elastomer Properties

Natural rubber, as normally used in bearing pads, is a nonlinear viscoelastic material capable of very large deformations. It is generally defined by a strain energy function which contains a number of arbitrary constants (Reference 3-5). For an isotropic body subjected to small strains, the strain energy function can be expressed in terms of two constants for the material--the compression modulus and the rigidity (shear) modulus.

The evaluation of all arbitrary constants may require considerable laboratory testing and complicated sample analyses. Such an evaluation is justified if the designer is faced with geometries and loads that warrant the use of a nonlinear theory. However, a large number of experimental and analytical studies of the behavior of rubber sheets bonded to rigid plates (References 3-6 through 3-8) have shown that the classical linear theory of elasticity is generally applicable to bearing design. A viscoelastic analysis, which is normally difficult, is not required.

The designer's objectives are to predict:

1. Stresses and strains in the pads under various loading conditions.
2. Life of the pads under these loads which are generally cyclic in nature.

Accurate predictions are possible if a thorough knowledge of the material behavior is available to the designer. The material properties that are required for a detailed stress analysis of the pads are:

1. Material stiffness

2. Bulk modulus or Poisson's ratio
3. Coefficient of linear thermal expansion

Instead of using Young's modulus for material stiffness as is customarily specified for metals, a modulus that is generally chosen to characterize the viscoelastic response of rubber is called the relaxation modulus.

Thiokol's observations have shown that a major cause of bearing failure is heat buildup during cyclic loading. Prediction of heat buildup requires a knowledge of some additional properties; these are:

1. Dynamic modulus and loss tangent
2. Thermal conductivity
3. Specific heat

Each of these properties will now be discussed separately along with suggested experimental methods for their determination.

3.1.2.1 Relaxation Modulus

Relaxation modulus is defined as the stress per unit applied strain. It is the relationship between the stress variation over time [$\sigma(t)$] associated with an instantaneously applied constant strain (ϵ_o) that is shown as follows:

$$\text{Relaxation Modulus} = \frac{\sigma(t)}{\epsilon_o} \tag{3-1}$$

Relaxation modulus can be defined in terms of shear stresses or tensile stresses. The relaxation modulus in shear is denoted by $G_{rel}(t)$ and will be discussed in this section because shear stresses are more dominant in most bearings than are tensile stresses. If required, tensile modulus values can be approximated by multiplying the shear values by 3.

The shear modulus of rubber is not constant, but varies with loading rate and temperature. The variation is significant at low temperatures and/or at high strain rates. The shear modulus is generally chosen to be consistent with the anticipated loading rate and temperature; it can be obtained from what has come to

be known as the "master relaxation curve" for the material. In order to determine the master relaxation curve, it is necessary to perform relaxation tests at different temperatures.

A standard test for relaxation modulus of vulcanized rubber is given in ASTM Procedure D1390-62. Procedures similar to those contained in Reference 3-9 could also be used. Another test that will provide accurate shear relaxation modulus values for helicopter bearings is designated the Quadruple Lap Shear (QLS) test. A QLS specimen is shown in Figure 3-1.

The procedures for relaxation tests--whether in tension, compression or shear--are basically the same, and they are discussed in Volume I.

Typical shear relaxation modulus data for TR-3012 rubber tested at three different temperatures are given in Figure 3-2. A tensile relaxation test was used and the tensile modulus values were divided by 3. The procedure for obtaining a master relaxation curve from this data is as follows:

1. Apply a temperature correction factor (T_s/T) to the data in Figure 3-2 and plot $G_{rel}\ T_s/T$ versus log t as shown in Figure 3-3. The temperature T_s is any arbitrary reference temperature (77° F in Figure 3-3) and T is the test temperature for a given curve. The temperatures are in degrees Kelvin or Rankine. The temperature correction factor was first introduced by Treloar (Reference 3-10).
2. Shift the temperature corrected values of $G_{rel}\ T_s/T$ along the log time axis using the William-Landel-Ferry (WLF) shift factor "log A_T" (Reference 3-11) defined by $\log A_T = [797.4 - 8.86\ (T-T_g)]/[93.24 + T-T_g]$ (temperatures are in degrees Fahrenheit). For example, the shift factors for 77°F and

-20°F are, respectively, -2.984 and +0.196. Therefore, if 77°F is taken as a reference temperature, the relaxation modulus data obtained at -20°F should be shifted along the log t axis by [0.196-(-2.984)] or 3.18 units.

The master relaxation curve obtained by the above procedure is presented in Figure 3-4. It shows that if the loading rate is slow (which corresponds to large time) and/or temperature is high, the shear modulus has a constant value of 96 psi. The curve can be used for other times (load rates) and/or temperature combinations to characterize the bearing pad shear stiffness for analysis purposes. The effect of time will become more apparent in the discussion on dynamic modulus.

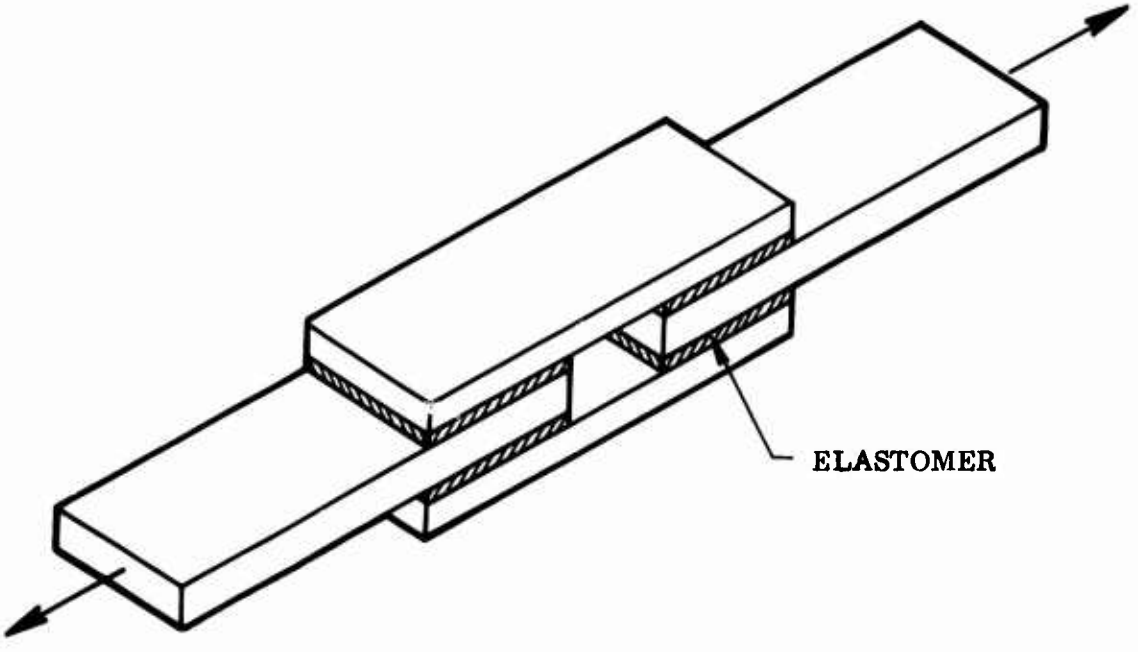

Figure 3-1. Quadruple lap shear specimen.

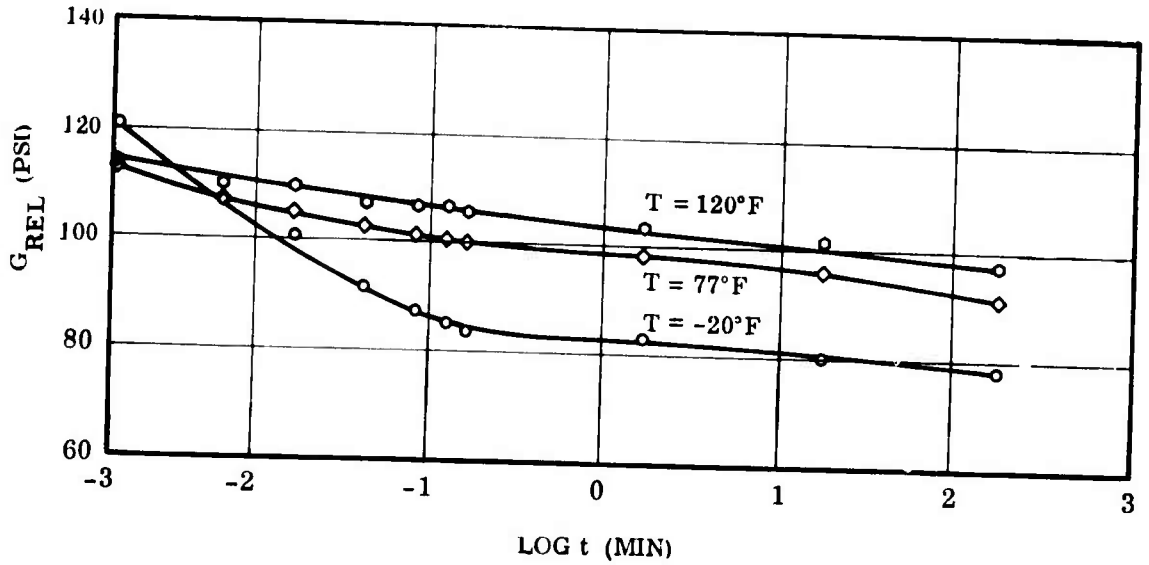

Figure 3-2. Relaxation modulus for TR-3012 elastomer at 30% strain.

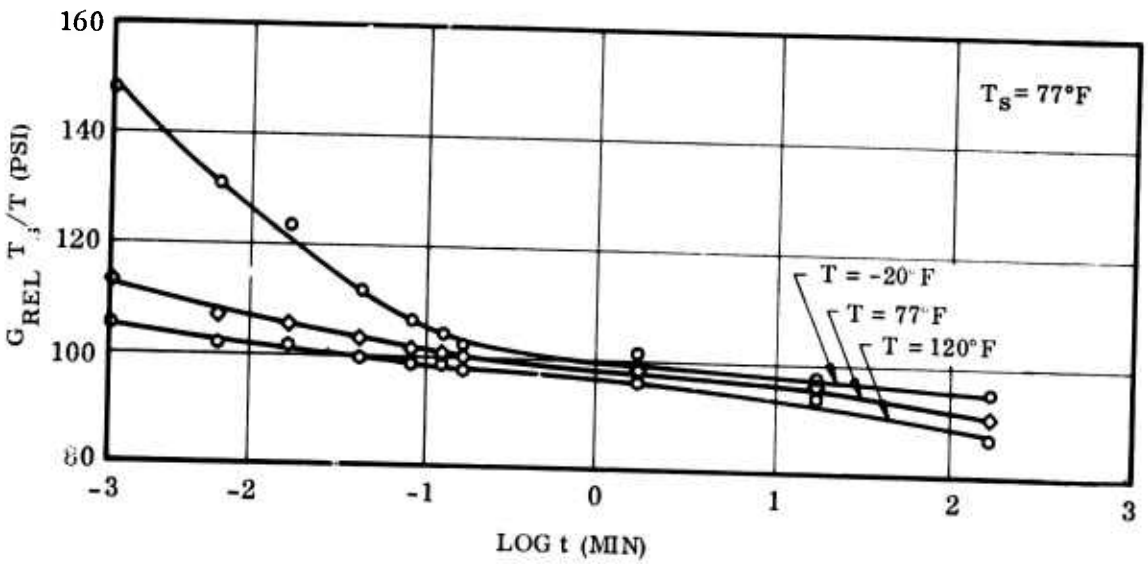

Figure 3-3. Temperature corrected relaxation modulus for TR-3012 elastomer at 30% strain.

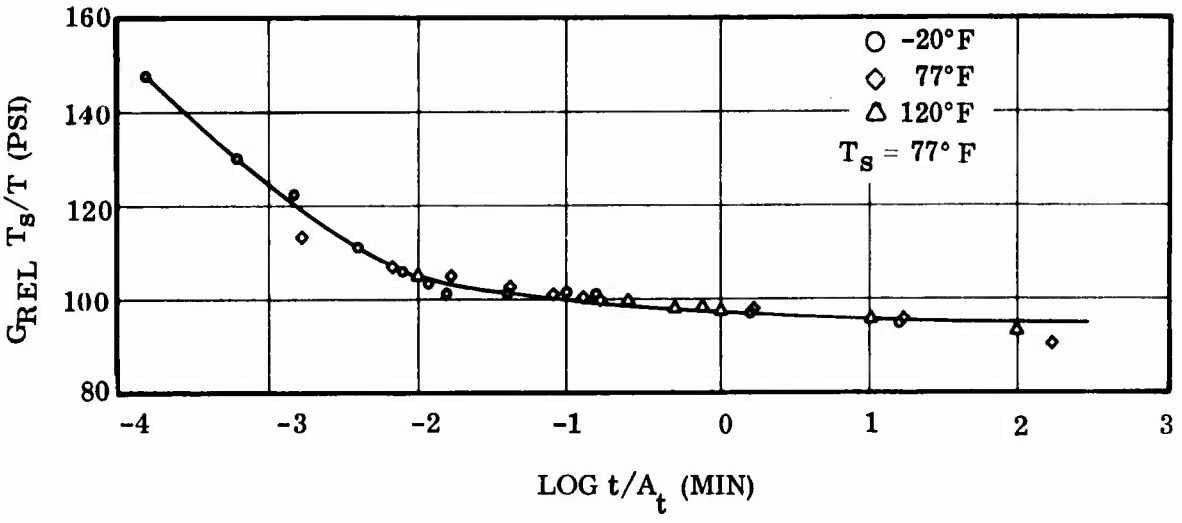

Figure 3-4. Master relaxation modulus for TR-3012 elastomer at 30% strain.

3.1.2.2 Bulk Modulus and Poisson's Ratio

The linear elastic material option in the finite-element computer program described in Section 6.0, Bearing Analysis, requires Young's modulus and Poisson's ratio (ν) to be inputted. The Young's modulus can be deduced from shear modulus as explained in the previous subsection. For accurate analysis of nearly incompressible materials (Poisson's ratio is close to 0.5) such as elastomeric bearing pads, the values of Poisson's ratio must be known to the fourth decimal place. The effect of Poisson's ratio on the calculated stresses is shown in Figure 3-5. They were determined analytically (Reference 3-12) in a solid Type I bearing pad (no center opening) due to an axial load when edge singularities were neglected.

Fairly accurate values of Poisson's ratio can be obtained by careful laboratory measurements of the axial load-deflection relationship for a bearing similar to that being analyzed. Proper value of Poisson's ratio can then be deduced by comparing them with finite-element analysis results of the bearing using the Young's modulus of the pad and various values of Poisson's ratio.

A second method is to obtain Poisson's ratio directly from bulk modulus (k) measurements using the formula giving $\nu = (3k - 2G_{rel})/2\,(3k + G_{rel})$ $\simeq 1/2\,(1 - G_{rel}/k)$. This formula is exact only for linear elastic materials. However, by using the value of G_{rel} from the master relaxation curve at the time and temperature of interest, the above equation can be successfully applied.

The bulk modulus is the reciprocal of material volume compressibility and for an isothermal condition is defined as

$$k = -V_o \frac{\partial P}{\partial V} \qquad (3\text{-}2)$$

where V_o = Initial Volume

V = Volume

P = Pressure

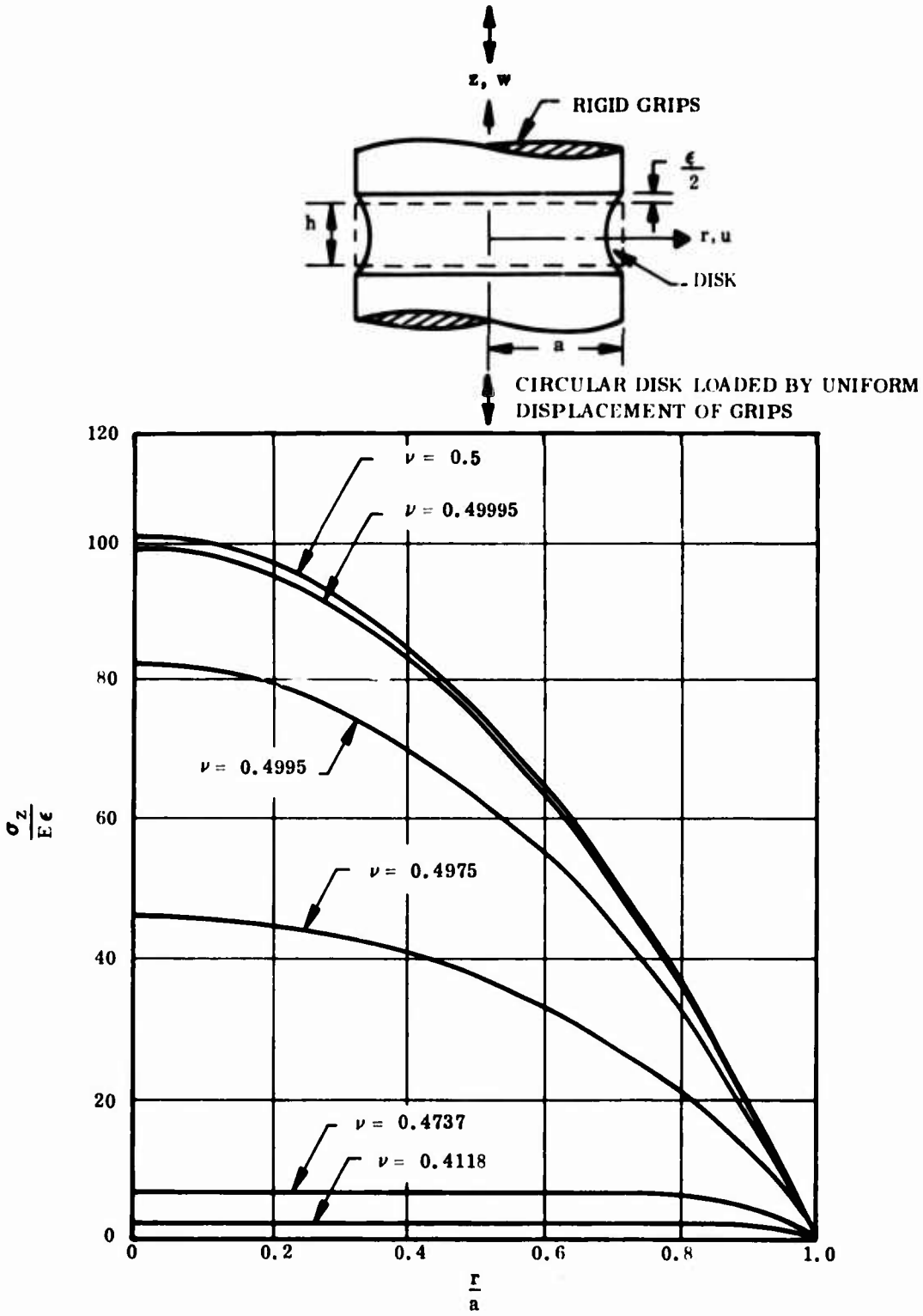

Figure 3-5. Normal stress (σ_z) in disk versus r/a when a/h = 10.

No standardized method is presently being used for obtaining bulk modulus. Any method for applying a hydrostatic pressure to a body of rubber and measuring the resulting volume decrease can be used. The major difficulty encountered is in obtaining an accurate measurement of volume change. Procedures have been developed using, in addition to others, pressurized gas, mercury, and oil (References 3-13, 3-14, and 3-15, respectively); the last two methods allow evaluation of dynamic bulk modulus. A pressurized oil method previously developed for viscoelastic solid propellants was used for evaluating elastomeric bearing rubber as described in Volume I.

The bulk modulus is generally considered to be a material property; i.e., a constant. In this case, the ratio $\partial P/\partial V$ in Equation 3-2 is a constant. For solid propellants and rubber materials, however, the curve relating the volume to the pressure may not be linear. In this case, the change in volume with respect to pressure is the instantaneous slope of the volume-pressure curve. The bulk modulus is then determined as a function or pressure over small incremental changes in pressure from the equation

$$k = -V_o \frac{\Delta P}{\Delta V} \tag{3-3}$$

The bulk modulus is generally constant at pressures over 500 psi. Figure 3-6 shows the bulk modulus dependency upon hydrostatic pressure for TR-3012 rubber.

3.1.2.3 Coefficient of Linear Thermal Expansion

The coefficient of linear thermal expansion (α) is used in thermal stress analysis of bearings. The α for rubber is typically more than 10 times that of steel. Since natural rubber is normally cured at 300° F and since bearings are often required to withstand temperatures of -65°F, the thermal stresses in many bearings (especially Type II) may be a major factor in bearing design.

Generally, α is obtained by first cooling the temperature of a laboratory sample to a low value (-165°F) and then raising the temperature slowly (0.2° to

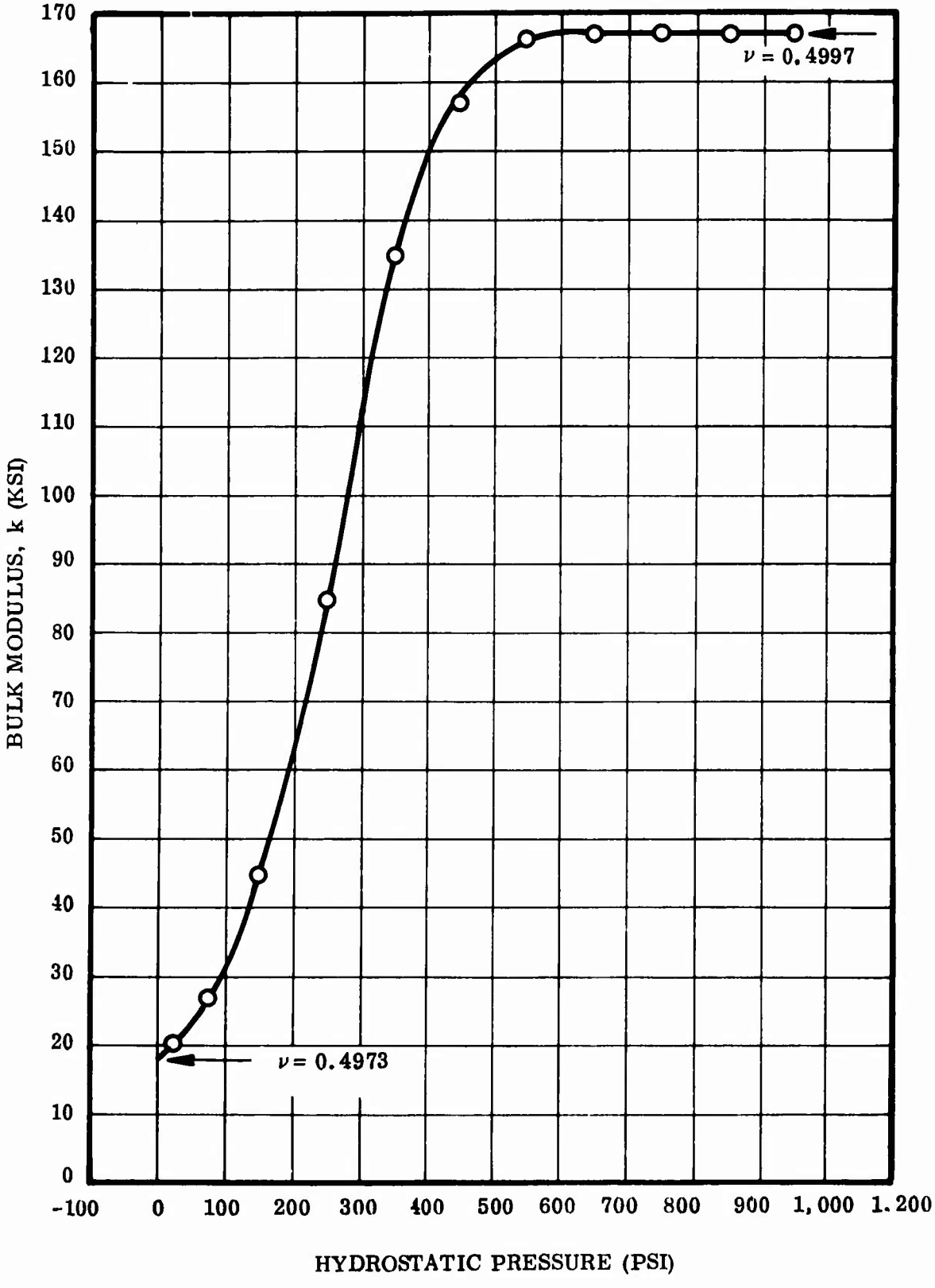

Figure 3-6. Bulk modulus dependency upon hydrostatic pressure.

2.0°F/minute) while monitoring sample elongation. The major difficulty in obtaining accurate α values for rubber stems from the need to allow free expansion of the rubber with negligible slump; other difficulties arise from the need to minimize surface friction and applied forces from displacement measuring equipment while recording extremely small changes in length. Many methods for avoiding these difficulties have been suggested (References 3-9, 3-16, and 3-17).

The test procedure used for determining α for TR-3012 rubber is given in Volume I. Figure 3-7 shows the variation of α with temperature.

In calculating the temperature correction factor for relaxation modulus determination, a parameter called the glass transition temperaure (T_g) was used. T_g is defined as the temperature at which the volumetric expansion coefficient changes from a value characteristic of a glass to that more characteristic of a liquid. The value of T_g is normally obtained by observing changes in α. For example, α changed from 34×10^{-6} in/in/°F to 97×10^{-6} in/in/°F at -106°F, which is the T_g for TR-3012 rubber.

3.1.2.4 Dynamic Modulus and Loss Tangent

Dynamic modulus and loss tangent determination is important when considering heat buildup in the pads due to cyclic loading. In fact, many fatigue failures can be attributed to reversion, which is a temperature-, time-, and strain-dependent phenomenon. Although temperature and reversion failure boundary prediction techniques have not been evaluated, a consideration of some of the properties required for such analyses has been included in the following discussion.

In order to explain dynamic modulus and loss tangent, it is desirable to include a brief discussion on dynamic behavior of viscoelastic materials. For this purpose, consider the application of a sinusoidal shear stress to a material. It will result in a sinusoidal shear strain. If the material exhibits ideal elastic behavior, the strain will be in phase with the stress and will vary with the same frequency. If the material is linearly viscoelastic, the strain will have the same

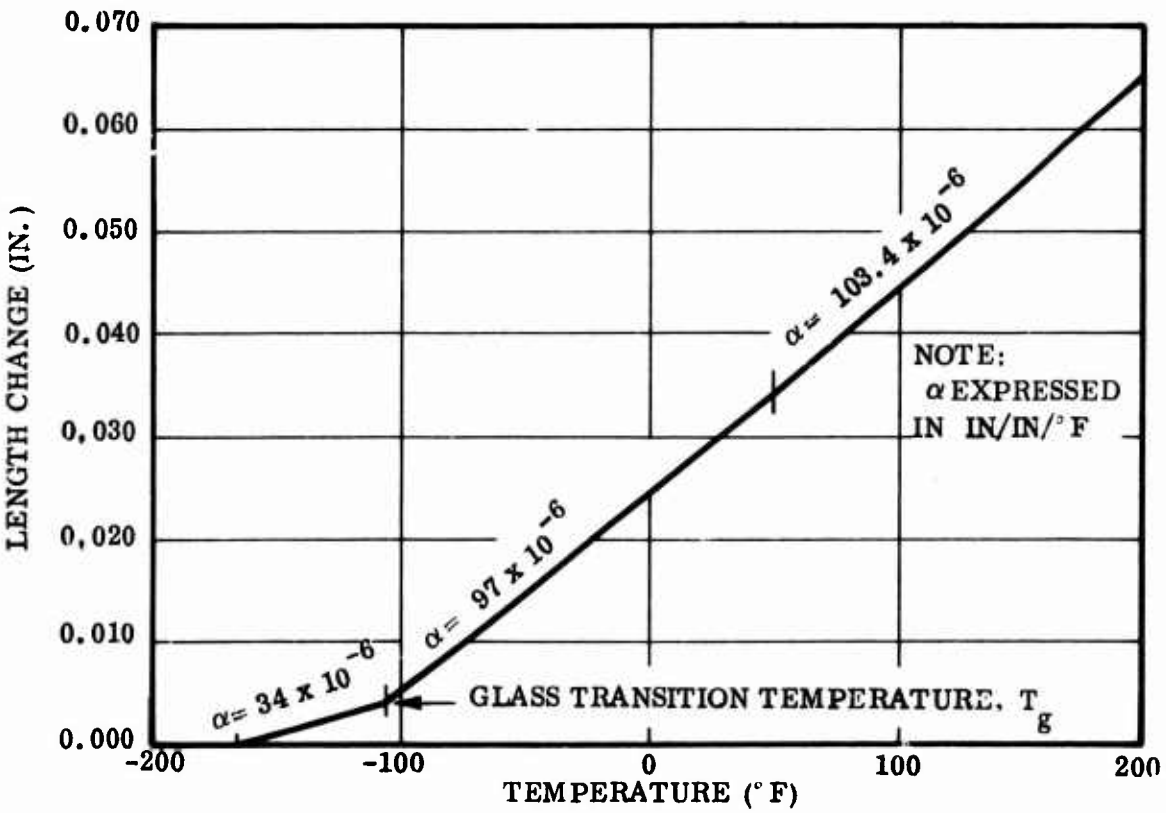

Figure 3-7. Coefficient of linear thermal expansion for TR-3012 elastomer.

frequency as the applied stress but will be out of phase with the stress. This relationship is shown in Figure 3-8, which represents the sinusoidal stress and strain behavior directly and in terms of a rotating radius vector. Analytically, it is convenient to represent the sinusoidal stress as the real part of a complex stress. Graphically, this complex stress would appear as a rotating vector in the complex plane, the length of which is the amplitude of the stress and the projection of which, on the real axis, gives the sinusoidally varying instantaneous real value of the stress.

Mathematically, the complex shear stresses and shear strains can be written in a trigonometric form as

$$\tau^* = \tau_a \ (\cos \ \omega t + i \sin \omega t) \tag{3-4}$$

$$\gamma^* = \gamma_a \ [\cos \ (\omega t - \delta) + i \sin \ (\omega t - \delta)] \tag{3-5}$$

where τ^* = Complex Stress

γ^* = Complex Strain

τ_a = Stress Amplitude

γ_a = Strain Amplitude

δ = Lag (or loss) Phase Angle

ω = Circular Frequency (rad/sec)

t = Time

Equations 3-4 and 3-5 can also be expressed in an exponential form as

$$\tau^* = \tau_a e^{i\omega t} \tag{3-6}$$

$$\gamma^* = \gamma_a e^{i\,(\omega t - \delta)} \tag{3-7}$$

The complex modulus (G*) is then defined as the ratio of the complex stress and complex strain; viz:

$$G^* \ (\omega) = \frac{\tau^*}{\gamma^*} \tag{3-8}$$

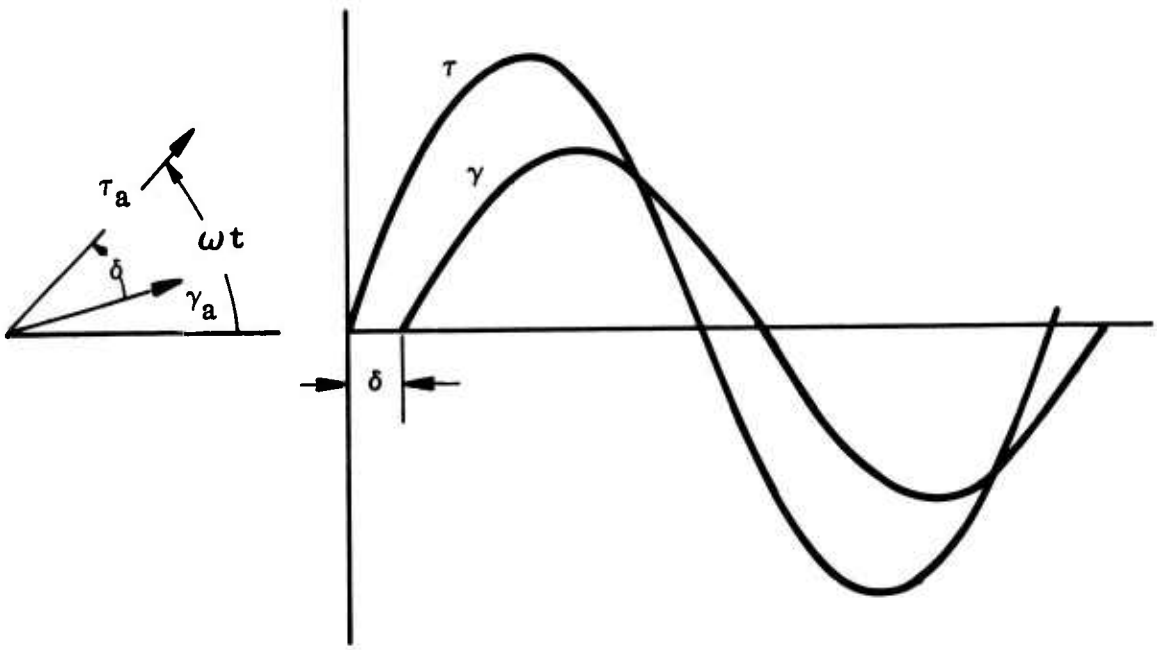

Figure 3-8. Dynamic stress and strain for a viscoelastic material.

Since G* is a complex number, it is normally written as

$$G^*(\omega) = G'(\omega) + i\, G''(\omega) \tag{3-9}$$

$G'(\omega)$ is called the real part of the complex modulus or the storage modulus since it is associated with the storage of the elastic energy in the body. $G''(\omega)$ is called the imaginary part of the complex modulus or loss modulus since it is associated with mechanical energy that is dissipated as heat. The loss tangent ($\tan\delta$) is defined as

$$\tan\delta = \frac{G''}{G'} \tag{3-10}$$

The loss tangent has special significance in bearing service life considerations, since the heat generation per cycle rate ($\dot{q}$) is proportional to $\sin\delta$ (Reference 3-18) and is given by

$$\dot{q} = 2\pi \sin\delta \int_{V_o} U\, dV_o \tag{3-11}$$

where the integrand is the maximum strain energy in the volume V_o during a given cycle.

The exact linear viscoelastic relationship between the dynamic modulus [$G^*(\omega)$] and the relaxation modulus [$G_{rel}(t)$] is

$$G^*(\omega) = i\omega\, L\left[G_{rel}(t)\right]_{S \to i\omega} \tag{3-12}$$

where L = Laplace transform operator

S = Laplace transform variable

Therefore, by curve fitting the relaxation data, Equation 3-12 can be used to obtain the dynamic modulus. This approach has provided fairly accurate values for $G'(\omega)$ in tire rubber; however, the $G''(\omega)$ values are generally underpredicted-by up to a factor of 2 in tire rubber- (Reference 3-19).

The formula below is also useful for approximate analyses.

$$G'(\omega) = G_{rel}(t)\Big|_{t = 1/\omega} \qquad (3\text{-}13)$$

Dynamic properties can be obtained by many different test techniques. One such technique is suggested in ASTM D945, "Test for Mechanical Properties of Vulcanizates Under Compressive or Shear Strains by the Mechanical Oscillograph." A second informative ASTM document is D2231-71, "Standard Recommended Practice for Forced Vibration Testing of Vulcanizates." An instrument that is very well suited for rubber dynamic property characterization is called a Rheovibron. It was developed by Toyo Measuring Instruments Co. Ltd., Tokyo. Dynamic property data obtained by this instrument for TR-3012 rubber is presented in Figures 3-9, 3-10, and 3-11. Complex modulus and loss tangent values were obtained over a wide range of temperatures and for frequencies of 11, 35, and 110 Hz.

It is necessary to obtain complex modulus data only over a temperature and frequency range for which a given bearing is required to operate. The most reliable values of complex modulus can be obtained by subjecting laboratory test specimens to conditions corresponding as nearly as possible to those of service. These conditions are: form of stress (shear or compression), static strain, dynamic amplitude, dynamic frequency (at least within one decade), and test temperature. Very precise data is, of course, obtained by using full-scale or scaled models.

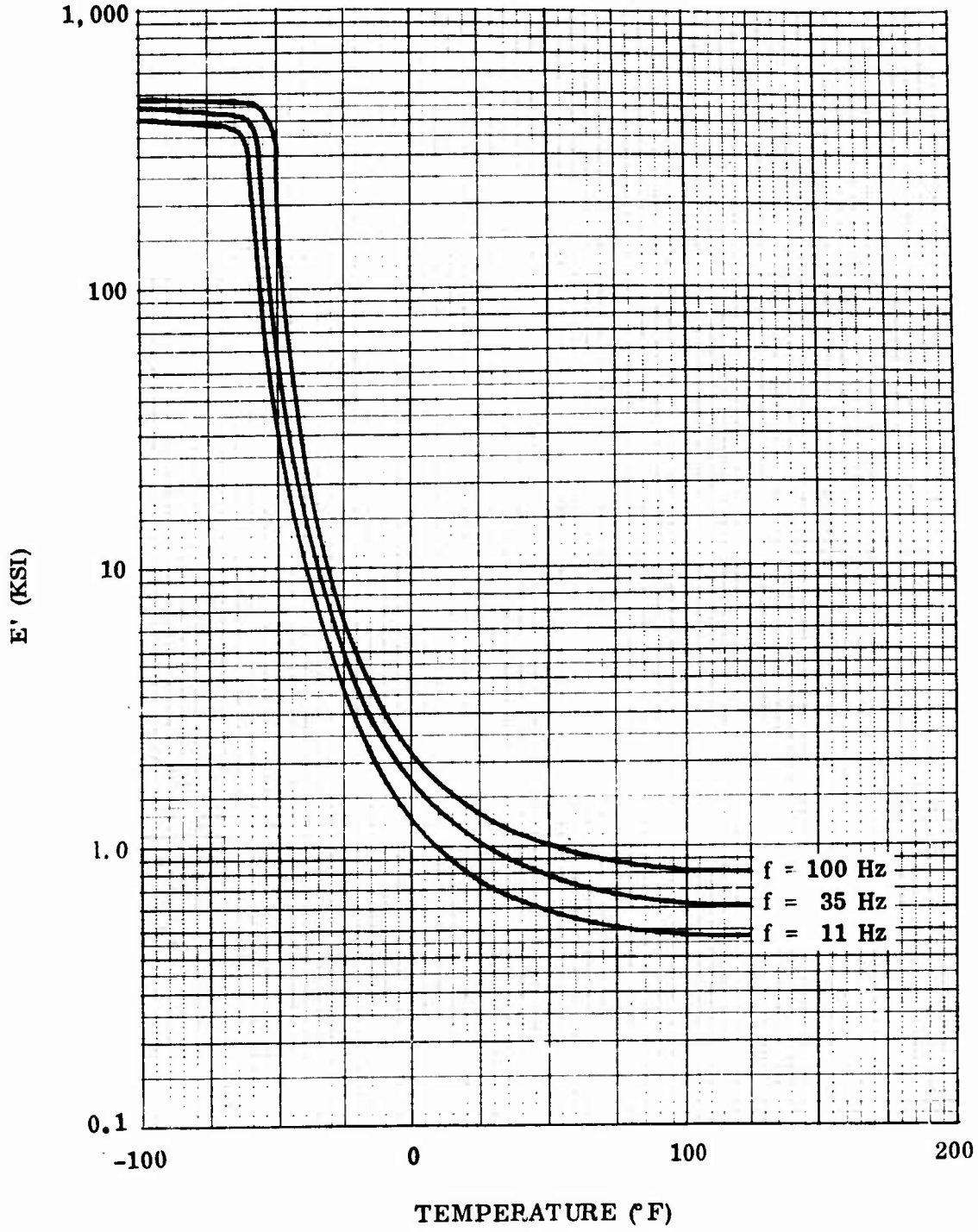

Figure 3-9. Real part of dynamic modulus.

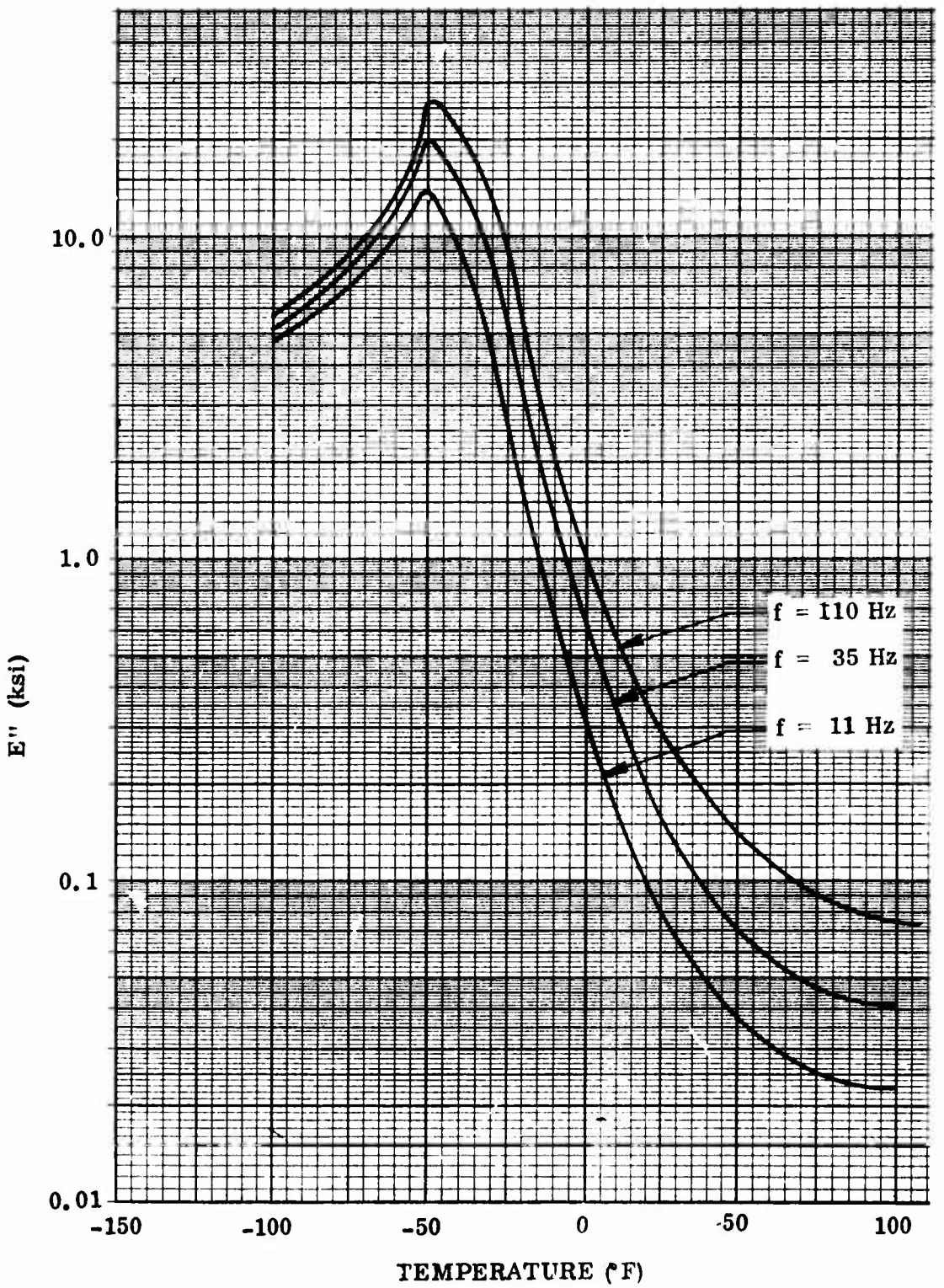

Figure 3-10. Imaginary part of dynamic modulus.

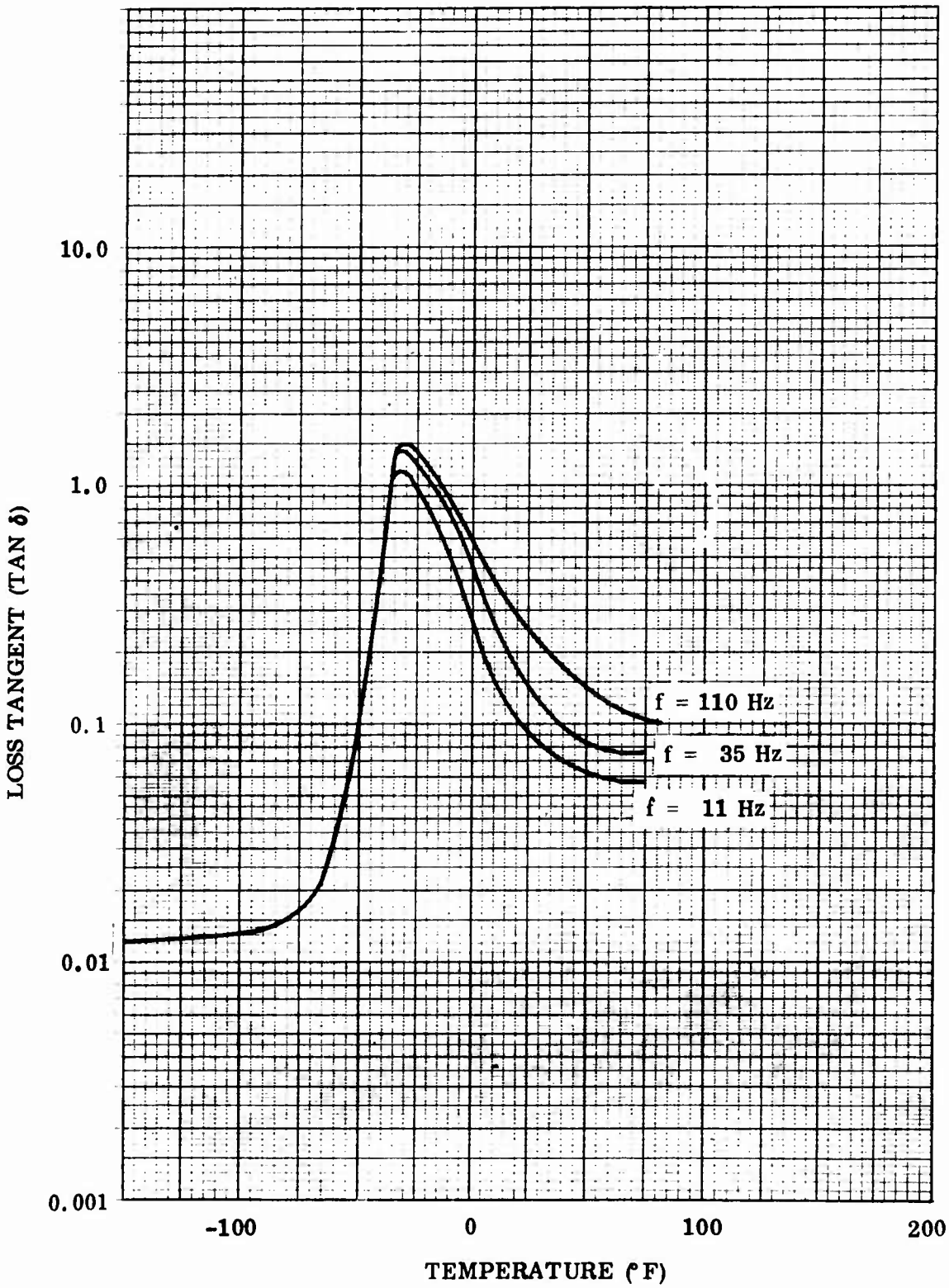

Figure 3-11. Loss tangent.

3.1.2.5 Thermal Conductivity and Specific Heat

The temperature actually developed in rubber depends on thermal conductivity as well as specific heat. The thermal conductivity of rubber formulations is very small; thus, the heat generated as a result of bearing cyclic loads is not readily dissipated. The thermal conductivity of a given rubber formulation is approximately an additive property proportional to the percentage of volume occupied by each constituent. Thus the quantities specified by weight fraction must be divided by the appropriate specific gravities.

The specific heat is also an additive property which can be calculated from the proportions of rubber and other constituents in the composition and the specific heats of the individual constituents.

Table 3-2 provides thermal conductivity, specific gravity and specific heat values for the important constituents in TR-3012 rubber. Because the other ingredients in the formulation are present in very small quantities, they need not be considered in the calculation of thermal conductivity and specific heat.

3.1.3 General Considerations

The above discussion was concerned with the determination of properties that are required for predicting bearing pad stresses and service life. The design engineer should also be aware of other distinguishing characteristics of rubber that differ from materials that are well characterized such as metals, wood, and concrete.

3.1.3.1 Mullins' Effect (Scragging)

At strain levels as low as 1 percent, and prior to exhibiting measurable dilatation, most filled rubber vulcanizates exhibit a stress softening and hysteresis phenomenon. This phenomenon is normally associated with microstructural failure prior to the formation of vacuoles and is termed the Mullins' effect. The significance of this effect in rubber testing is that the stress-strain curve is not identical for the first and second load cycles for the same applied strain. In fact,

TABLE 3-2

SPECIFIC HEATS, THERMAL CONDUCTIVITIES, AND SPECIFIC GRAVITIES OF TR-3012 INGREDIENTS[a]

Ingredients	Specific Heat (Btu/lbm/°F)	Thermal Conductivity (Btu/sq ft-hr-°F/in.)	Specific Gravity
Natural Rubber ("Pure Gum")	0.45 to 0.50[b]	0.928	0.92 to 0.98
Carbon Black	0.20	1.015 to 1.943	1.8
Zinc Oxide	0.12	4.06 to 4.785	5.606

[a]Reference 3-20

[b]Specific heat for most rubbers increases with temperature by about 0.0077 to 0.0028 per °F; values quoted are for 68° to 77°F.

a number of cycles (approximately 5) are required before a consistent stress-strain behavior is observed. Therefore, prestrains on test specimens should be carefully avoided if material properties are desired for first cycle loads (such as thermally induced loads applied after rubber cure). On the other hand, test specimens should be preloaded (scragged) to a level greater than the test level for a number of cycles before testing for mechanical properties used in predicting stresses due to cyclic loads. Care should be taken to avoid heat buildup during the scragging process by using a slow loading rate.

If a rubber specimen is allowed to sit in an unloaded condition for a period of time after cycling, the stress-strain behavior for many formulations reverts to nearly the first cycle response and, thus, indicates a healing phenomenon. This healing can take place in as little as 30 minutes at room temperature and after somewhat longer times at lower temperatures. Therefore, the rubber specimens should be tested soon after scragging.

3.1.3.2 Low-Temperature Crystallization

Certain rubbers crystallize when maintained at low temperatures. The rate of crystallization is greatest in the -15° to -40°F temperature range. A maximum crystallization rate is typically on the order of 50 percent crystallinity in 24 hours. Crystallization disappears rapidly as the temperature is increased. The effect of crystallization is to decrease the thermal coefficient of linear expansion. The stiffness (modulus) also increases by orders of magnitude greater than in the uncrystallized state. The increase in stiffness due to low-temperature crystallization prevents the use of the WLF shift factor at these temperatures. Therefore, a best curve fit using rubber exposed to an environmental temperature-time combination is suggested. Crystallization also increases fatigue life and tensile strength and provides excellent tear resistance.

3.2 REINFORCEMENT MATERIALS

The present contract was primarily concerned with the design of elastomer pads. However, the engineer should recognize that reinforcements (shims) can be critical to design.

Shims can be made of virtually any stiff material including steel, aluminum, stainless steel, titanium, and composite materials. The mechanical properties of these materials are much better characterized than those of rubber.

The physical size of the shim is a function of the loads and motions imposed on the bearing. Shim design is based on two principles; namely, stress analysis and failure criteria. The magnitude of the stresses due to the various loads on the bearing can be determined by finite-element analysis. Failure criteria are generally presented as strength values or failure envelopes. It is not our intent here to present the scores of rules and procedures that are normally covered under the subjects of "Strength of Materials" and "Properties of Materials." These rules and procedures have been used so generally in the engineering literature of the last few years that no modern practicing engineer can afford to ignore them.

Since the loads and motions on the bearing vary in time, the importance of fatigue as a factor in the design of shims should not be overlooked. Fatigue failures are generally produced by fractures propagating from points of high stress. High stress points are generally cracks, flaws, and voids; therefore, the shim designer should recognize their presence. This is especially true for high-strength metals which have low fracture toughness values and do not readily deform plastically around the flaws to absorb local overloads.

The methods of fracture mechanics will insure that a flaw will not cause premature failure. These methods are available in the literature (References 3-21 and 3-22). Information concerning yield strength, fracture toughness, Young's modulus, Poisson's ratio, and crack growth rate is usually required.

This information will determine the fracture resistance, fracture growth rate, and the maximum flaw size that can be tolerated in the shim for a given stress. Maximum flaw size in the shim can be detected by available nondestructive test inspection processes prior to bearing fabrication.

The lead-lag, flap, and pitch motions that are imposed on a bearing cause an alternating stress to be superimposed on a constant stress that exists due to the centrifugal force load. A knowledge of the number of cycles of loads or motion that the shims in the bearing can withstand without failure is useful in determining the bearing's life; this is given by fatigue test data.

Fatigue test data is obtained by determining the number of cycles to failure for a number of specimens stressed at various levels. Test results are plotted to make what is called the S-N diagram. It represents the variations between the number of cycles (N) for failure and the maximum stress (S). An example of such a curve for maraging steel (as taken from Reference 3-23) is shown in Figure 3-12. It shows that as the stress is reduced, the number of stress cycles required for failure increases. S-N curves for various metals can be found in Reference 3-24. The helicopter industry typically uses 70% of the S-N curve values as a 3σ design limit.

If the mean stress on a bearing is significant, fatigue life is influenced by the relation between variable and mean stress. Because of the considerable variation in test results to determine this influence, various empirical equations have been proposed. The most well known of these relations involves a method of plotting that makes what has become known as the Goodman diagram. The Goodman diagram for 17-4 PH stainless steel shown in Figure 3-13 was taken from Reference 3-25. An informative discussion on Goodman diagrams can be found in Reference 3-26.

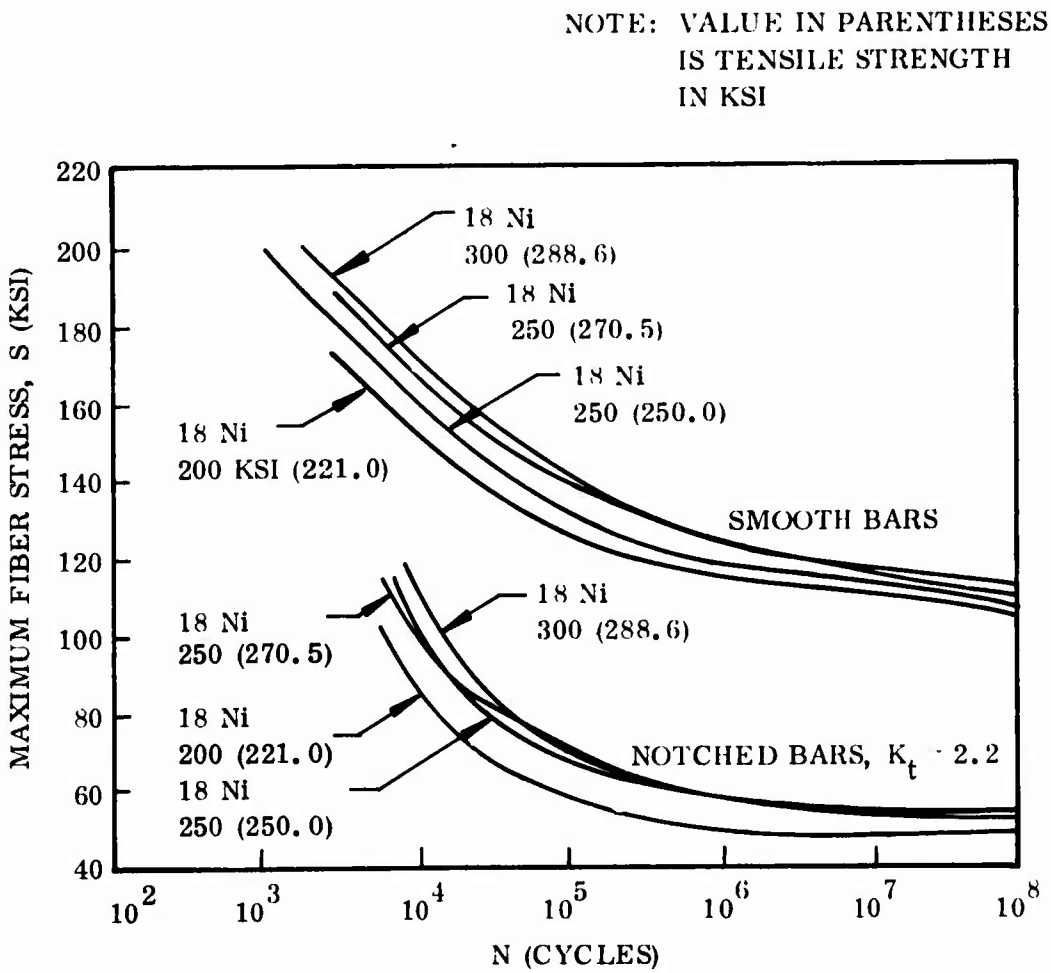

Figure 3-12. S-N curve for maraging steels.

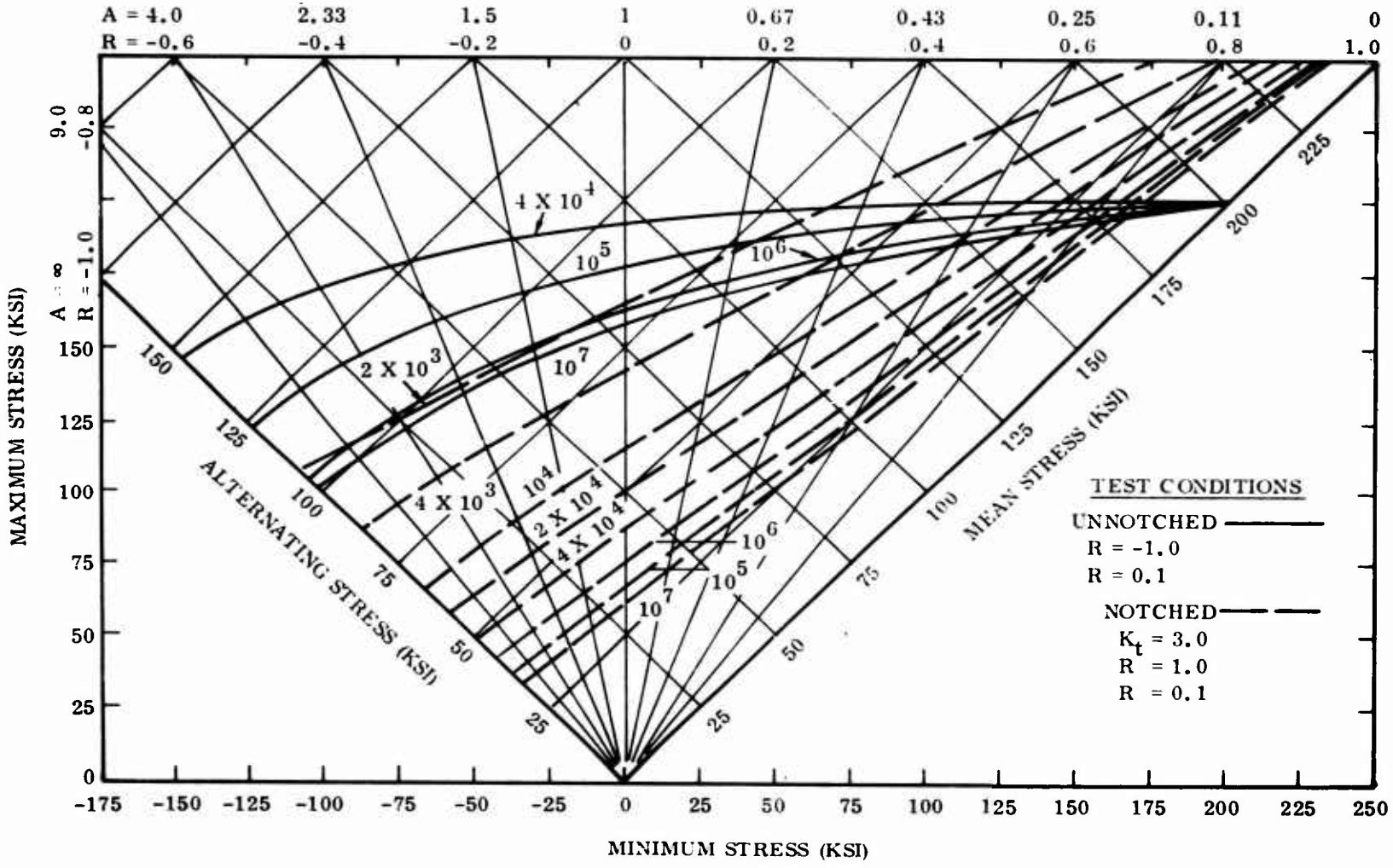

Figure 3-13. Goodman diagram for 17-4 Ph stainless steel.

4.0 TYPE I BEARING DESIGN

A Type I bearing consists of a column of flat circular elastomer pads separated by rigid shims (Figure 1-1). The shims greatly improve the load-carrying capability of the bearing by increasing the ratio of the loaded area to the area in which the elastomer is allowed to bulge or expand laterally. This ratio is commonly known as the "Shape Factor" and is denoted by S.

A Type I bearing is designed to react compressive axial loads and allow torsional rotation about its longitudinal axis. The axial load is due to the centrifugal force generated by the rotating blade, and the torsional motion is due to pitch or blade rotation about its own axis. A limited amount of bending and shear deformations are permitted although the bearing is not intended to accommodate these deformations in a typical helicopter application.

4.1 PROCEDURE

The purpose of this section is to describe a simple step-by-step procedure for design of Type I bearings. The designer is generally given the requirements for the bearing by the helicopter manufacturer. These requirements are listed for the operating times of the helicopter in a "Load-Motion Spectrum" table. A typical helicopter Load-Motion Spectrum is given in Section 9.0.

It is recommended that the design be carried out in the following three steps:

1. Preliminary Design I (Level 1) in which the rough size of the bearing is determined.
2. Preliminary Design II (Level 2) in which the design developed in Step 1 is refined.
3. Final Design (Level 3) in which the finite-element program (see Volume III) is used to pinpoint any problem areas.

4.1.1 Level 1 Design

A flow chart of the Level 1 design procedure is shown in Figure 4-1. The procedure is as follows:

1. Select elastomer formulation and develop material properties E, G, k, ν by the methods discussed in Section 3.0. A maximum shear stress fatigue failure surface of the type discussed in Section 9.0 is also required.
2. Define initial values for axial load (F_Z) and pitch angle from Load-Motion Spectrum table. Either maximum values at the cruise condition or values based on weighted average (proportional to time at load) can be chosen. The former may generally yield a conservative design. Note that the pitch angle specified in the spectrum table is the total pitch rotation (θ_Z^T) for the bearing.
3. Select an allowable compressive stress level (σ_Z^{all}) for the elastomer. The necessity of selecting an allowable stress level arises from the fact that the load-carrying capability of an elastomer pad increases as the shape factor is increased. This is shown by the relationship between the "real" Young's modulus (E) and the "apparent" Young's modulus (E_A) as given by Equations 4-4 and 4-5 and presented in Figure 4-2. For very low shape factors, $E_A \simeq E$; and in this case the advantage of restricting the area in which the elastomer is allowed to bulge is not utilized. For very high shape factors, on the other hand, $E_A \simeq k$; the bearing is too stiff to allow any appreciable flexibility in the bearing. It is advantageous to operate

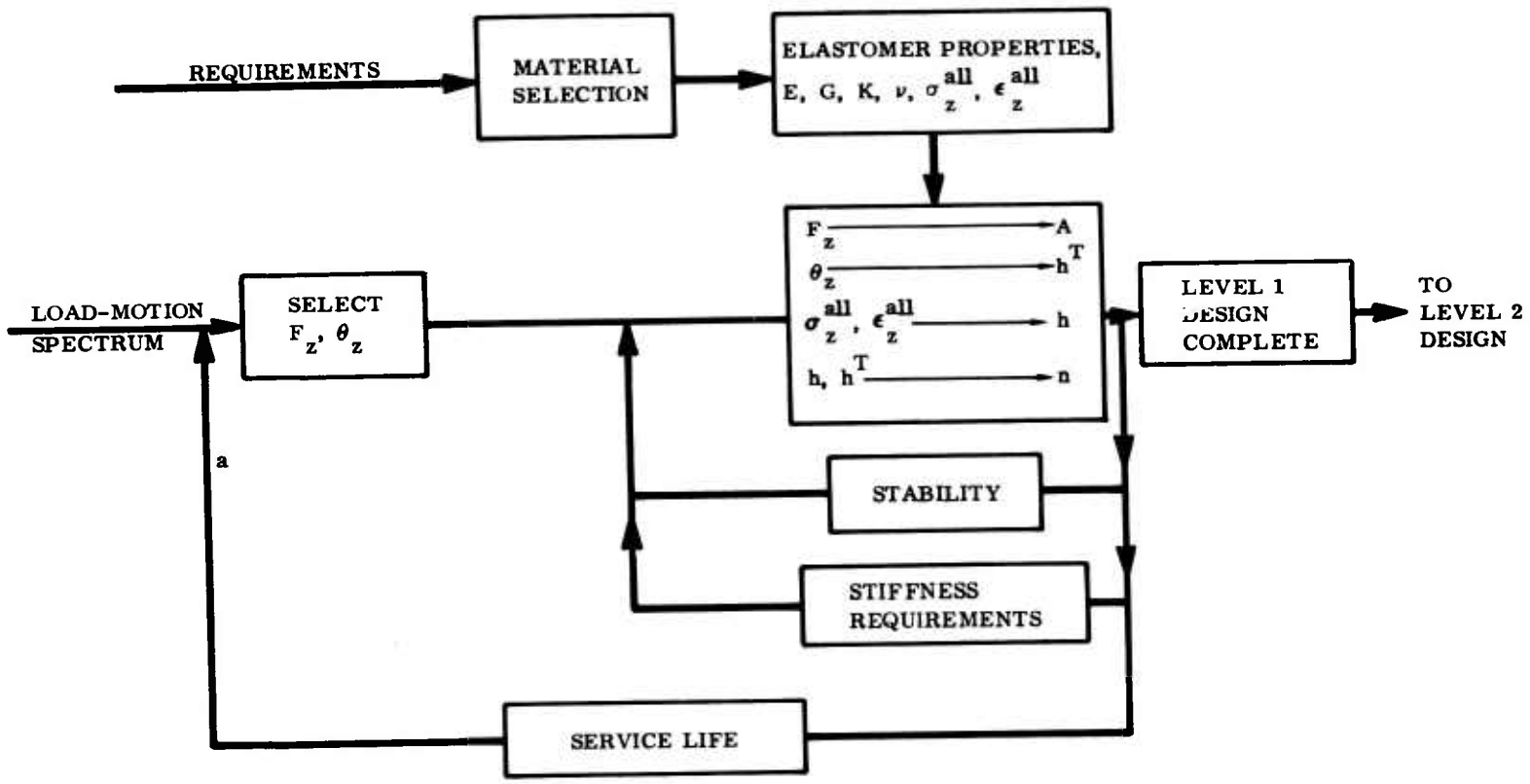

[a] EACH ITERATION REQUIRES EVALUATION OF DESIGN CONDITIONS (F_z, θ_z, ϵ_z^{all}) AND MATERIAL SELECTION

Figure 4-1. Level 1 design procedure flow for Type I bearings.

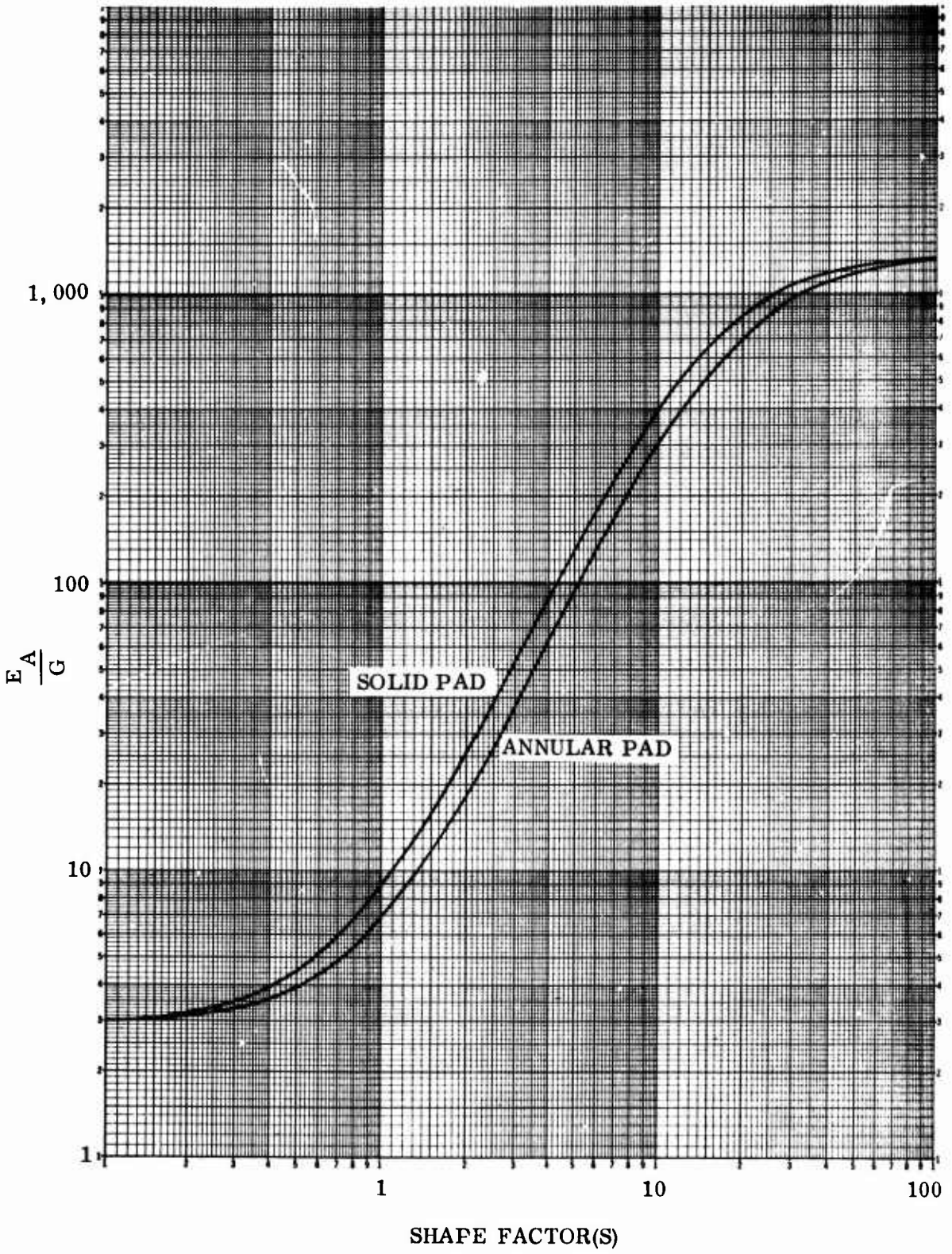

Figure 4-2. Apparent modulus versus shape factor for TR-3012 elastomer.

in the shape factor range of 2 to 15 for initial design purposes, as this will yield a reasonably sized bearing. A σ_z^{all} value of 5,000 psi is generally found to yield a shape factor in this range for typical bearing loads.

4. Assuming that $\sigma_z^{all} = \sigma_z^{ave}$, Equation 4-8 can be used to determine the cross-sectional area (A) and then the outer radius (r_o) since the inner radius (r_i) will, in general, be specified.

5. From the fatigue failure surface (Figure 9-2), select an average axial strain (ϵ_z^{ave}) that will provide a life (N) that is adequate (i.e., 30×10^6 cycles). A recommended value for ϵ_z^{ave} is 15 percent. For the assumed values of ϵ_z^{ave} and N, the maximum allowable oscillatory shear stress ($\tau_{r\theta}^{all}$) in the bearing, 52 psi, can be found in Figure 9-2.

6. The total elastomer thickness (h^T) is determined by using Equation 4-17 for the total pitch angle (θ_z^T) selected in Step 2.

7. The shape factor (S) is obtained by substituting Equation 4-3 in Equation 4-6 or 4-7. Since the inner and outer radii are known from Step 4, the expression for S given in Equations 4-6 and 4-7 will yield the elastomer pad thickness (h).

8. Since h^T and h are known, the number of elastomer pads (n) in the bearing can be calculated from the relationship $nh = h^T$.

9. Select shim thickness (t) as recommended in subsection 4.3. All geometric parameters are now known.

10. The bearing can be checked for stability by using Equation 4-23 to determine the buckling load (F_z^c). If F_z^c is greater than the axial load (F_z), then no stability problems exist. If F_z^c is less than F_z, the bearing has to be made more stable. This can be achieved by either increasing the outer radius (r_o) of the bearing or decreasing the total rubber thickness (h^T). Assuming that r_o is increased, then Equation 4-17 shows that h^T also has to be increased to hold the maximum allowable shear stress level constant at the value chosen in Step 5. Therefore, even though the ratio $\frac{r_o}{h^T}$ cannot be changed, F_z^c will still increase because examination of Equation 4-23 shows that the buckling load is directly proportional to $(r_o)^2$ and $(\frac{r_o}{h^T})^2$.

If r_o cannot be increased, then h^T has to be decreased. Equation 4-17 then will indicate that either the pitch angle (θ_z^T) requirement cannot be met--and has to be decreased--or the allowable shear stress level has to be increased--which would mean a shorter life for the bearing. The only approach to keeping the allowable shear stress level constant without affecting life is to decrease the average axial strain value (Figure 9-2).

It should be noted here that stability is generally not a problem in an annular bearing because the hub of the helicopter blade passes through it and prevents excessive lateral deformation.

11. Any stiffness requirement for the bearing can now be checked by using the necessary stiffness equations. For example, if the total torsional stiffness (K_θ^T) is specified, Equation 4-15 can be used to calculate K_θ^T for the geometry determined above. Either r_o or h^T has to be changed if the stiffness requirement is not met. For a bearing with a specified torsional stiffness, it is advisable to solve Equations 4-15 and 4-17 simultaneously for the two unknowns r_o and h^T instead of assuming σ_z^{all} as in Step 3 to determine r_o. If the total axial stiffness is specified, Equations 4-2 and 4-17 can be solved for r_o and h^T for a selected value of ϵ_z^{ave}.

12. For the given load-motion spectrum, check for adequacy of service life by using Equation 9-8 as discussed in Section 9.0. If the service life requirement of 30×10^6 cycles is not met, the ϵ_z^{ave} and/or $\tau_{r\theta}^{all}$ will need to be decreased and the design procedure repeated.

4.1.2 Level 2 Design

A flow chart of the Level 2 design procedure is shown in Figure 4-3. The iteration loops in the Level 1 design procedure will enable the designer to become familiar with the different parameters that affect bearing design. In Level 2 design, he can use the parametric curves that are presented in this subsection to refine the basic geometry generated by the Level 1 procedure. The parametric data is useful for indicating trends such as the effect of a geometric parameter on a particular design requirement. For example, Figure 4-4 shows the effect of varying $\frac{r_i}{r_o}$ and $\frac{r_o}{h}$ on the torsional stiffness (K_{θ_z}). Therefore, if K_{θ_z} is specified, several selections of $\frac{r_i}{r_o}$ and $\frac{r_o}{h}$ can be rapidly compared and the best values selected. These selections can be checked for stability using Figure 4-5, which shows the buckling load as a function of $\frac{r_o}{h^T}$ and $\frac{r_i}{r_o}$.

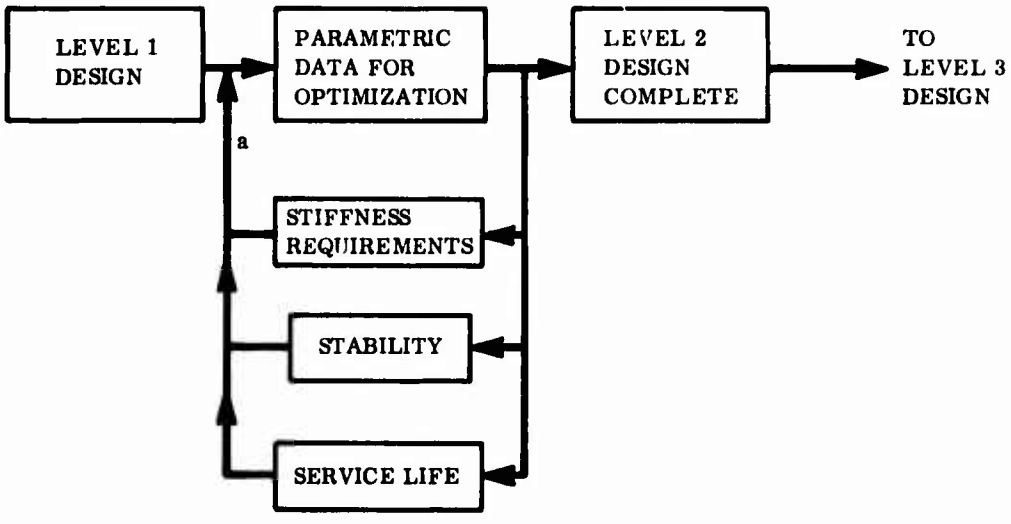

[a] EACH ITERATION REQUIRES EVALUATION OF DESIGN CONDITIONS (F_z, θ_z, ϵ_z^{all}) AND MATERIAL SELECTION

Figure 4-3. Level 2 design procedure flow for Type I bearings.

In Level 1 design, the allowable axial compressive stress (σ_z^{all}) and axial strain (ϵ_z^{all}) were selected in the initial stage of the design procedure. This determined the apparent modulus (E_A) given by Equation 4-3. However, for the same allowable axial strain, the allowable stress level can be significantly increased by choosing a slightly higher shape factor. This is because E_A and, hence, σ_z^{all} are proportional to S^2. Therefore, the axial stiffness is also increased by the same proportionality. In fact, in bearing design, the control of axial stiffness is achieved primarily by trading off shape factor against the compressive modulus.

4.1.3 Level 3 Design

The flow chart of the Level 3 design procedure is shown in Figure 4-6. The complete geometric description of the bearing is known after the completion of Level 2 design. The finite-element program will enable the designer to obtain a clear understanding of the structural behavior of the bearing. The versatility of the finite-element program is described in Section 7.0; a sample output of the computer program is given in Volume III. The computer output shows that the

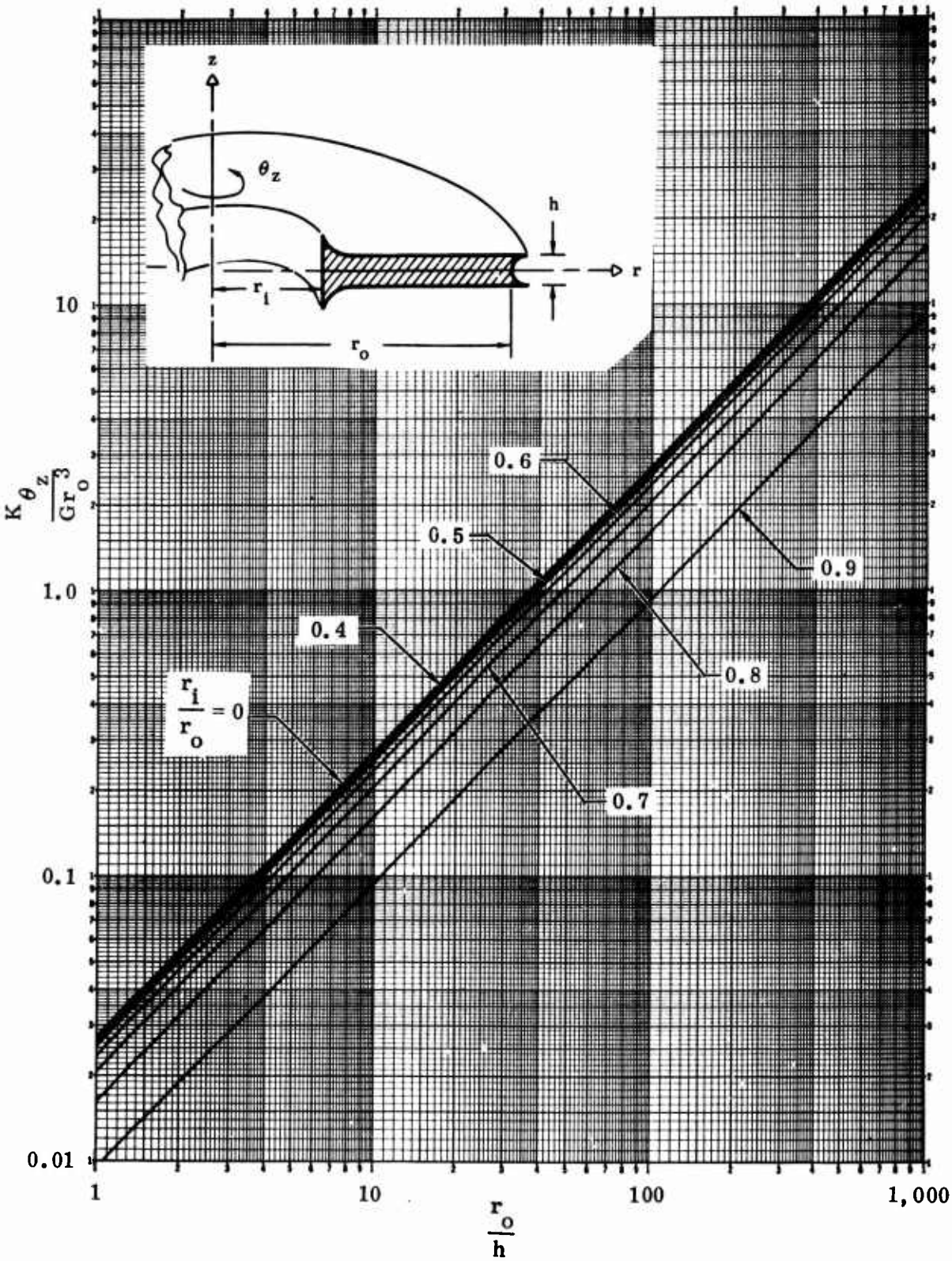

Figure 4-4. Torsional stiffness design curves for a TR-3012 Type I elastomer pad.

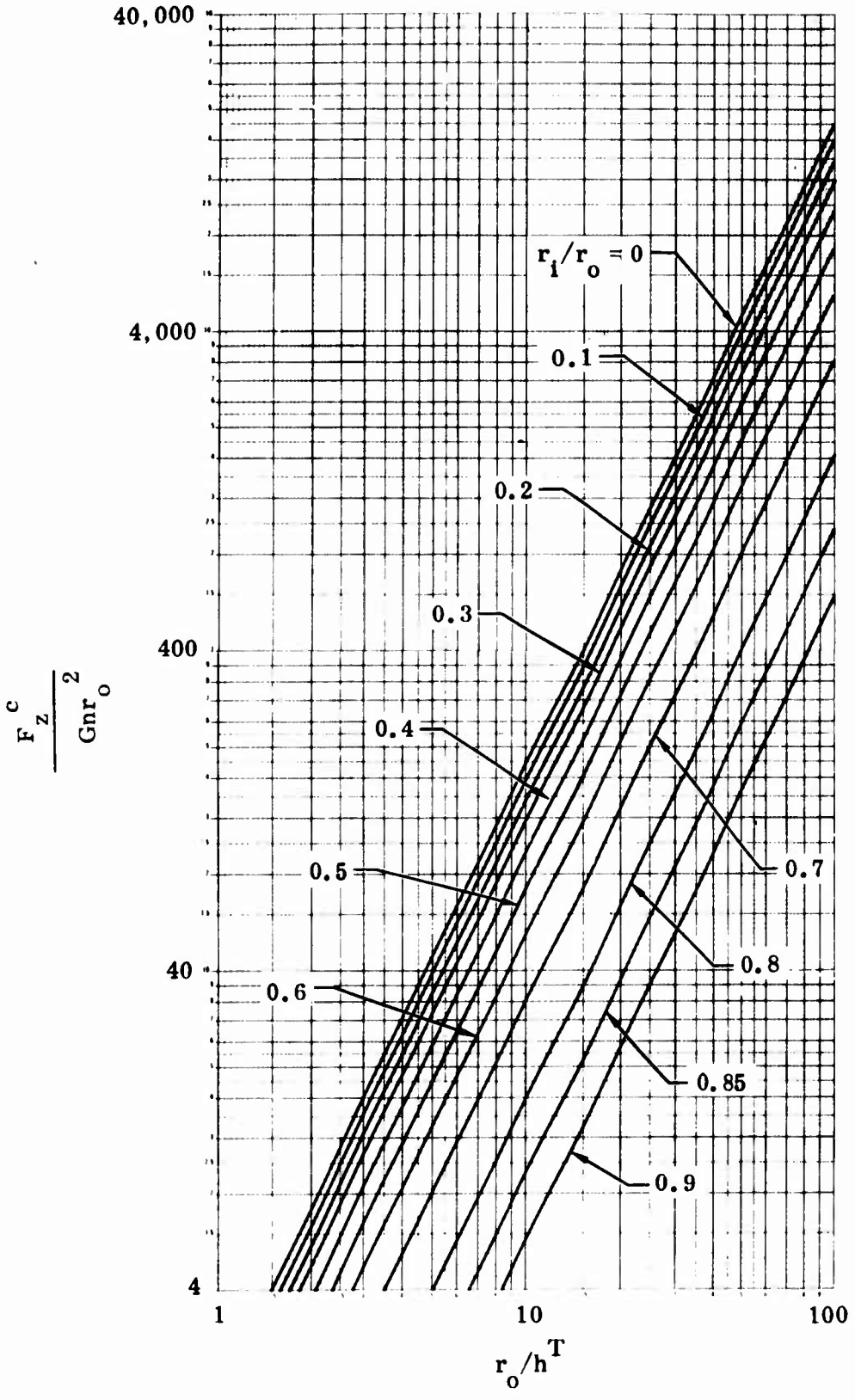

Figure 4-5. Stability design curve for Type I bearing.

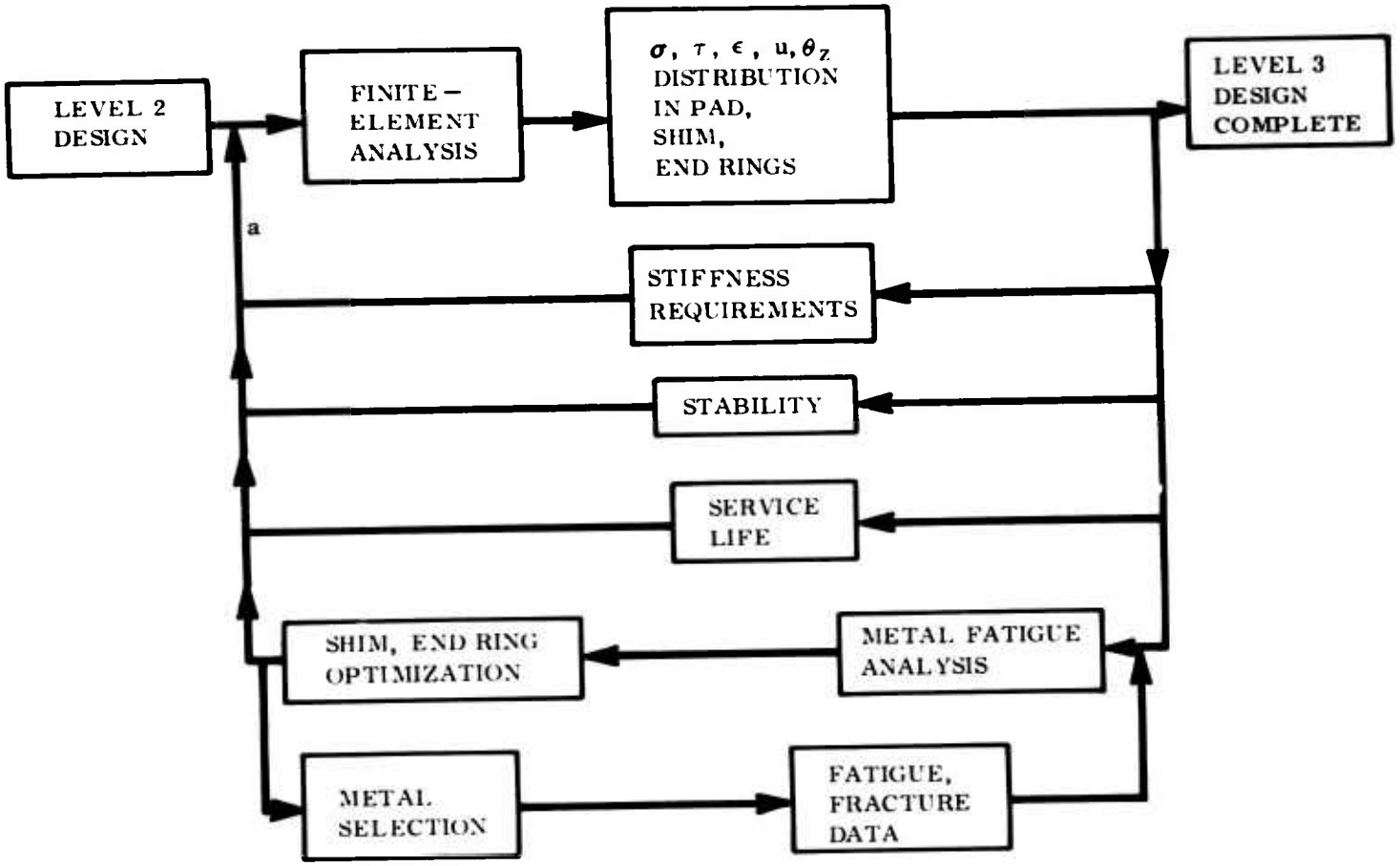

[a]EACH ITERATION REQUIRES EVALUATION OF DESIGN CONDITIONS (F_z, θ_z, ϵ_z^{all}) AND MATERIAL SELECTION

Figure 4-6. Level 3 design procedure flow for Type I bearings.

stress, strain, and displacement distributions can be obtained for the entire bearing for various applied loads. A careful evaluation of the computer output will reveal any problem areas in the bearing. The problem areas of major concern are:

1. Shim stresses.
2. Tensile stress in the elastomer due to thermal cool-down.
3. Tensile stresses in the elastomer due to vectoring (bending) loads.
4. Shear stresses that can cause bearing failure.

The above problem areas are discussed in detail in Section 9.0. Other problem areas such as stress singularities and methods to avoid them by providing radii at the edges of the elastomer pads and/or shims are also discussed. Shim material and design are discussed in subsection 3.2.

4.2 EQUATIONS

The equations required for a preliminary design are presented in this subsection. They are the final results of mathematical theories that can be found in the literature (References 3-18 and 4-1 through 4-6).

In preliminary design, information concerning the deflection of an elastomer pad under load (i.e., stiffness) is generally required. The stiffness equations given in this subsection apply to a single, Type I pad only. Total stiffness of the bearing is the reciprocal of the sum of the reciprocals of a single pad stiffness, i.e.:

$$\frac{1}{K_{Total}} = \frac{1}{K_1} + \frac{1}{K_2} + \frac{1}{K_3} + \cdots + \frac{1}{K_n} \qquad (4\text{-}1)$$

In torsion and transverse (shear) deformation modes, the shims do not affect the stiffness. Consequently, the single pad relationships can be used by substituting total height of rubber (h^T) in the stiffness equation for the single pad thickness.

There are five possible deformation modes for a Type I bearing: axial, radial, torsional, bending, and stability.

4.2.1 Axial Mode

The equations for the axial mode of deformation are:

1. Axial Stiffness (K_z)

$$K_z = \frac{F_z}{u_z^{ave}} = \frac{E_A A}{h} = \frac{E_A \pi (r_o^2 - r_i^2)}{h} = \frac{F_z}{\epsilon_z^{ave} h} \tag{4-2}$$

where E_A is the apparent compression modulus as given by

$$E_A = \frac{\sigma_z^{ave}}{\epsilon_z^{ave}} \tag{4-3}$$

E_A is related to E, G, k, and S by the relationship for solid pads ($r_i = o$):

$$\frac{1}{E_A} = \frac{1}{E+6GS^2} + \frac{1.25}{k} \tag{4-4}$$

and by the relationship for annular pads ($r_i = o$):

$$\frac{1}{E_A} = \frac{1}{E+4GS^2} + \frac{1.25}{k} \tag{4-5}$$

Equations (4-4) and (4-5) are presented in Figure 4-2 for TR-3012 rubber. For shape factors of 0.3 to 10, the above equations can be approximated by the relationship for solid pads $\left(S = \frac{r_o}{2h}\right)$:

$$E_A = E\,(1+2S^2) \tag{4-6}$$

and by the relationship for annular pads $\left(S = \frac{r_o - r_i}{2h}\right)$:

$$E_A = E\,(1+\tfrac{4}{3}S^2) \tag{4-7}$$

2. Average Axial Stress $\left(\sigma_z^{ave}\right)$:

$$\sigma_z^{ave} = \frac{F_z}{A} = \frac{F_z}{\pi(r_o^2 - r_i^2)} \tag{4-8}$$

3. Average Axial Deflection $\left(u_z^{ave}\right)$:

$$u_z^{ave} = \frac{F_z}{K_z} = \epsilon_z^{ave} h \tag{4-9}$$

4. Average Axial Strain $\left(\epsilon_z^{ave}\right)$:

$$\epsilon_z^{ave} = \frac{u_z^{ave}}{h} \tag{4-10}$$

4.2.2 Radial (Shear, Transverse, and Lateral) Mode

The equations for the radial mode of deformation are:

1. Stiffness (K_r):

$$K_r = \frac{F_r}{u_r^{max}} = \frac{GA}{h} = \frac{G\pi(r_o^2 - r_i^2)}{h} \tag{4-11}$$

2. Shear Stress (τ_{rz}):

$$\tau_{rz} = \frac{F_r}{A} = \frac{F_r}{\pi(r_o^2 - r_i^2)} \tag{4-12}$$

3. Shear Strain (γ_{rz}):

$$\gamma_{rz} = \frac{u_r}{h} \tag{4-13}$$

4. Maximum Deflection $\left(u_r^{max}\right)$:

$$u_r^{max} = \frac{F_r}{K_r} = \frac{F_r h}{G\pi(r_o^2 - r_i^2)} \tag{4-14}$$

4.2.3 Torsional Mode

The equations for the torsional mode of deformation are:

1. Stiffness $\left(K_{\theta_z}\right)$:

$$K_{\theta_z} = \frac{M_z}{\theta_z} = \frac{JG}{h} = \frac{\pi G}{2h}\left(r_o^4 - r_i^4\right) \tag{4-15}$$

The above equation is presented in Figure 4-4.

2. Shear Stress $(\tau_{r\theta})$:

$$\tau_{r\theta} = \frac{G\theta_z r}{h} \tag{4-16}$$

and

$$\tau_{r\theta}^{max} = \frac{G\theta_z r_o}{h} \tag{4-17}$$

3. Shear Strain $(\gamma_{r\theta})$:

$$\gamma_{r\theta} = \frac{\theta_z r}{h} \tag{4-18}$$

and

$$\gamma_{r\theta}^{max} = \frac{\theta_z r_o}{h} \tag{4-19}$$

4. Rotation (θ_z):

$$\theta_z = \frac{M_z}{K_{\theta_z}} = \frac{M_z h}{JG} \tag{4-20}$$

4.2.4 Bending (Vector) Mode

The equations for the bending mode of deformation are:

1. Stiffness $\left(K_{\theta_r}\right)$:

$$K_{\theta_r} = \frac{M_r}{\theta_r} = \frac{EI}{h}\left(1 + \frac{2}{3}S^2\right) \tag{4-21}$$

Equation 4-21 was derived in Reference 4-4 and is valid for solid elastomer pads only. However, for preliminary design purposes, it can also be used for annular pads. Figure 4-7 shows a dimensionless plot of bending stiffness (K_{θ_r}) versus shape factor (S) for different $\frac{r_i}{r_o}$ ratios. It was obtained by using the finite-element program and shows that the agreement between Equation 4-21 and the finite-element analysis is good for $\frac{r_i}{r_o} = 0$ for shape factors of less than 10. However, for other $\frac{r_i}{r_o}$ ratios, Equation 4-21 underpredicts the finite-element bending stiffness by about 15 percent.

2. Rotation (θ_r)

$$\theta_r = \frac{M_r}{K_{\theta_r}} \tag{4-22}$$

4.2.5 Stability Mode

For preliminary design purposes, critical buckling load (F_z^c) in a column of Type I pads can be determined by using the following relationship:

$$\frac{F_z^c}{Gn\, r_o^2} = \frac{\pi^2}{4\sqrt{2}} \left(\frac{r_o}{h^T}\right)^2 \left(1+\frac{r_i}{r_o}\right)\left(1-\frac{r_i}{r_o}\right)^2 \sqrt{1+\left(\frac{r_i}{r_o}\right)^2} \tag{4-23}$$

The above equation is valid for a Type I bearing with fixed ends and is presented in dimensionless form in Figure 4-5. Other end conditions are discussed in Section 8.0.

The procedure presented in Section 8.0 should be used to refine the predicted buckling load.

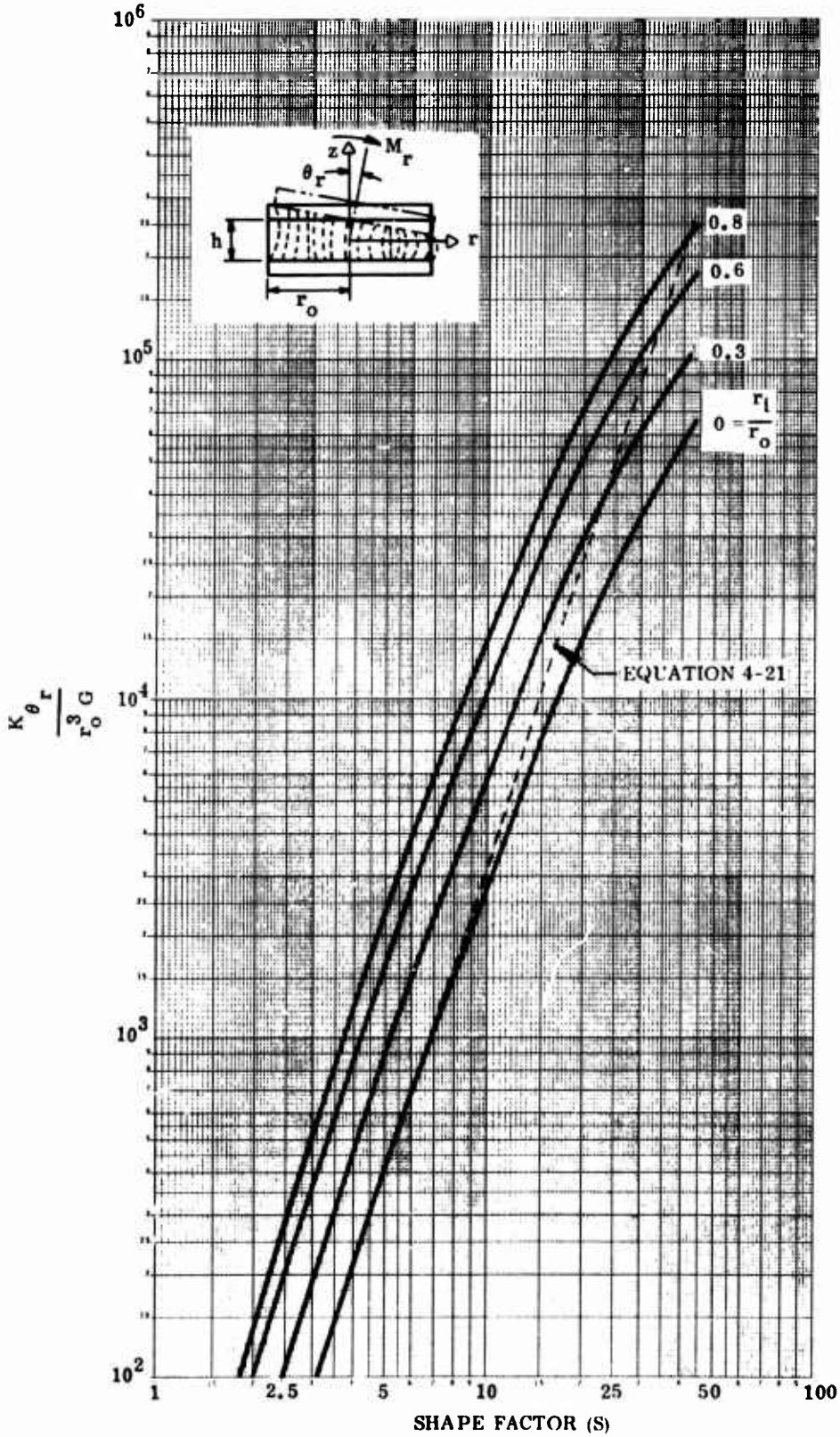

Figure 4-7. Bending stiffness versus shape factor for a TR-3012 Type I elastomer pad.

4.3 SHIM THICKNESS SELECTION

The thickness of the shims that are used in a Type I bearing are usually of the same order of magnitude as the elastomer pad. The thickness is generally governed by processing considerations. A very thin shim will not resist any bending and can cause premature buckling. A thick shim, on the other hand, will make the bearing heavier than necessary. A reliable rule-of-thumb is to make the shim thickness equal to the minimum elastomer pad thickness in the bearing. It is recommended that shim stresses be carefully evaluated during Level 3 design using the finite-element program.

5.0 TYPE II BEARING DESIGN

A Type II bearing consists of a cylindrical elastomeric annulus with rigid metal cylinders bonded to the inner and outer surfaces. Such a configuration allows the displacement of two rigid boundary cylinders relative to each other, in both axisymmetric and asymmetric modes. A typical bearing for helicopter application is made up of multiple elastomeric cylinders (pads) and metal shims as shown in Figure 1-2. This configuration has been used in teetering or feathering bearings as shown in Figure 2-1. The degeneration to one or a few pads is typical of dampers, one of which is shown in Figure 5-1.

Four principal loading modes are possible in the Type II bearing. These loading modes produce the following displacements when considering the outer cylinder fixed while the inner cylinder is displaced.

1. A rotation about its axis, referred to as torsional deflection as shown in Part A of Figure 5-2.
2. A translation in which each point moves parallel to the axis or axial deflection as shown in Part B of Figure 5-2.
3. A translation in which each point moves through an equal distance perpendicular to a plane containing the axis or radial deflection as shown in Part C of Figure 5-2.
4. A rotation of the axis in a radial plane about a point on itself midway between the plane ends of the elastic material or bending deflection as shown in Part D of Figure 5-2.

In typical helicopter applications, a Type II bearing has to react asymmetric radial loads (F_r) and provide torsional rotation (θ_z). Generally, F_r, θ_z, and the torsional stiffness $\left(K_{\theta_z}\right)$ are specified.

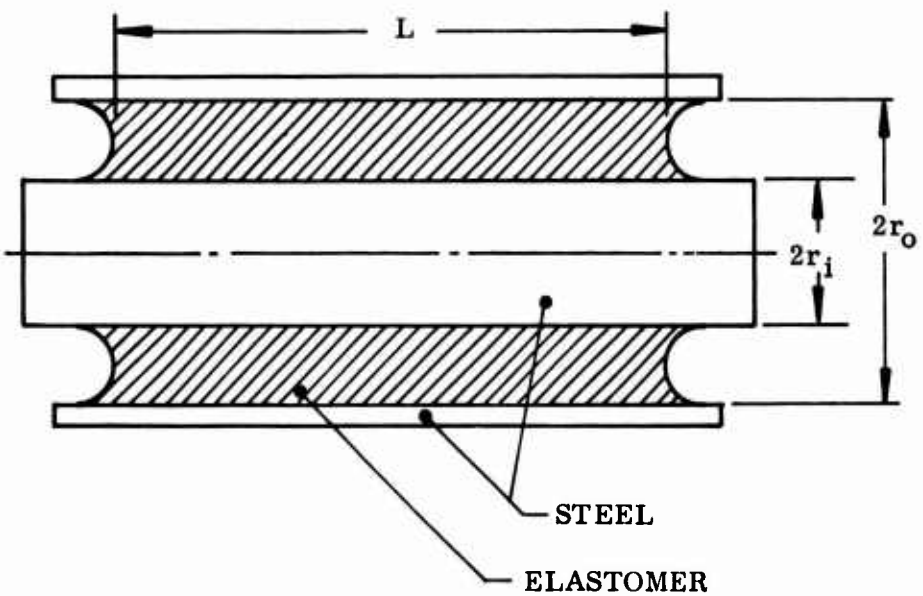

Figure 5-1. Type II elastomeric bearing damper.

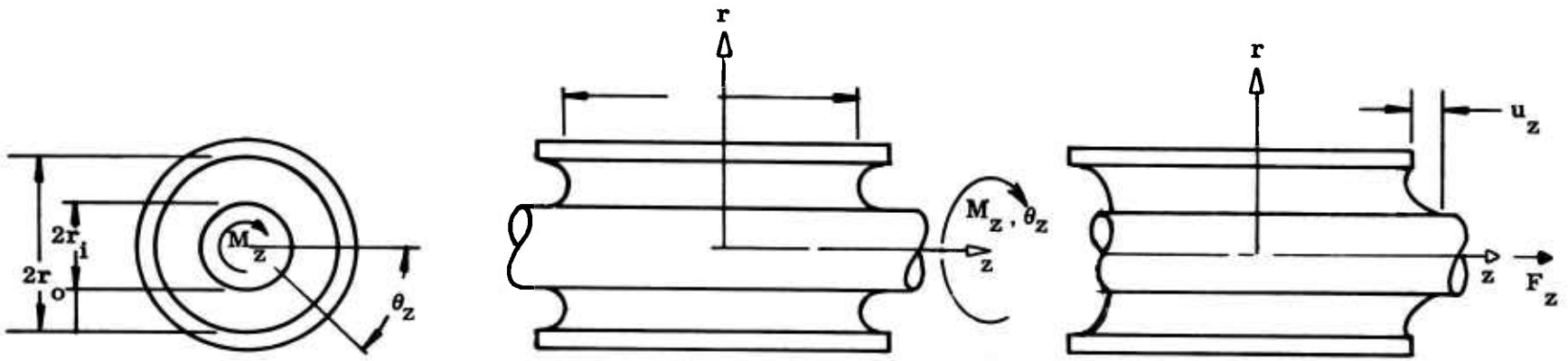

A. TORSIONAL

B. AXIAL

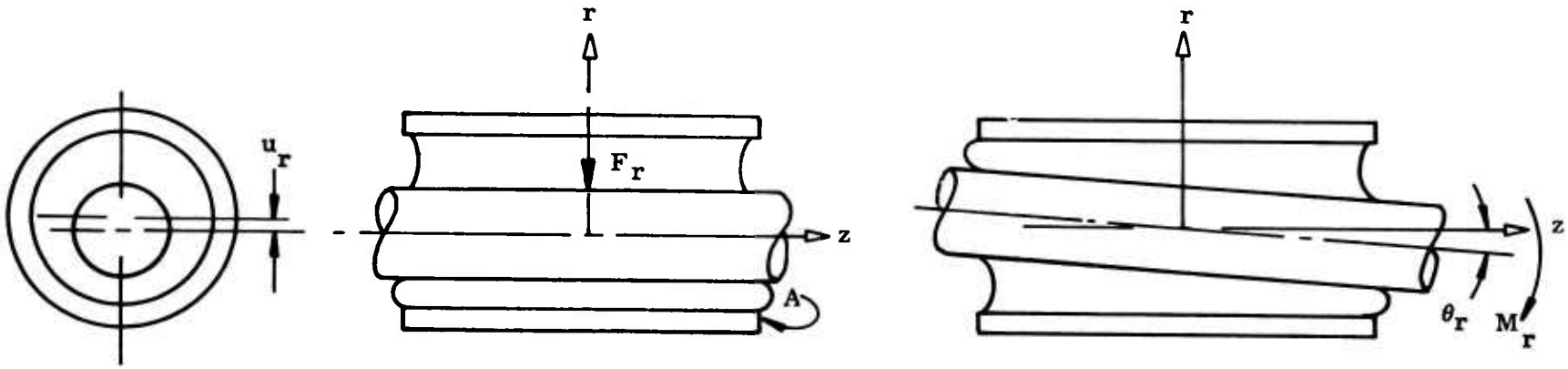

C. RADIAL

D. BENDING

Figure 5-2. Type II bearing loading modes.

5.1 PROCEDURE

The design procedure is similar to that for a Type I bearing and is carried out in three levels.

5.1.1 Level 1 Design

A flow chart for the Level 1 design procedure is given in Figure 5-3. The procedure is as follows:

1. Select elastomer formulation and develop material properties E, G, k, and ν. A shear stress failure surface of the type discussed in Section 9.0 is also required. Currently, little work has been accomplished in evaluating service life of a Type II bearing. Since no direct Type II service life data is available, it is recommended that the shear stress failure surface (Figure 9-4) be used for this preliminary design.
2. Define initial values for radial load (F_r), torsional displacement (θ_z), and torsional moment (M_z) in the same manner as discussed in the design of Type I bearings from the load-motion spectrum table.
3. Select an allowable compressive stress level (σ_r^{all}) = 5,000 psi as discussed in the design of Type I bearings. Since the radial load is reacted by the projected area of the bearing in the direction of the load, Equation 5-9 can be used to determine an equation for the product ($r_1 L$) assuming that $\sigma_r^{all} = \sigma_r^{ave}$.
4. From shear stress fatigue failure surface (Figure 9-4), select a curve to determine values for τ^{max} (which will be due to the torsional rotation), fatigue life (N),

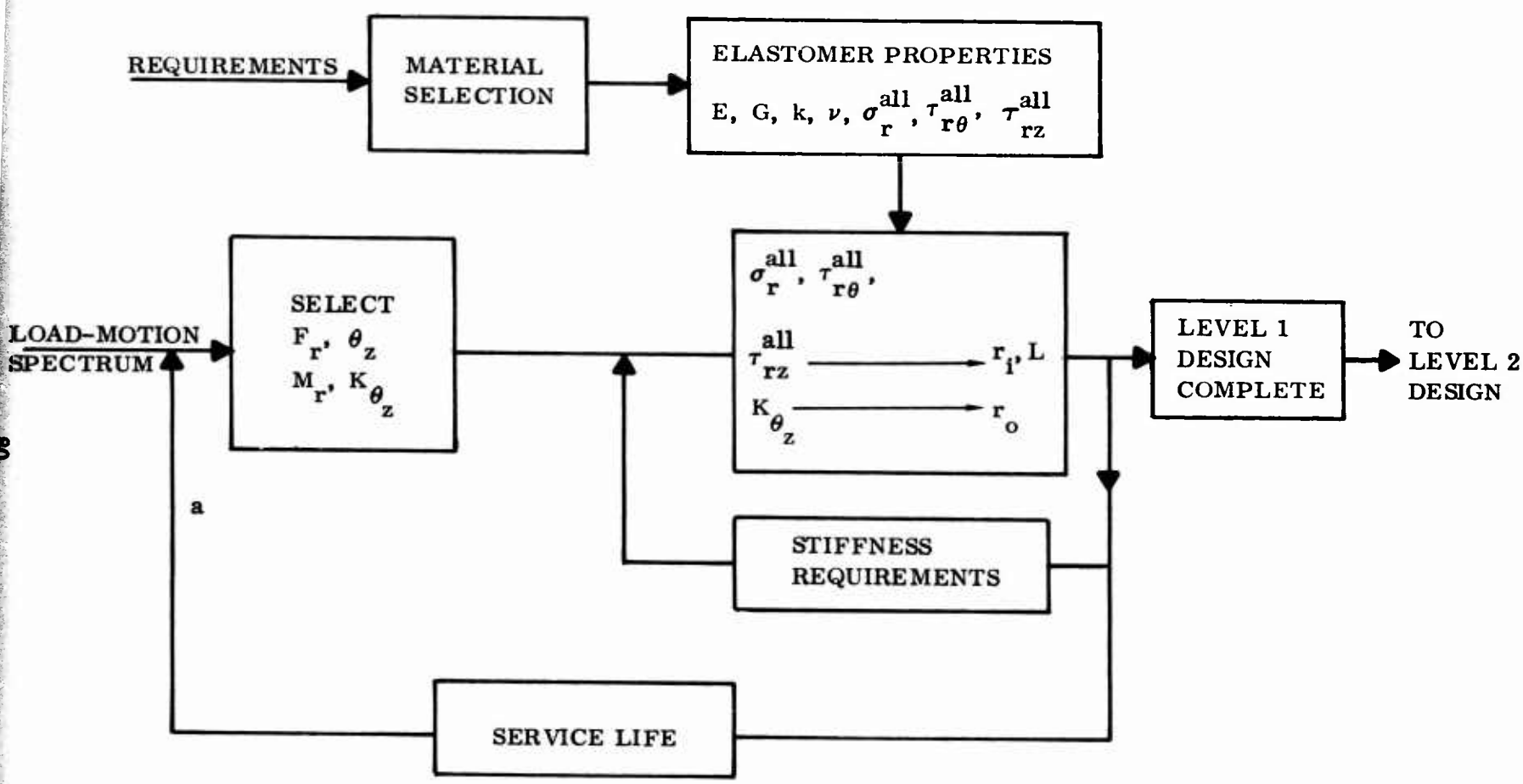

[a] EACH ITERATION REQUIRES EVALUATION OF DESIGN CONDITIONS (F_r, θ_z) AND MATERIAL SELECTION

Figure 5-3. Level 1 design procedure flow for Type II bearings.

and τ^{static}. For preliminary design purposes, curve number 2 is recommended because the values given by it do not differ significantly from curve number 1. Also, curve number 1 is for zero τ^{static} and bearings normally have a certain static load imposed on them. From curve number 2, values for τ^{max} and τ^{static} can be read off for a desired fatigue life.

5. In a Type II bearing, the maximum shear stress due to torsion will occur at the inner surface of the innermost pad (see Equation 5-5). Therefore, using the τ^{max} selected in Step 4 in Equation 5-5, an equation for $r_i^2 L$ can be obtained. This equation can be solved simultaneously with the equation determined in Step 3 to solve for the two unknowns r_i and L.
6. Since $\tau^{static} = \tau_{rz}$, the shear stress due to the radial load, Equation 5-8 can be used to determine the outside radius (r_o). All geometric parameters of the innermost pad are now known.
7. In this preliminary design, the bearing will be designed for constant torsional stiffness. From the geometric parameters of the innermost elastomer pad, its torsional stiffness can be calculated. Since the total torsional stiffness of the bearings is specified, the number of pads (n) can be determined by the formula: n = torsional stiffness of innermost pad/ torsional stiffness for entire bearing.
8. The inner radii for the next outer pad is determined by the shim thickness. Shim design is an area where more work is needed, and no equations exist for selecting its thickness. It is recommended that

the shim thickness be selected to be equal to the thickness of the innermost pad (r_o-r_i). Shim stresses, however, should be carefully evaluated using finite-element analysis in Level 3 design.

9. By selecting the shim thickness, the inner radius for the next elastomer pad is known. Equation 5-4 can be used to determine its outer radius, since each pad has the same torsional stiffness. The inner and outer radii of all pads can be determined in this manner.

10. The above procedure was for constant torsional stiffness in each pad. If the bearing has to be designed for constant service life in each pad, the procedure is slightly different. After the dimensions of the innermost pad are determined, Equation 5-5 can be plotted to show the variation of torsional shear stress with inner radius. Since this shear stress is proportional to ($1/r2$), the next outer pad will be subjected to a lower stress level. Therefore, using this new value for shear stress (τ^{max}), the fatigue surface curve can be used to determine τ^{static} for the same N value selected in Step 4. This τ^{static} will be higher than the value for the innermost pad. Equation 5-8 can then be used to determine the outer radius (r_o) for the second pad. As the dimensions for each pad are determined, the bearing is checked for overall torsional stiffness and pads are added until the specified stiffness requirement is met.

11. The constant torsional stiffness design approach yields a bearing in which the pad thickness is proportional

to r^3. An empirical approach for determining elastomeric pad thickness is to use a linear relationship between pad thickness and its radius. Since the innermost pad is subjected to the highest stress due to torsion and the outermost pad has the highest stress due to the radial load, this design approach has been found to yield a bearing that has the resultant peak stress uniformly distributed in the bearing.

12. Adequacy of service life should be evaluated using the procedure given in Section 9.0.

5.1.2 Level 2 Design

The Level 2 design procedure utilizes parametric data to refine the design developed in Level 1. The flow chart is given in Figure 5-4.

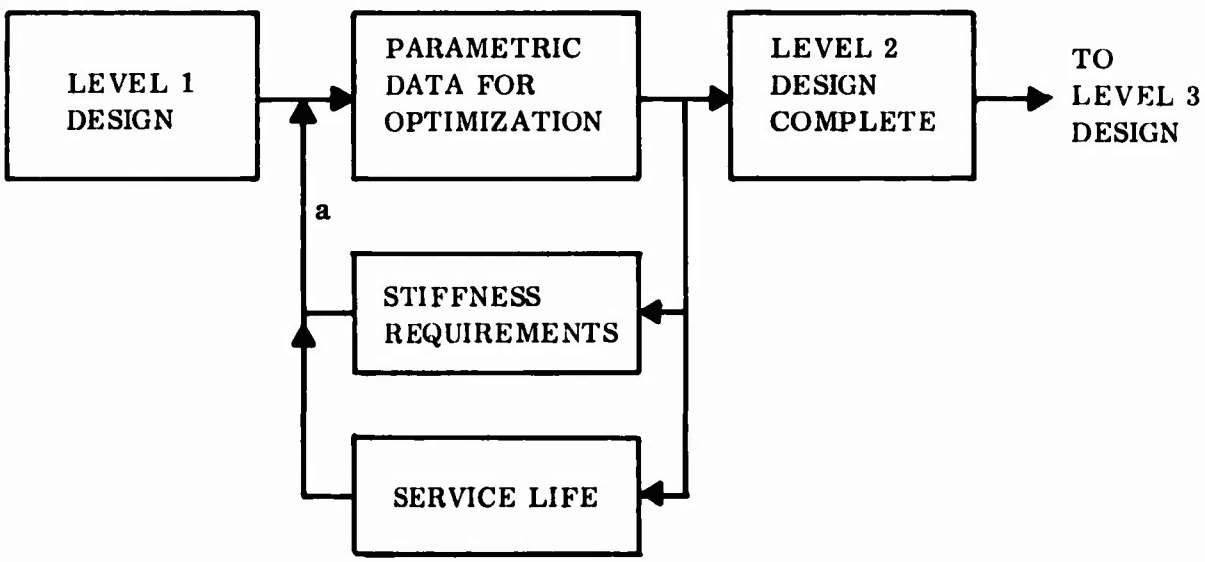

[a] EACH ITERATION REQUIRES EVALUATION OF DESIGN CONDITIONS (F_r, θ_z) AND MATERIAL SELECTION

Figure 5-4. Level 2 design procedure flow for Type II bearings.

Parametric design curves are presented for the loading conditions as follows:

1. Torsional in Figure 5-5.
2. Axial in Figures 5-6 and 5-7.
3. Radial in Figures 5-8 to 5-10.

The design curves are given in terms of dimensionless parameters in a range typical for helicopter applications. The curves were obtained by finite-element analysis for a single Type II elastomer pad having full radius ends (Figure 5-1).

Each loading type will now be considered individually for the application of the design curves.

5.1.2.1 Torsional Loads

Figure 5-5 shows the variation of torsional stiffness for a series of $\frac{r_i}{r_o}$ ratios.

Assume that the dimensions of the innermost pad have been calculated as discussed in the Level 1 design. Figure 5-5 can then be used to compare alternative values for the dimensions to meet stiffness requirement. Suppose, for example, that the bearing size is limited in the length direction and the value of L determined in Step 5 is excessive. Figure 5-5 and Equation (5-2) can be used to choose alternate values of L and determine its effects on stiffness and shear strain. If stiffness cannot be changed, then $\frac{r_i}{r_o}$ will have to be changed to meet this requirement. It may also be worth considering the use of a stiffer elastomer in the first few pads if this is necessary to meet the requirements.

5.1.2.2 Axial Loads

The trade-offs necessary to meet stiffness and strain requirements can be done in a manner similar to that used for torsional loading. The parametric curve for axial stiffness, enlarged in the $\frac{L}{r_o}$ range for typical helicopter applications, is presented in Figure 5-7. Type II bearings in helicopters generally have a $\frac{L}{r_o}$ ratio of two.

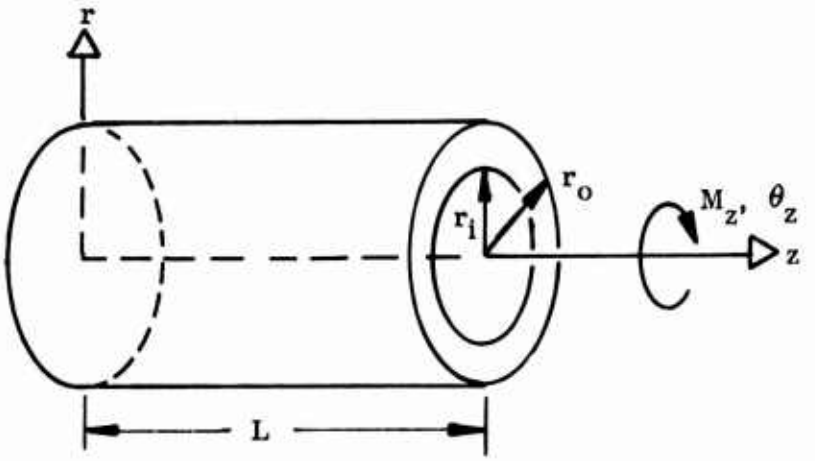

$$K_{\theta_z} = \frac{M_z}{\theta_z}; \text{ IN-LB/DEGREE}$$

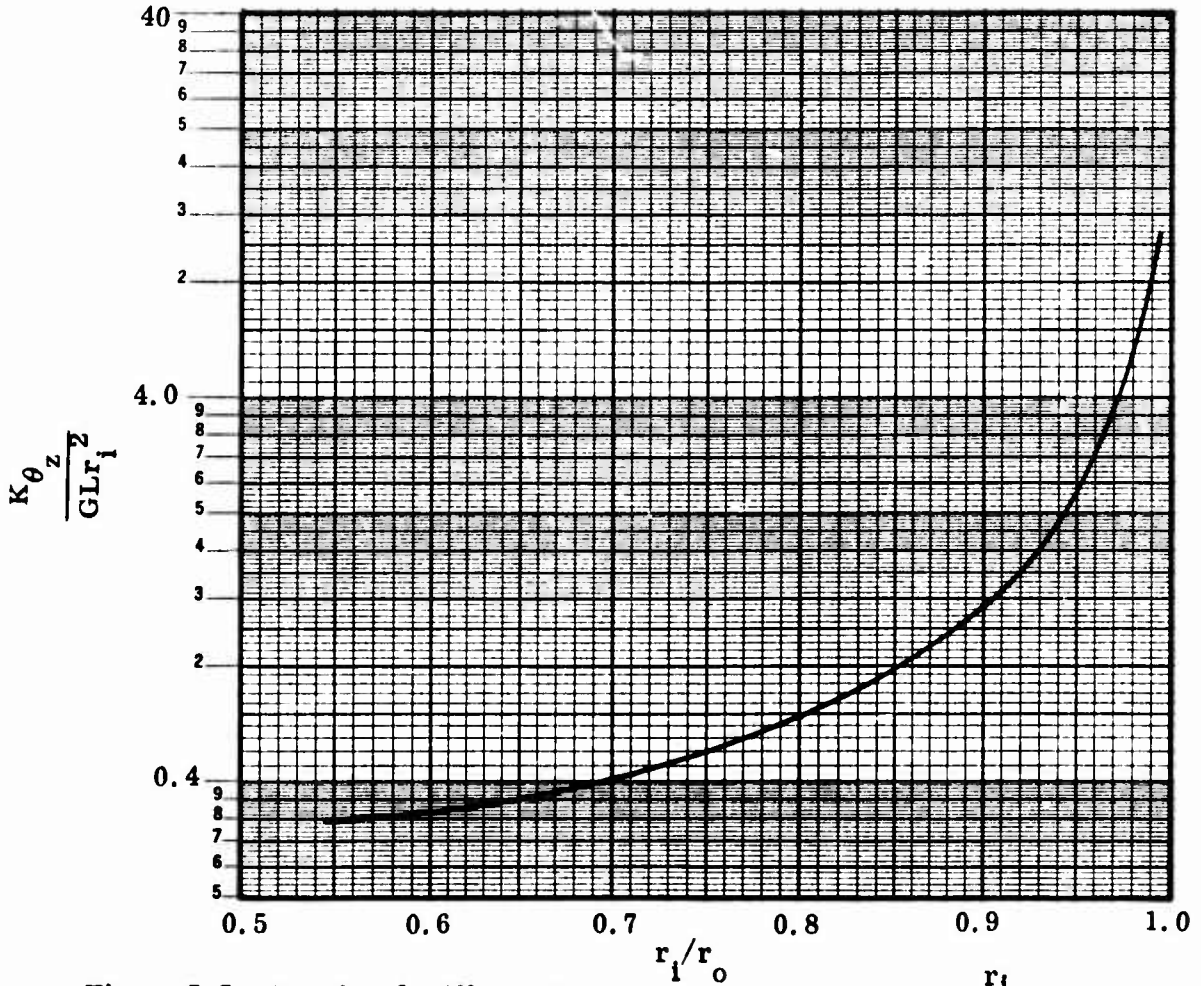

Figure 5-5. Torsional stiffness (K_{θ_z}) design curve for various $\frac{r_i}{r_o}$ ratios.

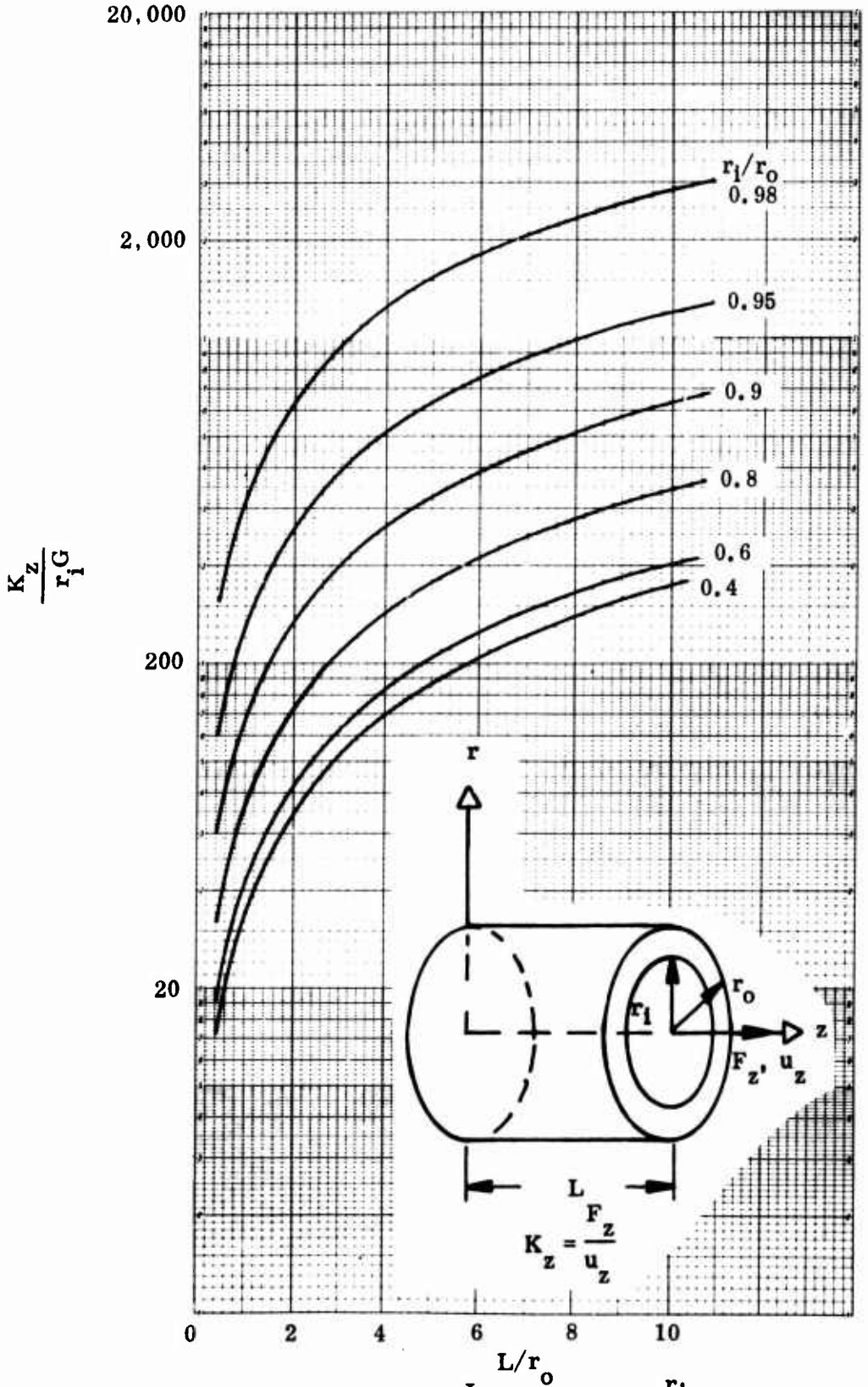

Figure 5-6. Axial stiffness (K_z) vs $\frac{L}{r_o}$ for various $\frac{r_i}{r_o}$ ratios.

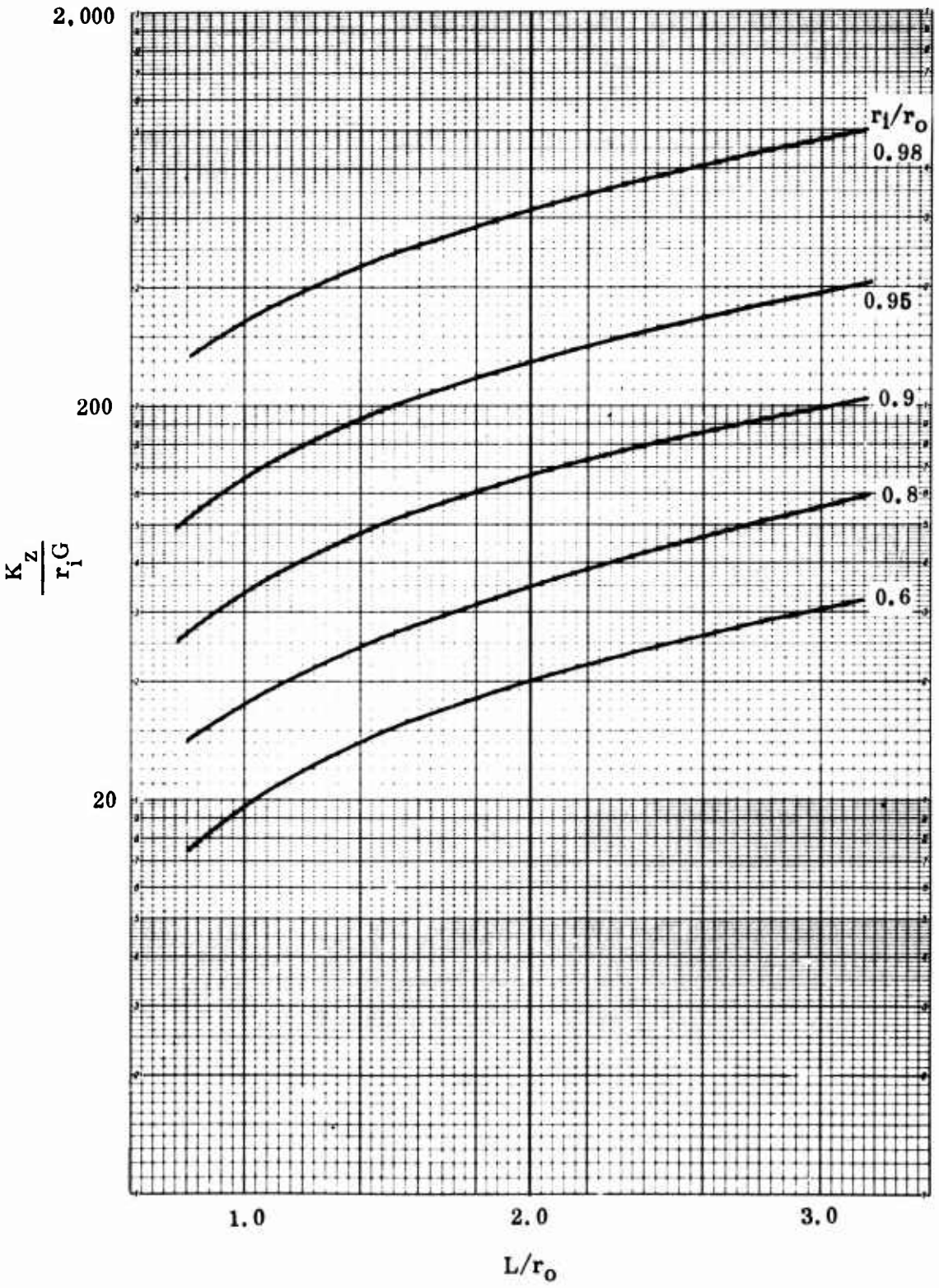

Figure 5-7. Axial stiffness design curves for helicopter applications.

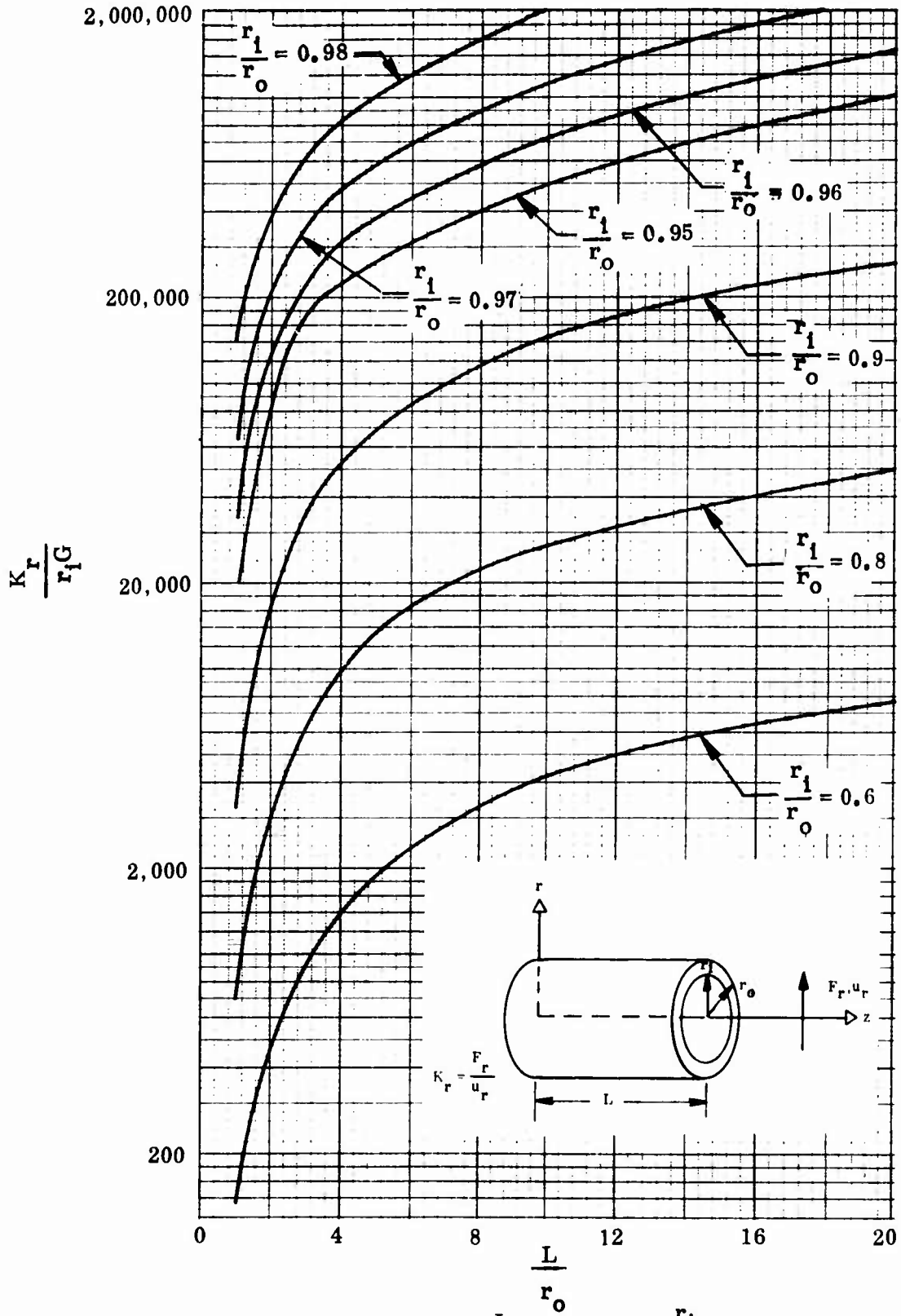

Figure 5-8 . Radial stiffness (K_r) vs $\frac{L}{r_o}$ for various $\frac{r_i}{r_o}$ ratios.

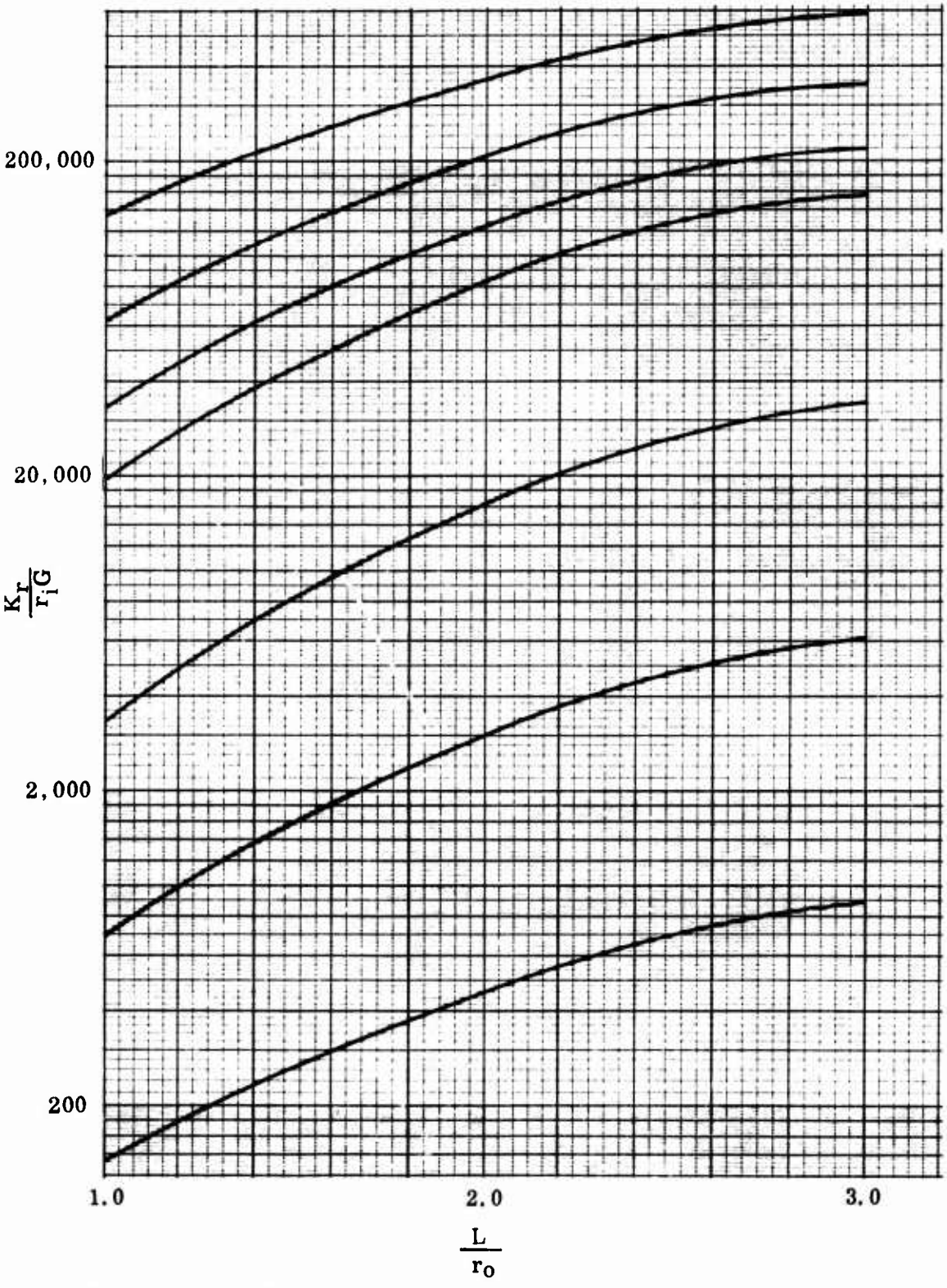

Figure 5-9. Radial stiffness design curves for helicopter applications.

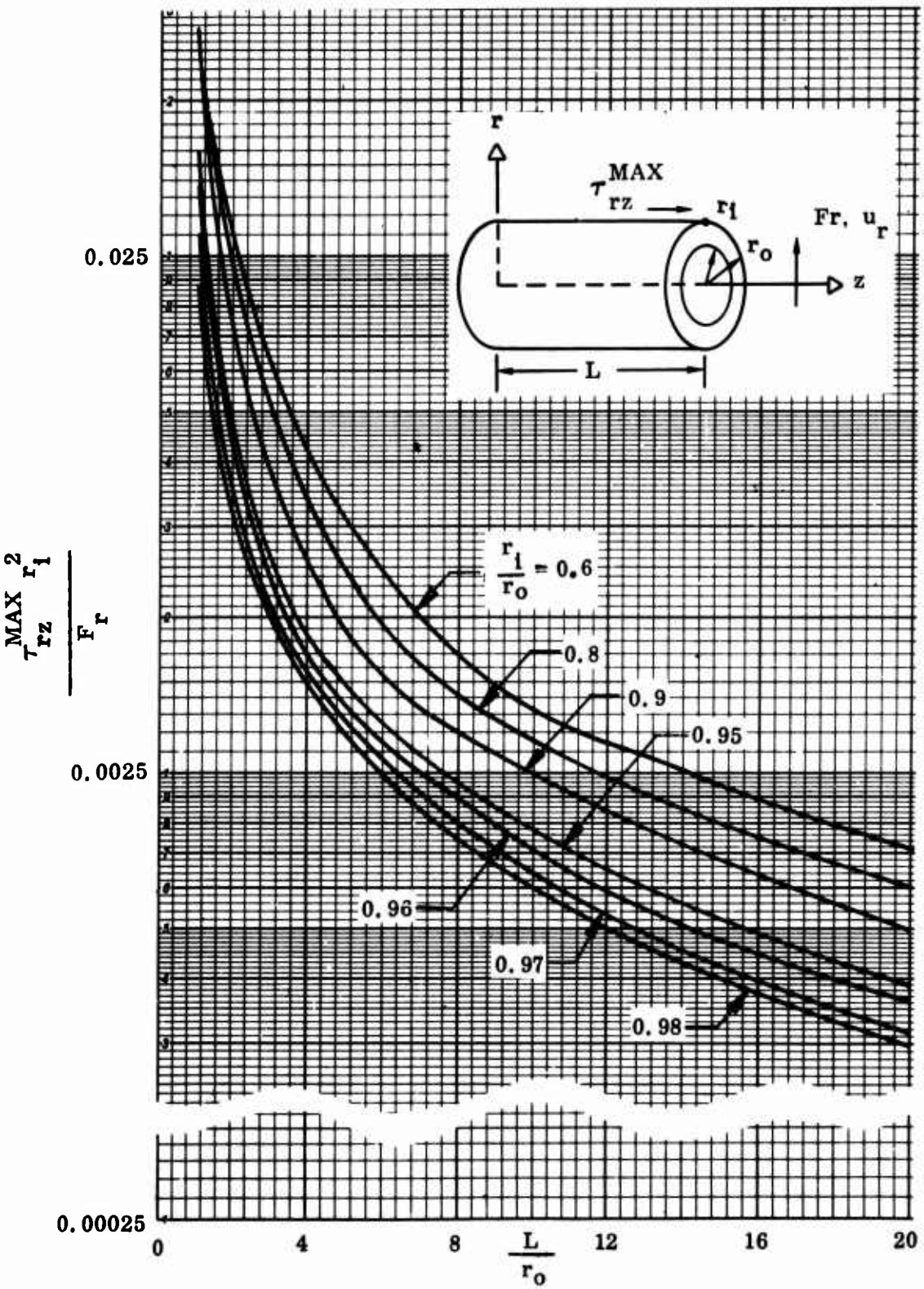

Figure 5-10. Maximum shear stress (τ_{rz}^{max}) due to radial load vs $\frac{L}{r_o}$ for various $\frac{r_i}{r_o}$ ratios.

5.1.2.3 Radial Loads

An enlarged radial stiffness curve in the $\frac{L}{r_o}$ range for helicopter applications is given in Figure 5-9. Other design curves are similar to those discussed for torsional loading.

Very limited experimental data for radial stiffness exist for thin pads. A comparison of experimentally measured stiffness with that predicted by the design curves indicates a factor of four difference, with the measured value being the lower. There are two reasons which might possibly account for this discrepancy:

1. When a Type II bearing is loaded radially, the compression half of the bearing is very stiff while the tensile half is very soft. Low tension stiffness could be due to cavitation or internal cracking of the elastomer (References 3-6, 4-4 and 5-1). It is quite possible that this behavior could account for as much as a factor of two.
2. The design curves were drawn for an elastomer with a Poisson's ratio of 0.4997. Figure 5-11 shows the effect of Poisson's ratio on radial stiffness for a thin elastomer pad with $\frac{r_i}{r_o}$ ratio of 0.98. Radial stiffness is very sensitive to changes in Poisson's ratio; this indicates that a knowledge of Poisson's ratio up to the fourth decimal place is necessary for accurate prediction. This would imply that the shape factor of the bearing is high and that bulk compression cannot be neglected.

Experimental results for the radial loading of Type II bearings are contained in Reference 5-1. They became available while this manual was being prepared; hence, the results could not be compared with theoretical predictions.

5.1.3 Level 3 Design

The flow chart for the Level 3 design procedure is given in Figure 5-12. It utilizes the finite-element computer program to determine stress, strain and displacement distributions in the entire bearing under various loading conditions. A careful evaluation of these distributions will determine if the design is satisfactory. The finite-element analysis will enable the designer to improve predictions on service life by using strain energy density as the fatigue failure criterion.

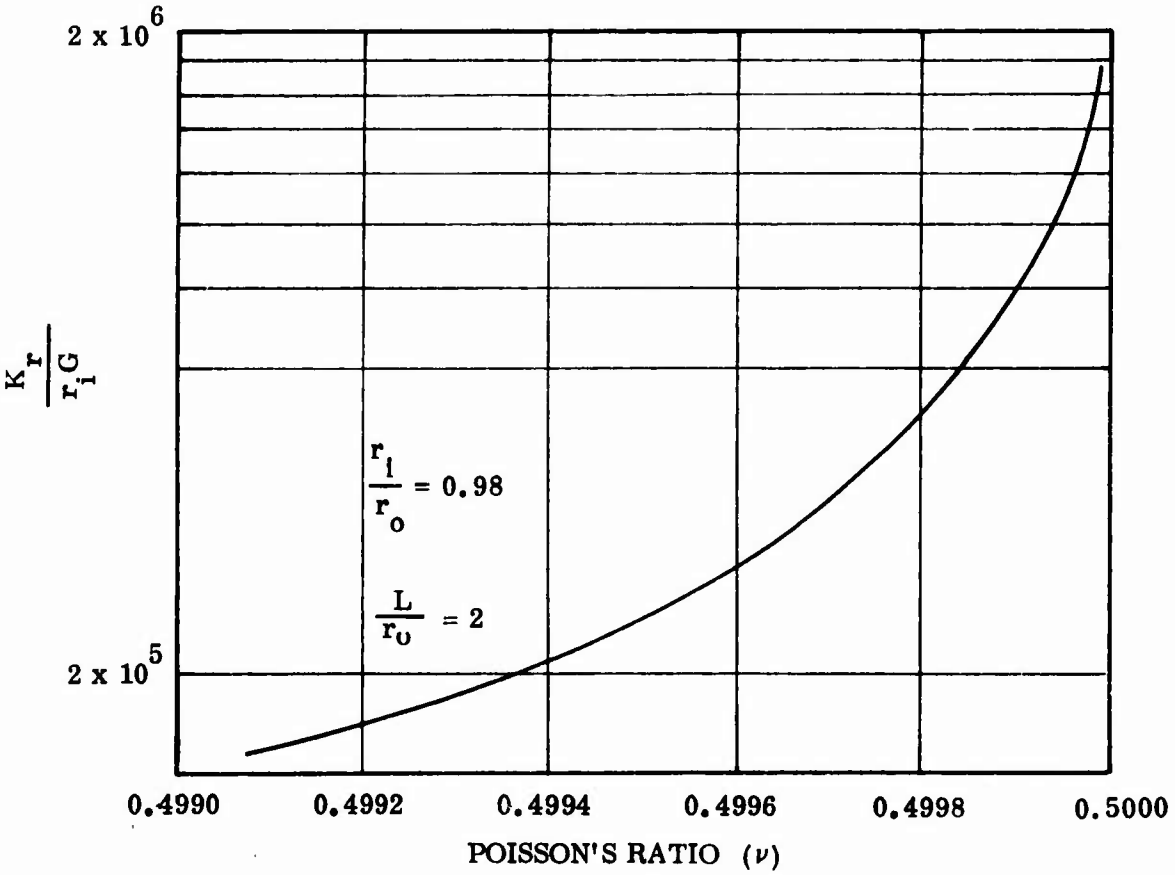

Figure 5-11. Effect of Poisson's ratio on radial stiffness.

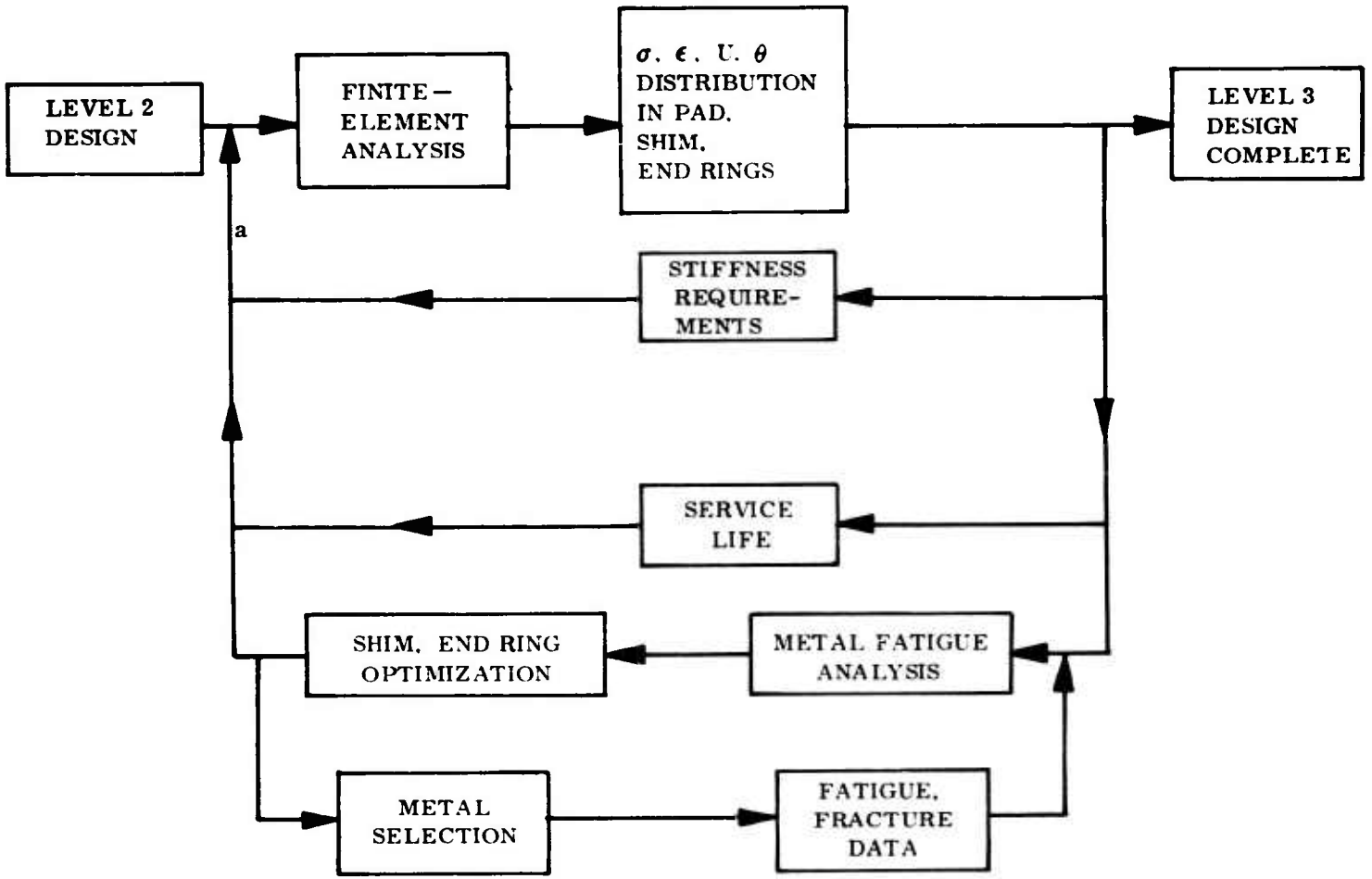

[a]EACH ITERATION REQUIRES EVALUATION OF DESIGN CONDITIONS (F_r, θ_z) AND MATERIAL SELECTION

Figure 5-12. Level 3 design procedure flow for Type II bearings.

5.2 EQUATIONS

The preliminary design equations for a single elastomer pad in a Type II bearing are given below for the axial, torsional, and radial loading modes. Analysis of the bending mode is difficult and closed-form equations are not available.

5.2.1 Axial Mode

The equations for the axial mode of deformation are:

1. Stiffness (K_z):

$$K_z = \frac{F_z}{u_z} = \frac{2.73\ GL}{\mathrm{Log}_{10}\left(\frac{r_o}{r_i}\right)} \tag{5-1}$$

2. Shear Stress (τ_{rz}):

$$\tau_{rz} = \frac{F_z}{2\pi rL} \qquad \text{(Note: Shear stress is maximum at } r = r_i\text{)} \tag{5-2}$$

3. Shear Strain (γ_{rz}):

$$\gamma_{rz} = \frac{\tau_{rz}}{G} \tag{5-3}$$

5.2.2 Torsional Mode

The equations for the torsional mode of deformation are:

1. Stiffness (K_{θ_z}):

$$K_{\theta_z} = \frac{4\pi GL}{\left(\frac{1}{r_i}\right)^2 - \left(\frac{1}{r_o}\right)^2} \tag{5-4}$$

2. Shear Stress ($\tau_{r\theta}$)

$$\tau_{r\theta} = \frac{M_z}{2\pi r^2 L} \qquad \text{(Note: Shear stress is maximum at } r = r_i\text{)} \tag{5-5}$$

3. Shear Strain ($\gamma_{r\theta}$) :

$$\gamma_{r\theta} = \frac{\tau_{r\theta}}{G} \tag{5-6}$$

5.2.3 Radial Mode

The equations for the radial mode of deformation are:

1. Stiffness[a] (K_r):

$$K_r = \frac{F_r}{u_r^{ave}} = 24\pi G r_o \left(\frac{r_o}{h}\right)^3 \left(\frac{L}{2r_o} - \text{Tanh}\,\frac{L}{2r_o}\right) \tag{5-7}$$

2. Maximum Shear Stress $\left(\tau_{rz}^{max}\right)$

$$\tau_{rz}^{max} = \frac{F_r h \left(\text{Tanh}\,\frac{L}{2r_o}\right)}{4\pi r_o^3 \left(\frac{L}{2r_o} - \text{Tanh}\,\frac{L}{2r_o}\right)} \tag{5-8}$$

Maximum shear stress location is at point A as shown in part C of Figure 5-2.

3. Average Radial Stress $\left(\sigma_r^{ave}\right)$:

$$\sigma_r^{ave} = \frac{F_r}{2r^{ave}L} \tag{5-9}$$

The average radius (r^{ave}) is $\frac{r_o + r_i}{2}$; for thin pads $r^{ave} \simeq r_i$.

[a]For compressible materials, the radial stiffness is given by

$$K_r = \frac{2Gr_o}{\left[\phi_r \left(\frac{h}{2r_o}\right)^3 + 0.8\left(\frac{h}{L}\right)\left(\frac{G}{k}\right)\right]} \tag{5-10}$$

The radial stiffness factor (ϕ_r) is presented in Figure 5-13.

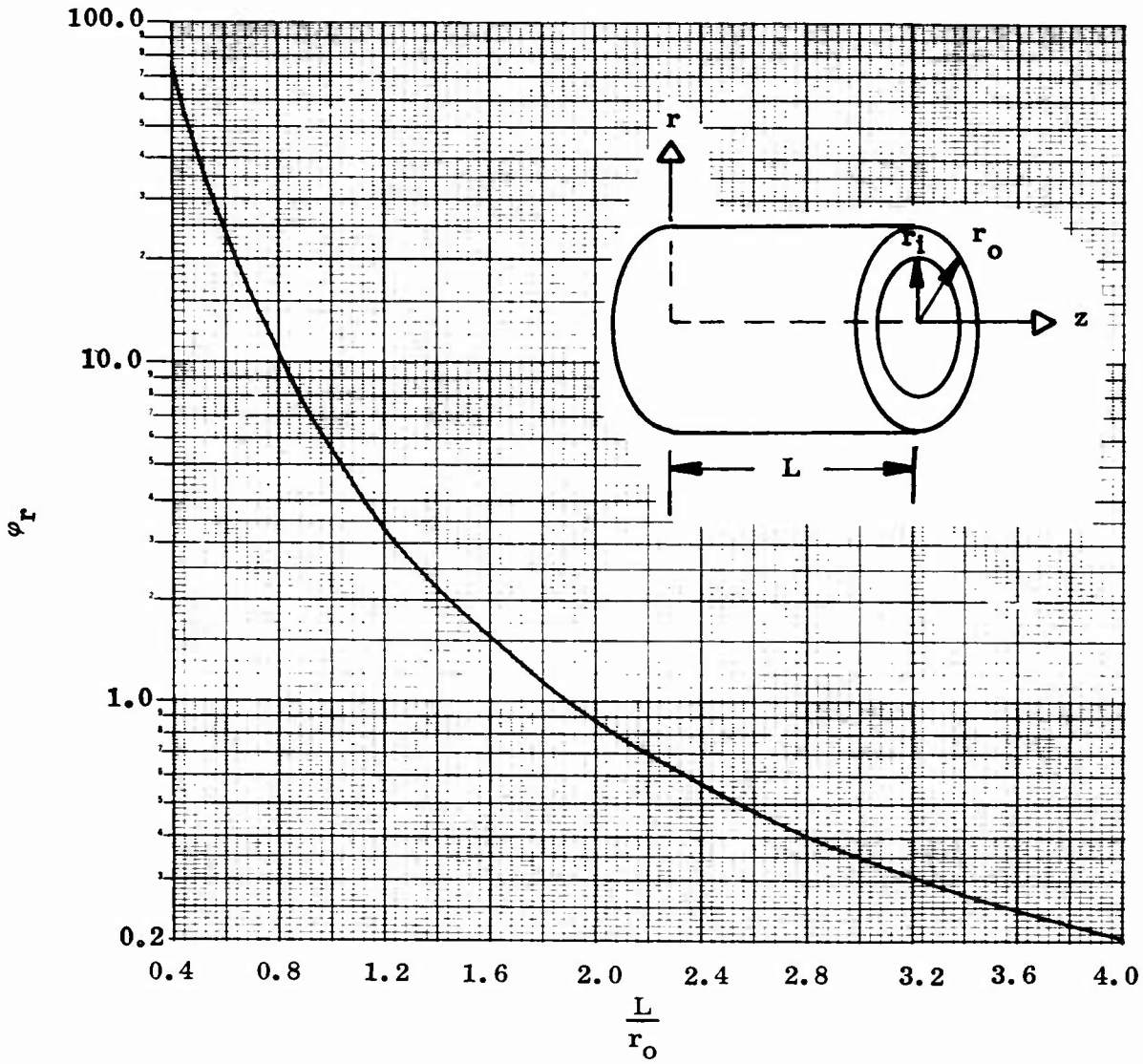

Figure 5-13. Radial stiffness factor for various L/r_o ratios.

5.3 MANUFACTURING CONSIDERATIONS

A Type II bearing has very high tensile stresses induced in the elastomer during cool-down from the molding temperature to ambient. Figure 5-14 shows the hydrostatic tensile stress in a Type II elastomer pad cured at 300° F and cooled to 70° F. Tensile stress in elastomers should be avoided, since cavitation is initiated when the stresses are about 3/4 of the elastomer tensile modulus (Reference 5-2). Therefore, if the bearing is to have a reasonable service life, it is necessary that these induced thermal stresses be minimized.

Pressure molding has been used in an attempt to reduce induced stresses. The applied pressure decreases the inner housing diameter and increases the outer housing diameter of the bearing. Upon release of the pressure, the housing shrinks on to the elastomer pad, resulting in a state of compressive stress. It is also possible that a high molding pressure causes sufficient bulk compression in the elastomer which, upon release of the pressure, could result in a compressive stress state.

Currently, preliminary design curves are not available to treat the cure and thermal-induced stresses. It is recommended that these stresses be obtained by using the finite-element computer program in the following steps:

1. Obtain deformed geometry of the housing and shims at molding temperature and pressure. Note that there is no elastomer (void element) in the finite-element model in this step.
2. Incorporate elastomer in the finite-element model after Step 1. Apply a thermal load on the entire bearing together with a negative molding pressure on the exposed core ends (elastomer and shim areas) to effectively remove the pressure applied in Step 1. The thermal load should consider cool-down to minimum storage temperature.

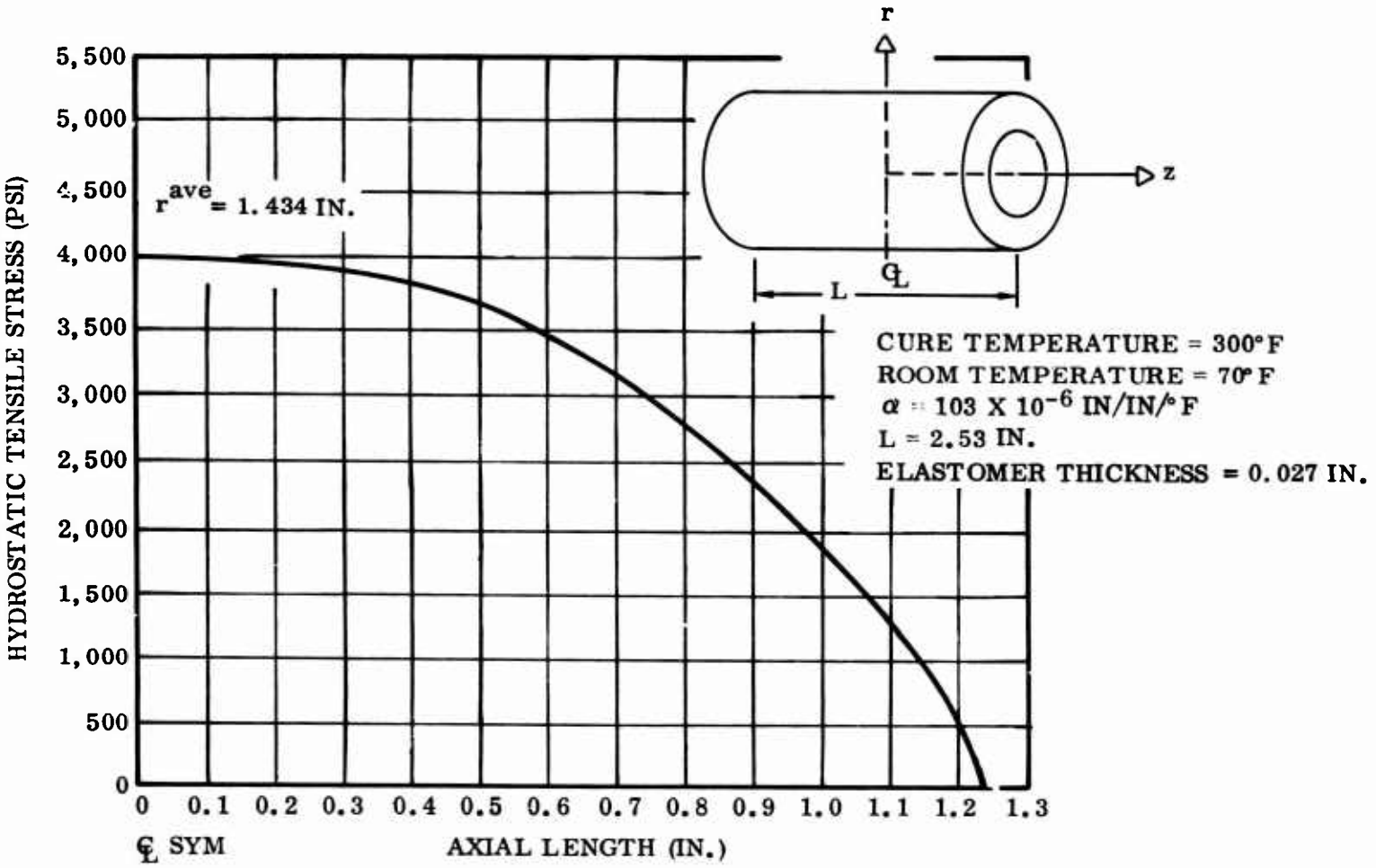

Figure 5-14. Hydrostatic tensile stress in a Type II elastomer pad due to thermal cool-down.

3. Superimpose thermal and radial loads prescribed on geometry obtained in Step 3.
4. Evaluate resultant stress field from Steps 2 and 3 to determine if critical tensile stresses are present in the bearing.

6.0 TYPE III BEARING DESIGN

A Type III bearing consists of alternate layers of spherically shaped rubber pads and shims (Figure 1-3). It is designed to react axial loads and allow motion about all three axes. In a typical helicopter application, it will support the centrifugal force load and allow blade pitch, flap, and lead-lag motions. In helicopter terminology, the minimum spherical radius end of the bearing is normally referred to as the "inboard", end and the maximum spherical radius end is called the "outboard" end. The outboard end is generally fixed, while the inboard end is free to move.

6.1 PROCEDURE

The design procedure is similar to that of a Type I bearing. The reader is referred to an r-z cross section of a Type III bearing in Figure 6-1 for some of the geometric parameters that are unique to this bearing and used in the text.

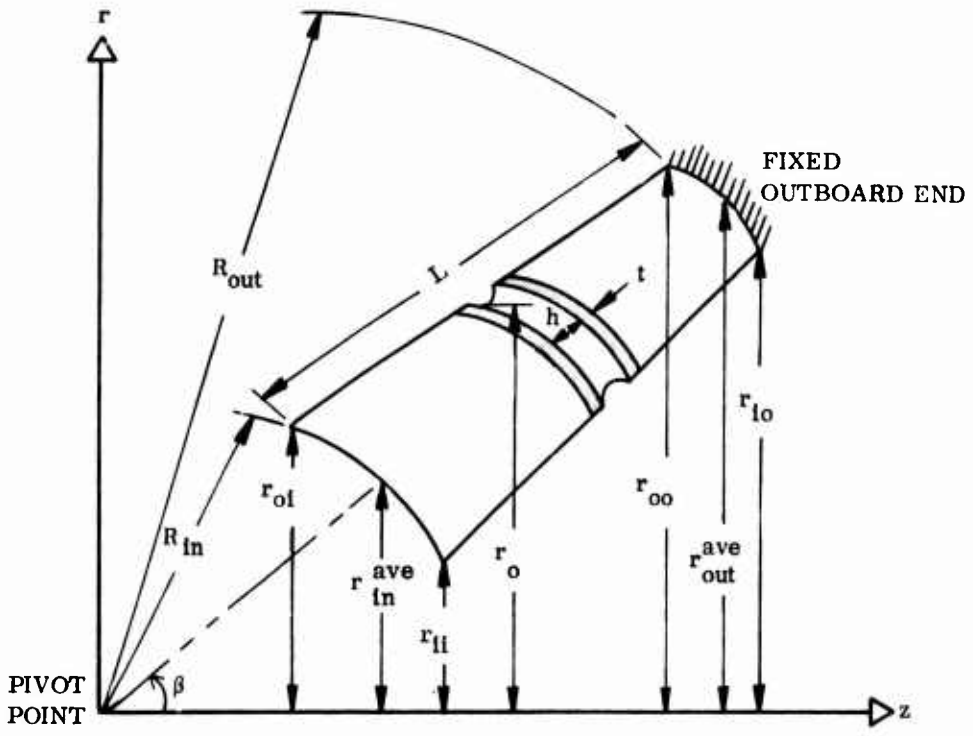

Figure 6-1. Type III bearing nomenclature.

6.1.1 Level 1 Design

A flow chart of the Level 1 design procedure is given in Figure 6-2. The procedure is as follows:

1. Select an elastomer formulation with known properties E, G, k, ν. A maximum shear strain failure surface of the type discussed in Section 9.0 is also required.
2. Define initial value for axial load (F_z) pitch angle (θ_z^T) and flap angle (θ_x^T) from load-motion spectrum table as discussed in the design of Type I bearings (Section 4.0).
3. Select an allowable axial strain (ϵ_z^{all}) and an allowable axial stress (σ_z^{all}) as discussed in the design of Type I bearings. Values of $\epsilon_z^{all} = 15\%$ and $\sigma_z^{all} = 5,000$ psi are recommended. Assuming that $\sigma_z^{all} = \sigma_z^{ave}$, Equation 6-4 can be used to determine E_A and the projected area (A). Since r_{ii} is specified, r_{oi} can be determined. Also, since E_A is related to the shape factor (S) by Equations 4-6 and 4-7, S can be calculated.
4. Select a value for the included half angle (β) of the bearing. For this preliminary design, a value of 45 degrees is recommended. Assuming that the inboard end average radius is $\left(r_{in}^{ave} = \frac{r_{oi} + r_{ii}}{2}\right)$, the pivot point can be located by construction or by simple trigonometric relationships.
5. The shear strain failure surface is used to read off the γ^{all} value for the chosen $\epsilon_z^{ave} = 15\%$ and acceptable life value of, say, 30×10^6 cycles. The shear strain in a Type III bearing is the result of the strains due to pitch and vector rotations and is given by

$$\gamma^{all} = \sqrt{\gamma_{r\theta}^2 + \gamma_{R\phi}^2} \qquad (6\text{-}1)$$

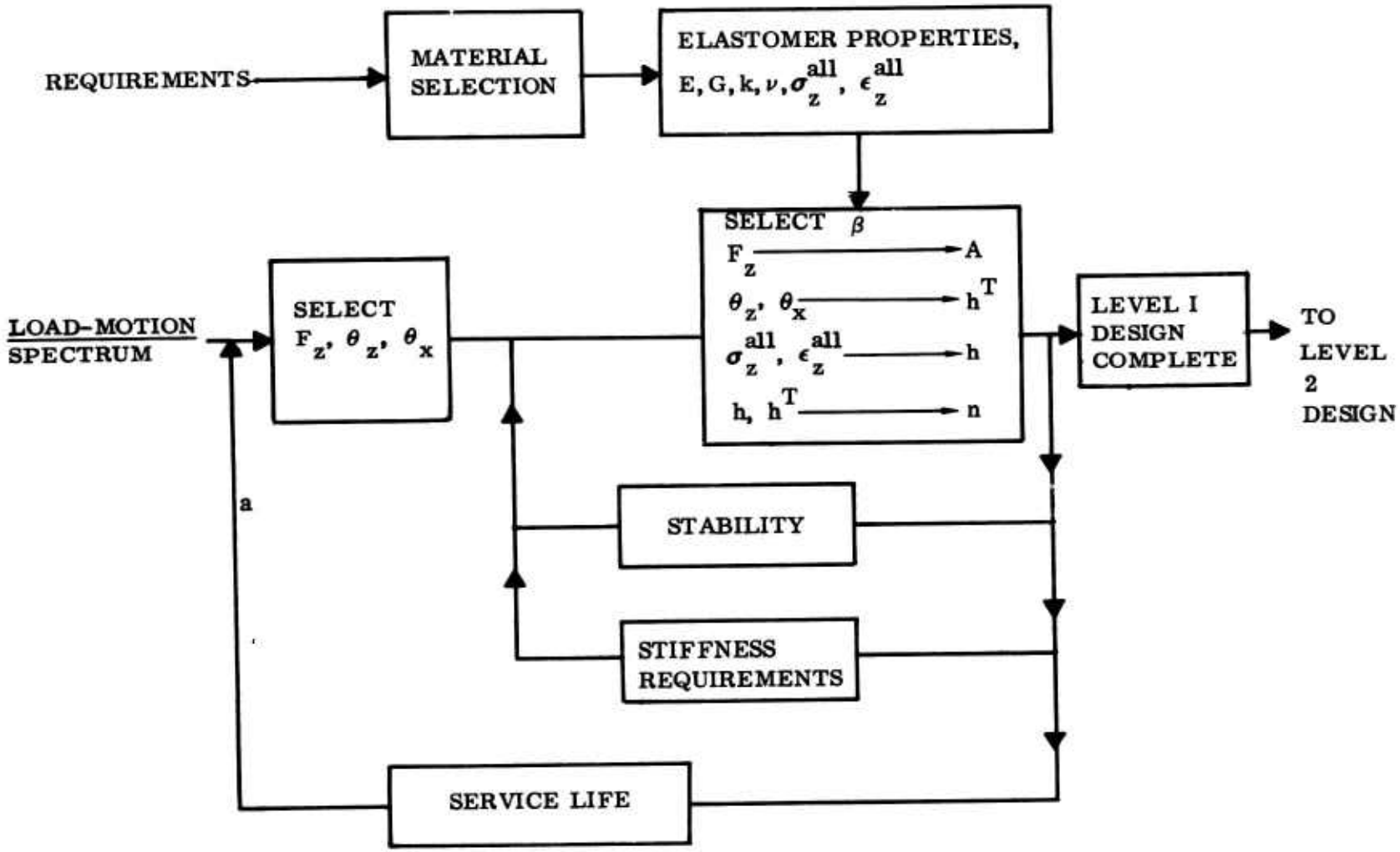

[a]EACH ITERATION REQUIRES EVALUATION OF DESIGN CONDITIONS (F_z, θ_z, ϵ_z^{all}) AND MATERIAL SELECTION

Figure 6-2. Level 1 design procedure flow for Type III bearings.

The shear strain due to the lead-lag motion is not included in Equation 6-1 since it is generally small and out of phase with $\gamma_{r\theta}$ and $\gamma_{R\phi}$. This omission will result in a conservative design because the lead-lag motion reduces the magnitude of the shear strain in the bearing.

Equation 6-1 can be expanded using Equations 6-6 and 6-8 to yield

$$\gamma_{all} = \sqrt{\left\{\frac{\theta_z^T J^{ave}}{h^T} \frac{G^{ave}}{G} \frac{r_o}{J}\right\}^2 + \left\{\theta_r^T \frac{R^{ave}}{h^T}\left(\frac{R^{ave} A^{ave} G^{ave}}{RAG}\right)\right\}^2} \qquad (6\text{-}2)$$

The first iteration of this preliminary design is simplified by assuming $J^{ave} = J$, $r_o = r_{oi}$, $R^{ave} = R = (R_{in} + h^T)$, $G^{ave} = G$, and $A^{ave} = A$. Since the total flap angle (θ_r^T) and the total pitch angle (θ_z^T) are chosen in Step 2, the only unknown in Equation 6-2, namely, h^T, can be determined.

6. Shim stresses are highest in Type III bearings during vectoring. It is recommended that shim thickness be chosen equal to the elastomer pad thickness. Therefore, since $t^T = h^T$, the length of the bearing ($L = t^T + h^T$) can be calculated.

7. For this preliminary design, each pad can be assumed to have the same projected area (A). Therefore, the inner and outer radii (r_{io} and r_{oo}), respectively, at the outboard end can be determined. Note that the average radius at the outboard end (r_{out}^{ave}) is measured from the z axis to the point of intersection of a straight line of slope β and an arc of spherical radius, R_{out}, given by $R_{out} = R_{in} + L$.

8. Since the basic envelope of the bearing is now defined and S is known in Step 3, the pad thickness (h) can be determined for the middle pad. Assuming that all pads have the same thickness, the number of pads can be calculated. All geometric parameters of the bearing are now defined.

9. The second iteration can be carried out without making the assumptions used in simplifying Equation 6-2 in Step 5. This will yield more accurate values for the geometric parameters.

10. Check bearing for stability by using Equation 6-7 for bending stiffness and Equation 6-9 for shear stiffness of the middle pad in the buckling Equation 8-1 presented in Section 8.0. If bearing is unstable, these stiffnesses may have to be increased. Bending stiffness can be increased by increasing β. Shear stiffness can be increased by reducing the pad thickness or increasing the cross-sectional area. As in the design of a Type I bearing, care should be taken that values ϵ_z^{ave} and γ^{all} chosen in Steps 3 and 5, respectively, are not violated. If they are not met, new values of ϵ_z^{ave} and γ^{all} may have to be chosen.

11. Check for any stiffness requirement as discussed in the design of Type I bearings.

12. Check for service life as explained in Section 9.0.

6.1.2 Level 2 Design

The flow chart for the Level 2 design procedure is given in Figure 6-3.

In the Level 2 design, the designer can refine the Level 1 design by noting the effect of some of the important parameters in the design equations. For example, Equation 6-8 shows that all pads will have the same bending strain, if the

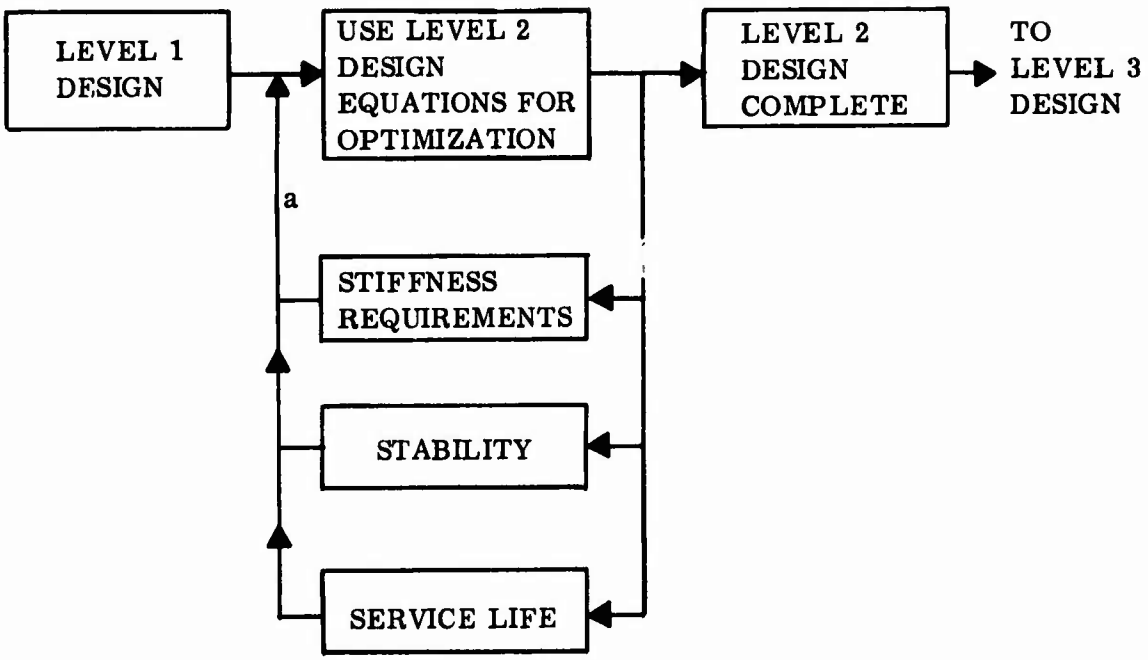

[a]EACH ITERATION REQUIRES EVALUATION OF DESIGN CONDITIONS (F_z, θ_z, ϵ_z^{all}) AND MATERIAL SELECTION

Figure 6-3. Level 2 design procedure flow for Type III bearings.

parameter RA is kept constant in the bearing. On the other hand, Equation 6-6 shows that all pads will have the same torsional strain, if the parameter $\frac{r_o}{J}$ is kept constant. Therefore, if the bearing is to be designed for the same strain in each pad, a compromise between Equations 6-6 and 6-8 will have to be reached.

Since an important consideration in service life is shear strain, methods for minimizing the shear strain should be investigated. One approach is to make the spherical elastomer pads with different moduli.

Another parameter that can be modified at this stage is the included half angle (β). If the axial load (F_Z) is considerably less than the buckling load, β can be reduced. However, the minimum value of β is determined by the maximum flap angle of the blade shaft, and adequate clearance should be provided between the outboard end and the shaft in the maximum flap position.

The detailed design equations given in Subsection 6.2 can also be used at this time to determine the stiffness and stress in each pad. They have not been plotted in a parametric form because of their complex nature. However, some observations for the important equations are provided.

The maximum shear stress failure surface criteria can also be evaluated in Level 2 design by using the detailed design equations for shear stress.

6.1.3 Level 3 Design

It has probably become obvious to the designer that Type III bearing design is rather complicated. The finite-element analysis becomes a powerful tool in analyzing this bearing. The Level 3 design procedure is the same as for a Type I bearing (Figure 4-3). The detailed design equations will help the designer in noting the effect of a geometric parameter such as pad thickness or spherical radius on stiffnesses, stresses and strains, so he may not have to use a trial and error approach in Level 3 to modify the design to meet the prescribed requirements.

The areas of concern have been identified in the design of Type I bearing. Close attention should be given to these areas. Improved service life parameters such as strain energy density or maximum shear stress should be used to refine prediction of bearing fatigue life. The procedure for this prediction is given in Section 9.0.

6.2 EQUATIONS

The equations that are used in the preliminary design of Type III bearings are given below. They are modifications of the design equations for a Type I bearing with spherical pads and shims. Therefore, they should be used for Level 1 design only. The Level 2 design equations that apply for a spherical pad are given in Paragraph 6.2.2.

6.2.1 Level 1 Design

The preliminary design equations for the four modes of deformation of a Type III bearing are given below.

6.2.1.1 Axial Mode

The equations for the axial mode of deformation are:

1. Stiffness (K_Z):

$$K_Z = \frac{A\,E_A}{h^T} \tag{6-3}$$

Note: E_A is given by Equations 4-4 and 4-5.

2. Average Strain (ϵ_z^{ave}):

$$\epsilon_z^{ave} = \frac{F_z}{A\,E_A} = \frac{\sigma_z^{ave}}{E_A} \tag{6-4}$$

6.2.1.2 Torsional Mode

The equations for the torsional mode of deformation are:

1. Stiffness (K_{θ_Z}):

$$K_{\theta_Z} = \frac{JG}{h^T} \tag{6-5}$$

2. Shear Strain ($\gamma_{r\theta}$):

$$\gamma_{r\theta} = \frac{\theta_z^T\,J^{ave}}{h^T}\;\frac{r_o}{J}\;\frac{G^{ave}}{G} \tag{6-6}$$

In the above equation, J^{ave} and J are the polar moments of inertia of the middle pad in the bearing and any individual pad, respectively. The outside radius of an

individual pad is r_o. G^{ave} and G are the shear moduli of the middle pad and any individual pad, respectively.

6.2.1.3 Vectoring (Bending, Flapping) Mode

The equations for the vectoring mode of deformation are:

1. Stiffness ($K_{\theta r}$):

$$K_{\theta r} = \frac{GAR^2}{h^T} \tag{6-7}$$

Since the Type III bearing is axially symmetric,

$K_{\theta x} = K_{\theta y} = K_{\theta r}$.

2. Shear Strain ($\gamma_{R\phi}$):

$$\gamma_{R\phi} = \frac{\theta_r^T R^{ave}}{h^T} \quad \frac{R^{ave} A^{ave}}{RA} \quad \frac{G^{ave}}{G} \tag{6-8}$$

In the above equation, R^{ave} and A^{ave} refer to the middle pad in the bearing and R&A refer to any individual pad.

6.2.1.4 Shear (Transverse, Radial) Mode

The equations for the shear mode of deformation are:

1. Stiffness (K_r):

$$K_r = \frac{GA^{ave}}{h^T} \tag{6-9}$$

Since the Type III bearing is axially symmetric,

$K_x = K_y = K_r$.

2. Shear Strain (γ_{rz}):

$$\gamma_{rz} = \frac{u_r^T}{h^T} \tag{6-10}$$

where u_r^T = total radial displacement for the entire bearing.

6.2.2 Level 2 Design

The following equations apply for a single spherical pad only.

6.2.2.1 Axial Mode

The equations for the axial mode of deformation are:

1. Average Deflection (u_z^{ave}):

$$u_z^{ave} = \frac{F_z h^3}{1.5\pi G r_o^4 \phi_a} + \frac{1.25 F_z h}{k\pi (r_o^2 - r_i^2)} \quad (6\text{-}11)$$

The axial stiffness factor (ϕ_a) is given in Figure 6-4.

2. Stiffness (K_Z):

$$K_z = \frac{F_z}{u_z^{ave}} \quad (6\text{-}12)$$

3. Maximum Axial Stress (σ_z^{max}):

$$\sigma_z^{max} = \frac{F_z \phi_{as}}{\pi r_o^2} \quad (6\text{-}13)$$

The axial stress factor (ϕ_{as}) is given in Figure 6-5.

4. Maximum Shear Stress at r_i or Inner Radius ($\tau_{r_i}^{max}$):

$$\tau_{r_i}^{max} = \frac{F_z h \phi_{si}}{\pi r_o^3} \quad (6\text{-}14)$$

5. Maximum Shear Stress at r_o or Outer Radius ($\tau_{r_o}^{max}$):

$$\tau_{r_o}^{max} = \frac{F_z h \phi_{so}}{\pi r_o^3} \quad (6\text{-}15)$$

The shear stress factors (ϕ_{si} and ϕ_{so}) are given in Figures 6-6 and 6-7, respectively.

6.2.2.1.1 Observations on Equations 6-11 and 6-12

The following observations should be considered:

1. If $S < 15$, $u_z^{ave} \alpha h^3$. Therefore, stiffness is very sensitive to pad thickness h.
2. If $S > 30$, the second term in Equation 6-11 is far greater than the first term. Therefore, stiffness will be inversely proportional to h.

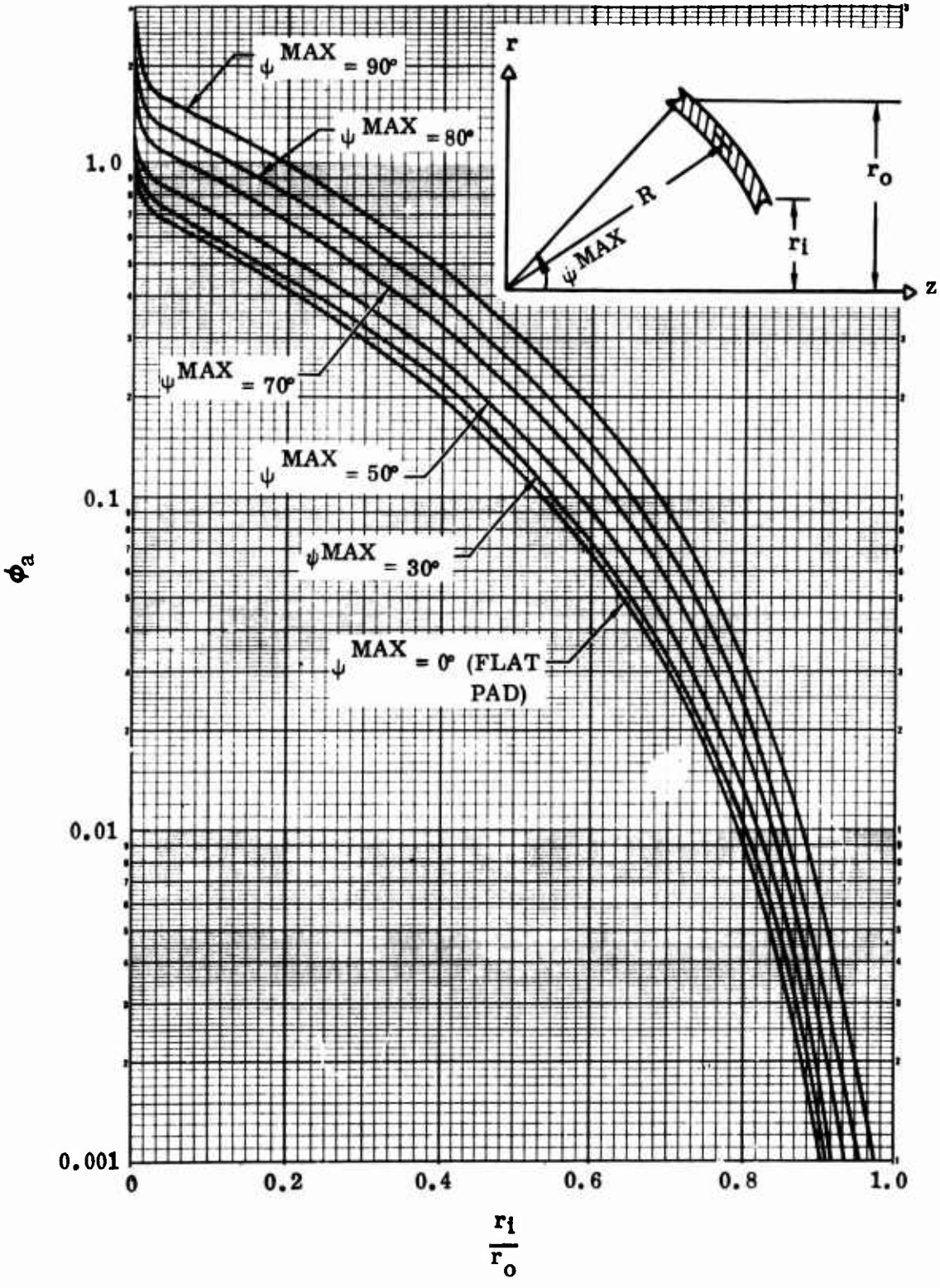

Figure 6-4. Axial stiffness factor (ϕ_a) vs $\frac{r_i}{r_o}$ ratio.

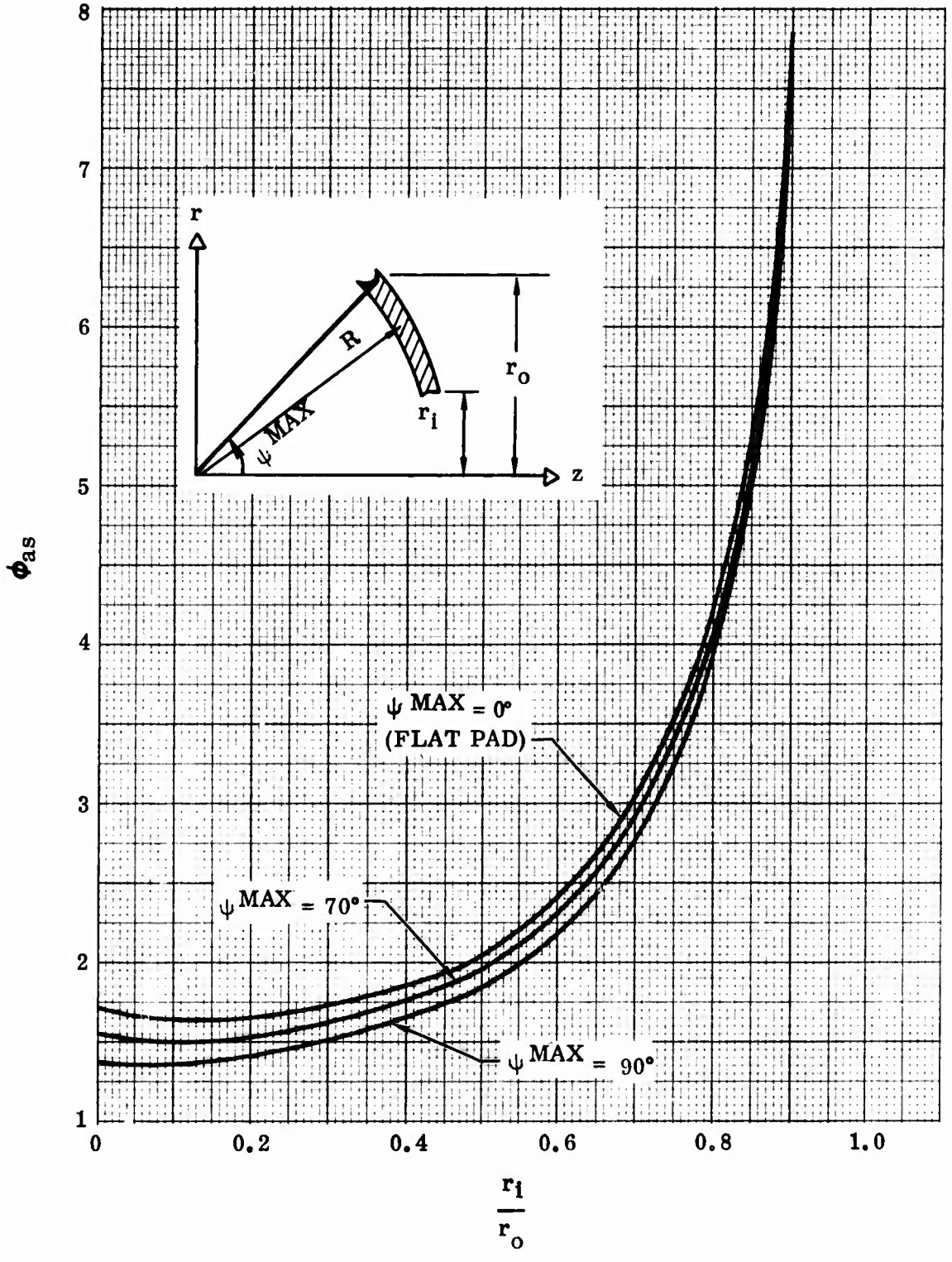

Figure 6-5. Axial stress factor (ϕ_{as}) vs $\frac{r_i}{r_o}$ ratio.

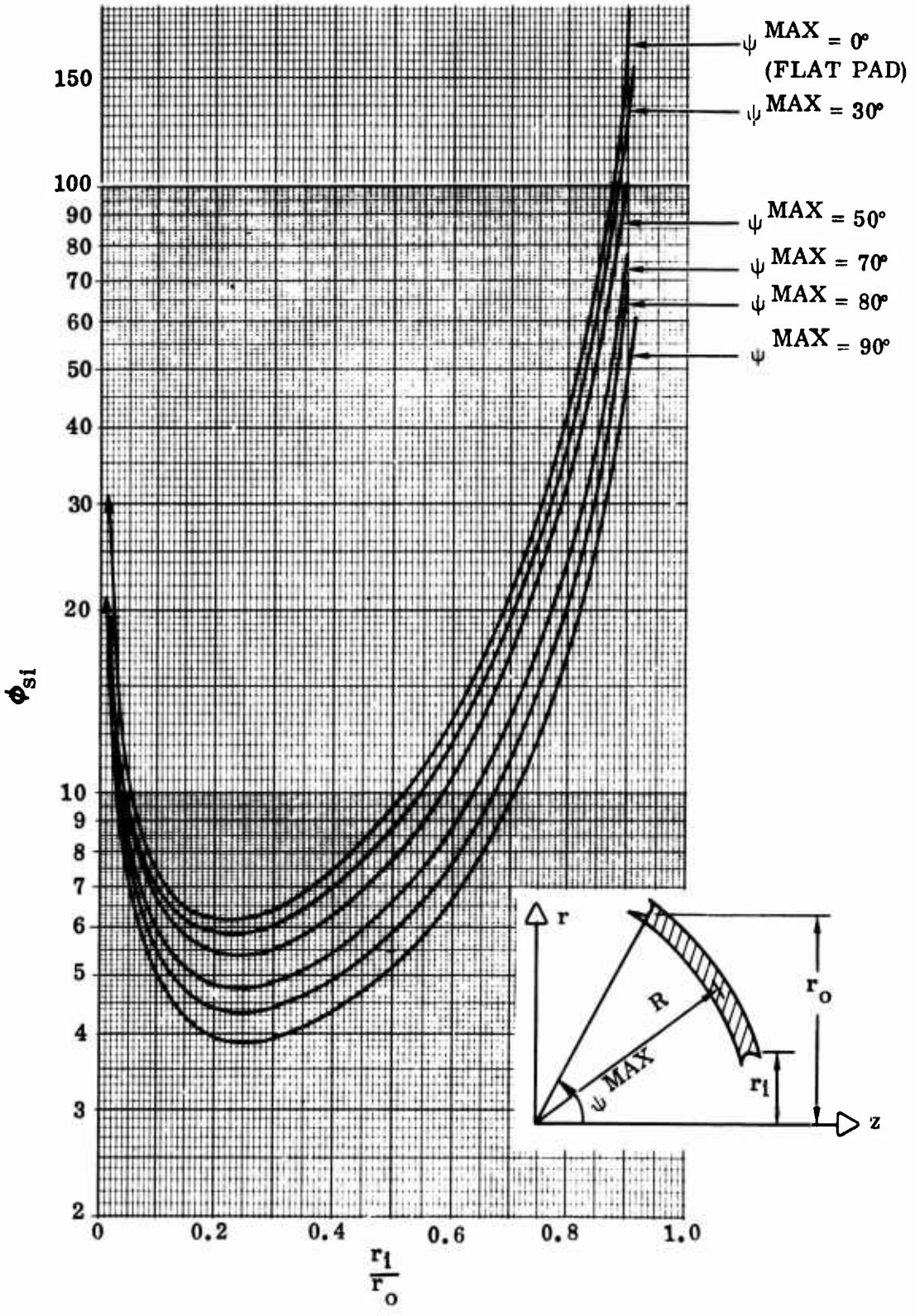

Figure 6-6. Inner radius shear stress factor (ϕ_{si}) vs $\frac{r_i}{r_o}$ ratio.

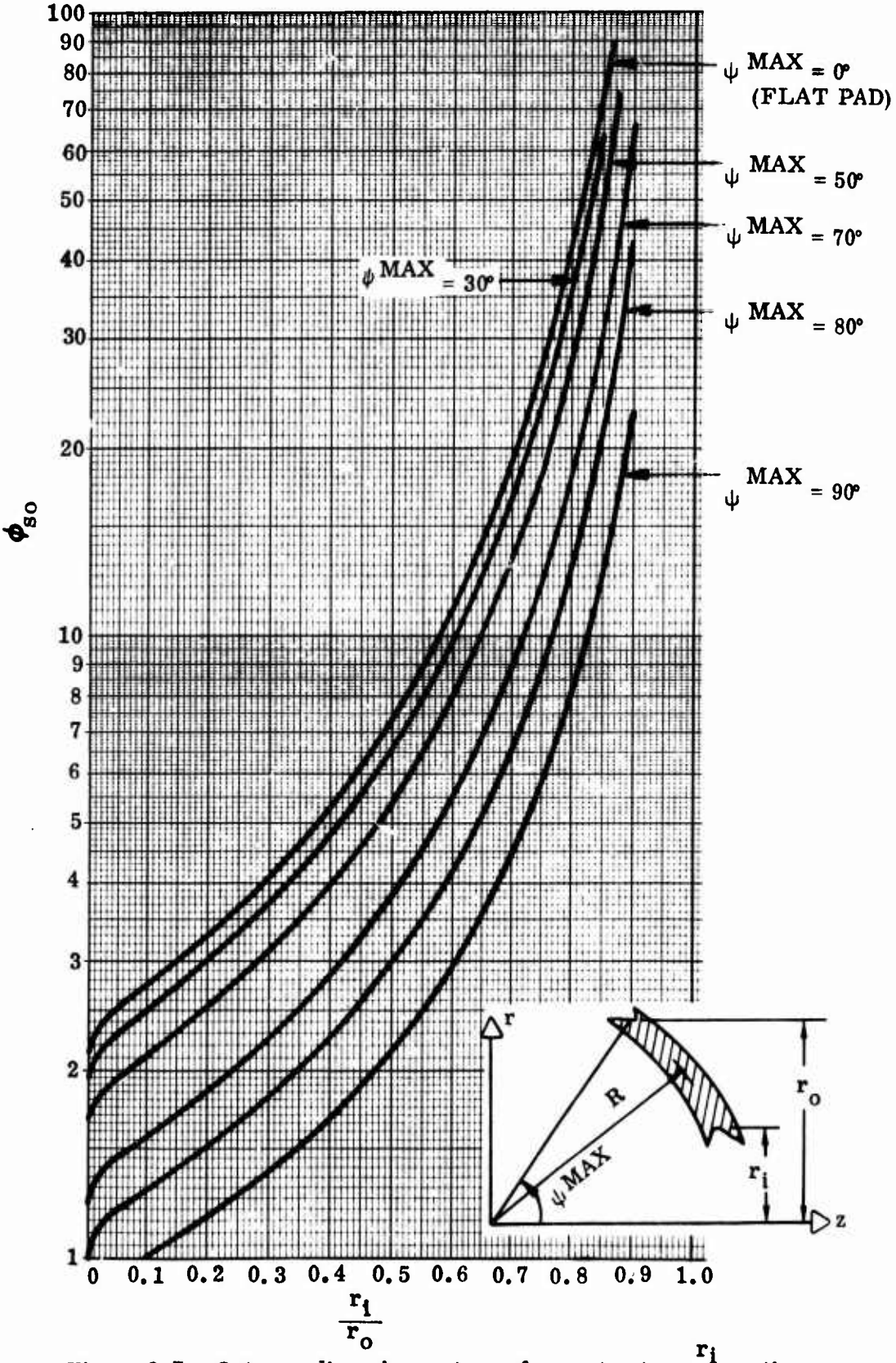

Figure 6-7. Outer radius shear stress factor (φ_{so}) vs $\frac{r_i}{r_o}$ ratio.

3. Stiffness is significantly reduced by the presence of a small center hole placed in a solid pad.
4. For a bearing with multiple pads, the reciprocal of the total axial stiffness is given by the sum of the reciprocals of the individual pad stiffnesses.

6.2.2.1.2 Observations on Equation 6-13

The following observations should be considered:

1. Axial stress is zero at r_o and r_i and maximum near the average radius $\left(r^{ave} = \frac{r_o + r_i}{2}\right)$.
2. For a solid pad, maximum stress is at the centerline (zero radius).

6.2.2.1.3 Observations on Equations 6-14 and 6-15

The following observations should be considered:

1. Shear stress is maximum at the bondline between elastomer pad and shim.
2. Shear stress distribution in the pad is maximum at the inner and outer radius (r_o and r_i), respectively. It is zero at a point approximately midway between r_o and r_i. The shear stress is highest at the inner radius.
3. Shear strains at the inner and outer radii can be determined by dividing Equations 6-14 and 6-15, respectively, by the shear modulus (G).

6.2.2.2 Torsional Mode

The equations for the torsional mode of deformation are:

1. Torsional Deflection (θ_z):

$$\theta_z = \frac{2M_z h}{\pi G\left\{r_o^4 \phi_{t_o} - r_i^4 \phi_{t_i}\right\}} \qquad (6\text{-}16)$$

2. Torsional Stiffness (K_{θ_z}):

$$K_{\theta_z} = \frac{\pi G}{2h} \left\{ r_o^4 \phi_{t_o} - r_i^4 \phi_{t_i} \right\} \qquad (6\text{-}17)$$

The torsional stiffness factor (ϕ_t) is presented in Figure 6-8. The sub-subscripts i and o indicate that ϕ_t is evaluated at the inner and outer edge, respectively.

3. Shear Stress ($\tau_{r\theta}$):

$$\tau_{r\theta} = \frac{G\theta_z r}{h} \qquad (6\text{-}18)$$

6.2.2.2.1 Observations on Equations 6-16 and 6-17

The following observations should be considered:

1. Torsional deflection is proportional to h. Therefore, adding reinforcements will not affect stiffness.
2. Stiffness is not significantly affected by changing spherical radius.
3. For bearing included angles up to 40 degrees, the values ϕ_{t_i} and ϕ_{t_o} do not change significantly from a value of one (Figure 6-8). Therefore, stiffness is directly proportional to the polar moment of inertia (J) of the bearing cross section.
4. Stiffness is not greatly affected by the presence of a center hole.
5. For a bearing with multiple pads, the reciprocal of the total torsional stiffness is equal to the sum of the reciprocals of the individual pad torsional stiffnesses.

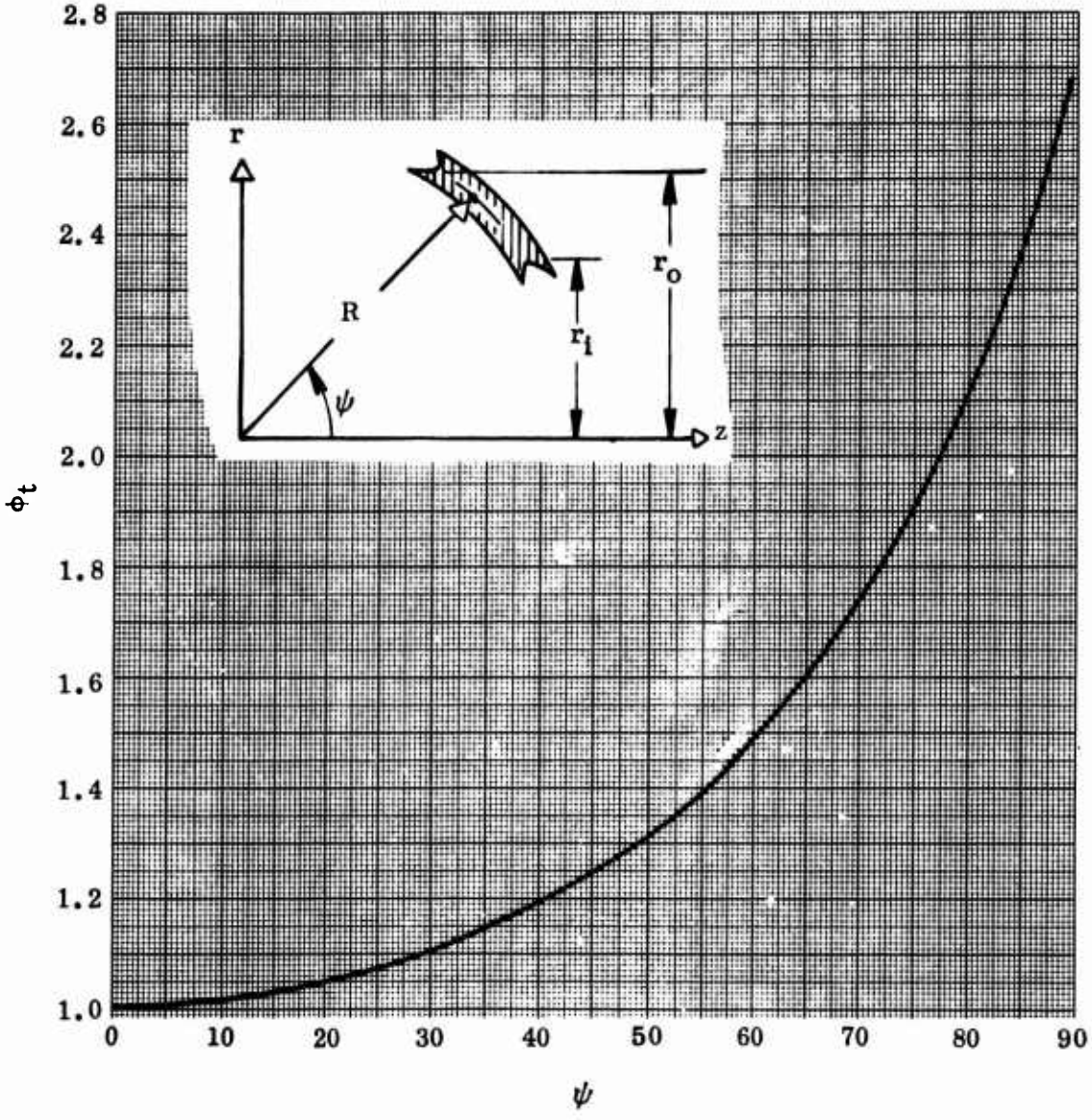

Figure 6-8. Torsional stiffness factor(ϕ_t) vs ψ.

6.2.2.2.2 Observations on Equation 6-18

The following observations should be considered:

1. Shear stress is constant through the pad thickness.
2. Shear stress is maximum at the outer radius.
3. Shear strain is obtained by the formula: $\gamma = \frac{\tau}{G}$.

6.2.2.3 Bending and Shear (or Transverse) Modes

The bending and shear modes of deformation on loading are interrelated. Hence, they will be analyzed together.

The loads that are required to displace the center of curvature (C) shown in Figure 6-9 by u_x in the x- direction are a shear force (F_x) and a moment (M_y) applied at C. These loads are given by

$$F_x = u_x \frac{r_o^2 \pi R^2 G}{h^3} \quad \phi_D = u_x C_1 \tag{6-19}$$

$$M_y = u_x \frac{\pi RG}{h} (r_i^2 - r_o^2) = u_x C_2 \tag{6-20}$$

The transverse stiffness factor (ϕ_D) is given in Figure 6-10.

The forces that are necessary to achieve pure rotation (θ_y) about the center of curvature without any translation (Figure 6-11) are given by

$$F_x = \theta_y \frac{\pi RG}{h} (r_i^2 - r_o^2) = \theta_y C_2 \tag{6-21}$$

$$M_y = \theta_y \frac{R^2 \pi G}{h} \left\{ r_o^2 \phi_{B_o} - r_i^2 \phi_{B_i} \right\} = \theta_y C_3 \tag{6-22}$$

The bending stiffness factor (ϕ_B) is presented in Figure 6-12. The sub-subscripts o and i with ϕ_B refer to the outer and inner edge of the bearing, respectively.

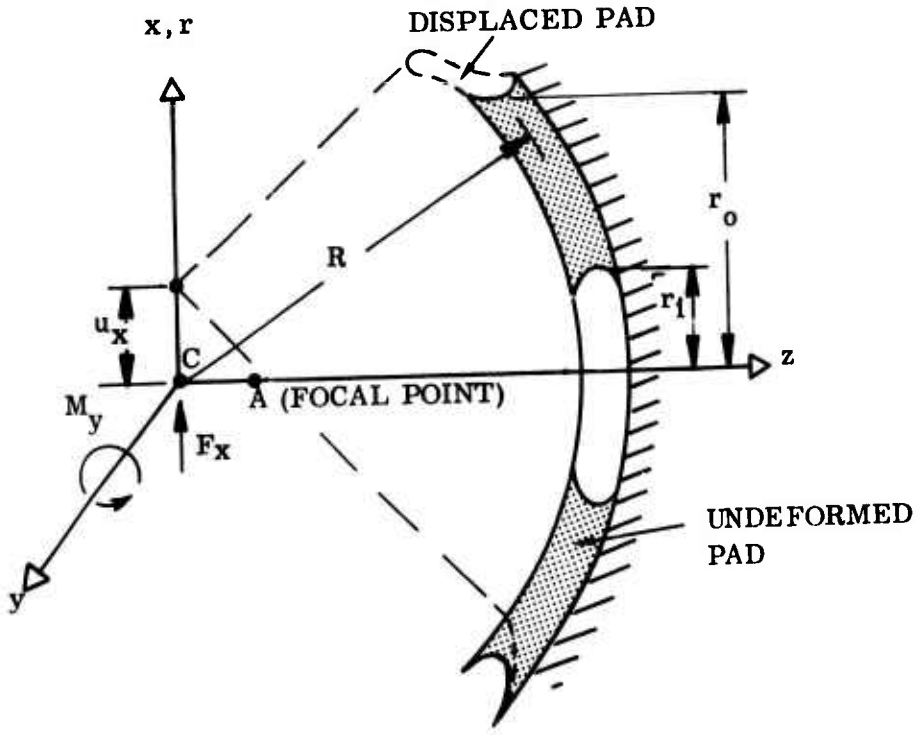

Figure 6-9. Transverse displacement in Type III bearing.

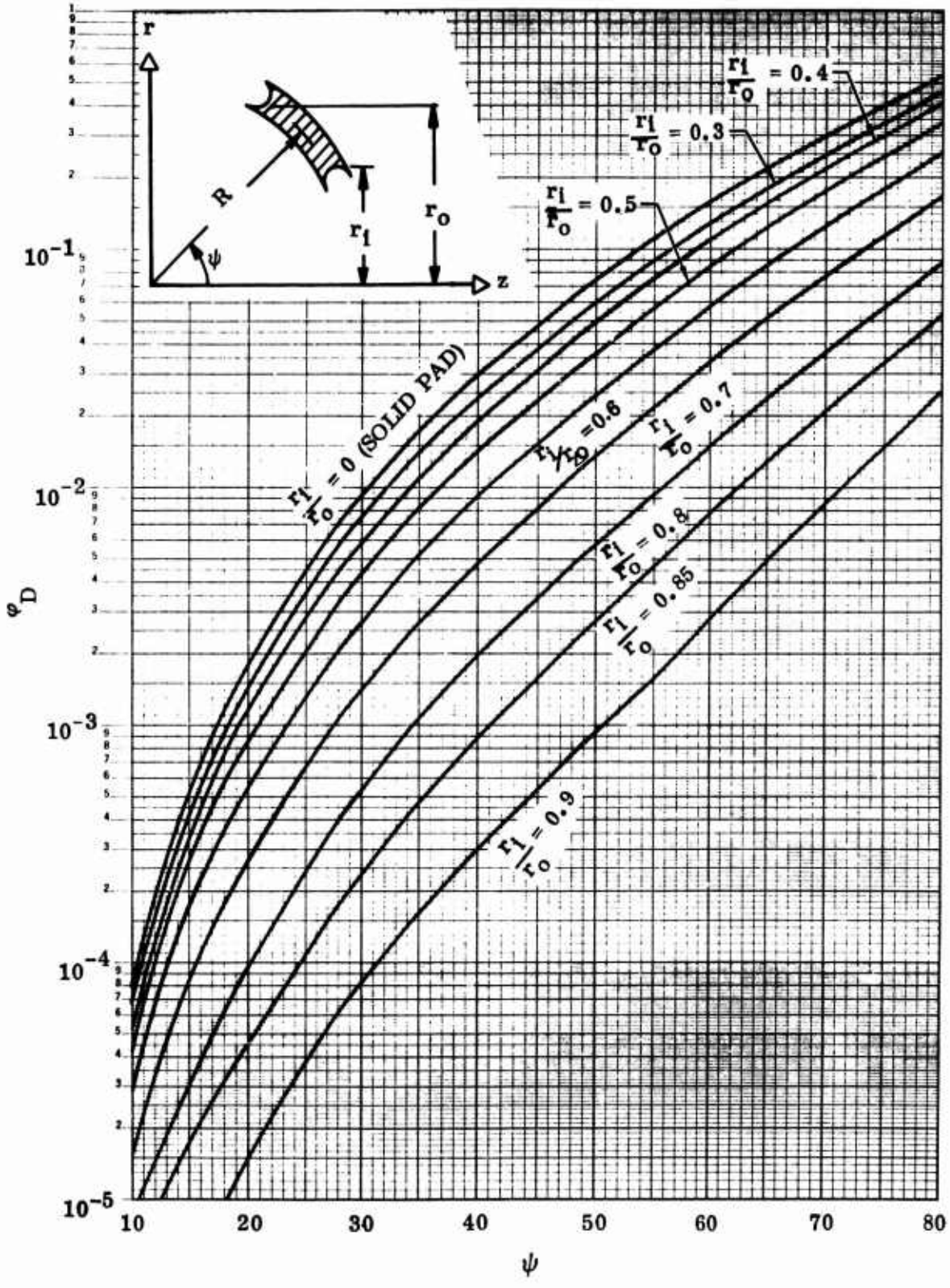

Figure 6-10. Transverse stiffness factor (ϕ_D) vs ψ.

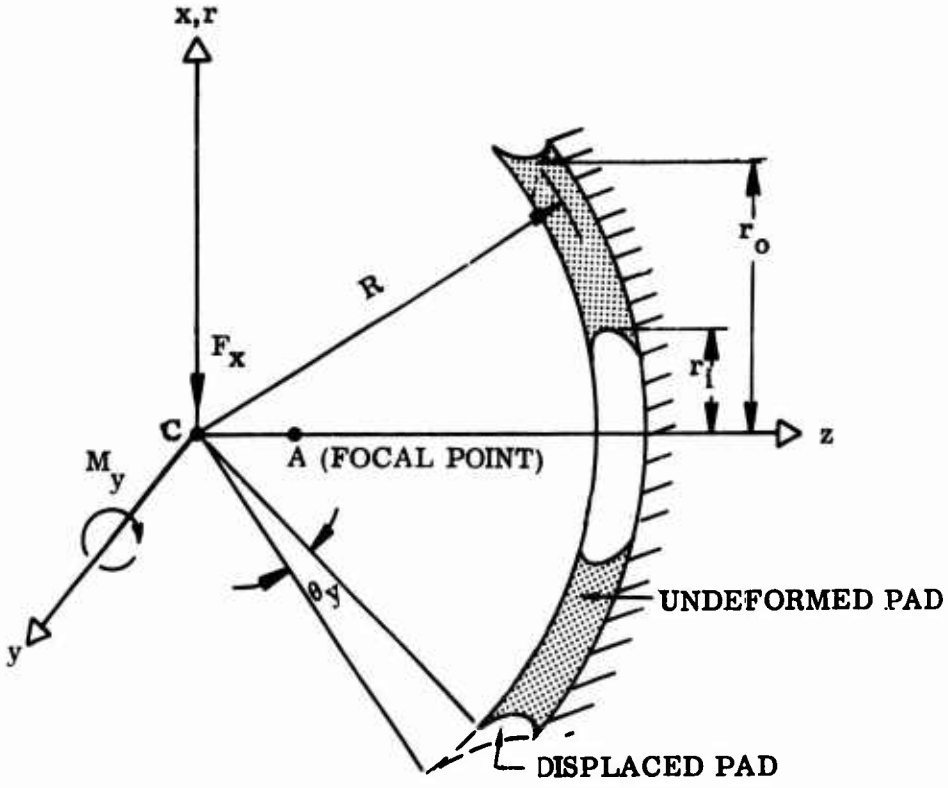

Figure 6-11. Rotation in type III bearings.

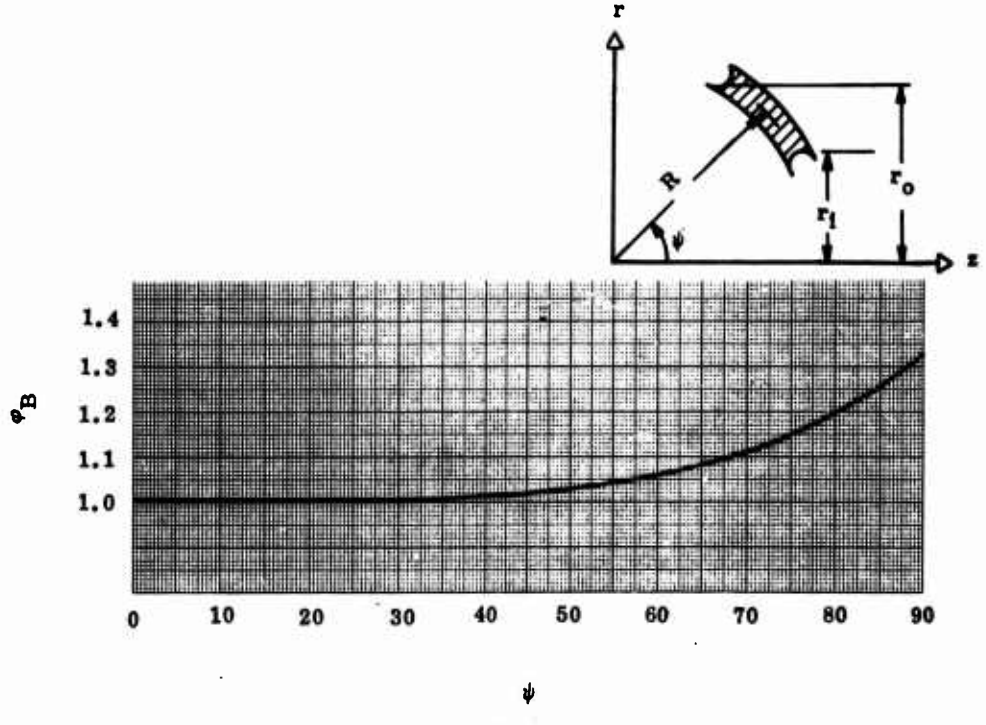

Figure 6-12. Bending stiffness factor (φ_B) vs ψ.

Since a Type III bearing is axially symmetric, $F_X = F_r$, $M_y = M_r$, $u_X = u_r$, and $\theta_y = \theta_r$. Equations 6-19 through 6-22 can be combined to give the relations

$$u_r = a_1 F_r + a_2 M_r \tag{6-23}$$

$$\theta_r = a_2 F_r + a_3 M_r \tag{6-24}$$

where a_1, a_2, and a_3 are given by

$$a_1 = \frac{C_3}{C_1C_3 - C_2^2} \tag{6-25}$$

$$a_2 = \frac{-C_2}{C_1C_3 - C_2^2} \tag{6-26}$$

and

$$a_3 = \frac{C_1}{C_1C_3 - C_2^2} \tag{6-27}$$

Equations 6-23 and 6-24 give the deflection (u_r) and rotation (θ_r) due to applied loads F_r and M_r. Therefore, for example, a radial load, $F_r = F$, applied at the center of curvature with $M_r = 0$ will cause a deflection $u_r = a_1F$ and a rotation $\theta_r = a_2F$. However, the radial load if applied at a point A that is, $\frac{C_2}{C_1}$ units to the right of point C shown in Figure 6-9 will not cause any rotation. The moment (M_r), if applied at the point A, will cause pure rotation about A. Therefore, the point A is commonly referred to as the focal point of the pad.

6.2.2.4 Radial and Bending Stiffness

The radial and bending stiffness of a Type III bearing can now be defined. The radial stiffness (K_r) is given by

$$K_r = \frac{F_r}{u_r} = \frac{1}{a_1} \text{ with } M_r = 0 \tag{6-28}$$

The bending stiffness (K_{θ_r}) is given by

$$K_{\theta_r} = \frac{M_r}{\theta_r} = \frac{1}{a_3} \text{ with } F_r = 0 \tag{6-29}$$

6.2.2.4.1 Observations on Equation 6-28

The following observations should be considered

1. Radial stiffness is proportional to $\frac{1}{h^3}$ and R^2.
2. The presence of a small hole (up to $\frac{r_i}{r_o} = 0.3$) will not reduce the radial stiffness significantly from that for a solid pad.

6.2.2.4.2 Observations on Equation 6-29

The following observations should be considered:

1. Bending stiffness is proportional to $\frac{1}{h}$ and R^2.
2. The presence of a small hole (up to $\frac{r_i}{r_o} = 0.3$) will not reduce the bending stiffness significantly from that for a solid pad.

6.2.2.5 Shear Stress Due to Translation and Rotation

The shear stress resulting from a rotation (θ_r) is given by

$$\tau_{R\phi} = \frac{\theta_r R G}{h} \qquad (6\text{-}30)$$

Because of the coupling between bending and transverse loading, it is difficult to determine the total bending or radial stiffness of an entire bearing based on the corresponding stiffness of a single pad. Also, a bearing of multiple pads may have the same center of curvature, but not the same focal point. Therefore, the use of the finite-element analysis is recommended for determining the stiffness.

7.0 BEARING ANALYSIS

This section briefly describes the features of the computer program and tells how it can be used to model typical bearing geometries. The features are discussed separately in the subsections that follow.

7.1 COMPUTER PROGRAM FEATURES

There are basically five separate features in the computer program in addition to the input and output features; the program features are summarized in Figure 7-1. A brief description of each feature follows.

7.1.1 Axisymmetric

This is the basic feature in the computer program. It uses linear elasticity theory together with the assumption of a linear displacement element to obtain solutions. If additional accuracy is desired, the user has the option to use the isoparametric element. This feature will evaluate loads and displacements that are axisymmetric, i.e., independent of the circumferential coordinate. Thermal loads can be superimposed.

7.1.2 Nonlinear Axisymmetric

This feature evaluates axisymmetric loads and displacements for problems where large displacements and strains as well as nonlinear material properties are encountered. The user has two separate options; namely, the incremental load option and the total load option. In the incremental load option, all loads and displacements for the boundary conditions may be applied in increments. In the total load option, the nonlinear terms in the strain displacement relations are taken into consideration. The two options can be combined to have a large deformation iteration inside each incremental loading loop. Nonlinearity of material properties are taken into account by constructing tables of material properties versus strain or temperature and referring to the table for each iteration. The nonlinear material properties are discussed in Paragraph 7.3.2.

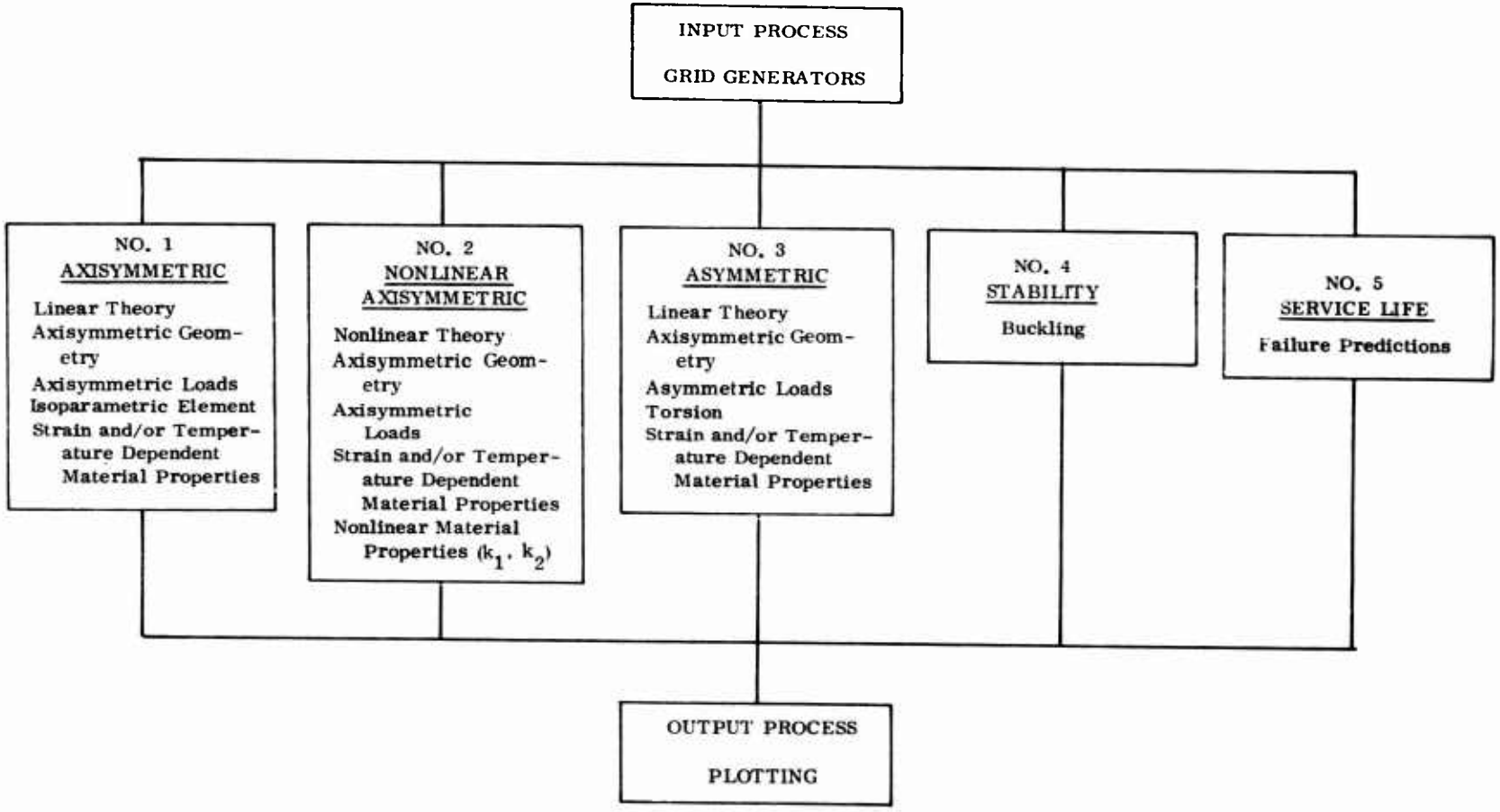

Figure 7-1. Computer program features summary.

7.1.3 Asymmetric

Bearing geometries with applied loads and displacements that are not axisymmetric can be analyzed by using this feature. It is necessary to express these loads and displacements as a set of Fourier series expansions in the circumferential coordinate. The general problem is separated into a series of two-dimensional problems for each harmonic of the Fourier series and then combined. Unlike the axisymmetric feature described in Paragraph 7.1.1, this feature will allow the user to analyze an axisymmetric problem with combined axial, torsional, and thermal loads. The O-harmonic of this feature must be used for torsional analysis.

7.1.4 Stability

At the present time, buckling loads for only Type I bearings can be analyzed using this feature.

7.1.5 Service Life

This feature combines the bearing stress analysis output of different imposed loads and displacements to calculate the failure parameters necessary for service life prediction. These failure parameters are generally expressed as octahedral shear stress, strain energy, strain energy density, and maximum shear stress.

7.2 FINITE-ELEMENT PROGRAM GUIDELINES

Guidelines for obtaining the best possible results using the finite-element program are given in the following paragraphs.

7.2.1 Symmetry

The finite-element method requires that the problem to be analyzed be subdivided into a finite number of trapezoidal elements superimposed on a coordinate system. The coordinate system chosen identifies the coordinates of element corners; these element corners are called nodes. It is important to choose a coordinate system that takes maximum advantage of the symmetry of the problem.

Figure 7-2 shows the transverse cross section of an axisymmetric body in the r-z plane. This is an example of a general two-dimensional problem which can be analyzed under various loading conditions. From the theory of elasticity, the solution of this problem depends on both axial and radial coordinates and is independent of the circumferential coordinate.

The torsion problem is a special type of two-dimensional problem in which the solution depends on the radial and circumferential coordinates only.

Figure 7-3 shows the cross section of an axisymmetric body being acted upon by asymmetric loads. It is possible to include the circumferential variation of the load and still take advantage of the axisymmetric geometry by using the asymmetric load feature of the finite-element program. The nonsymmetrical loading condition requires a Fourier series expansion representation in the circumferential coordinate. The general three-dimensional problem is then separated into a series of two-dimensional problems for each harmonic of the Fourier series. These problems are solved separately and then combined.

7.2.2 Grid Considerations

The grid structure of a finite-element model is chosen to closely approximate the contours of the actual body to be analyzed after consideration of symmetry advantage. Grid lines are developed so that they fall on natural material boundaries.

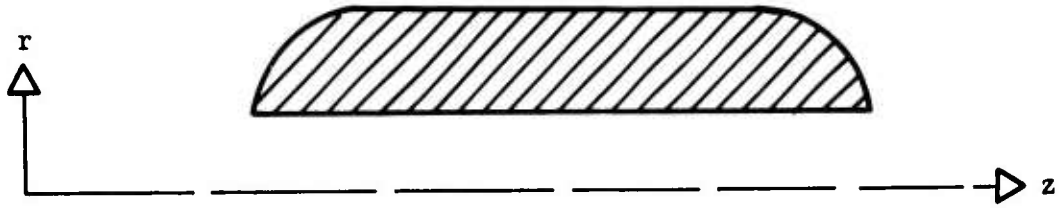

Figure 7-2. Axisymmetric body of finite length.

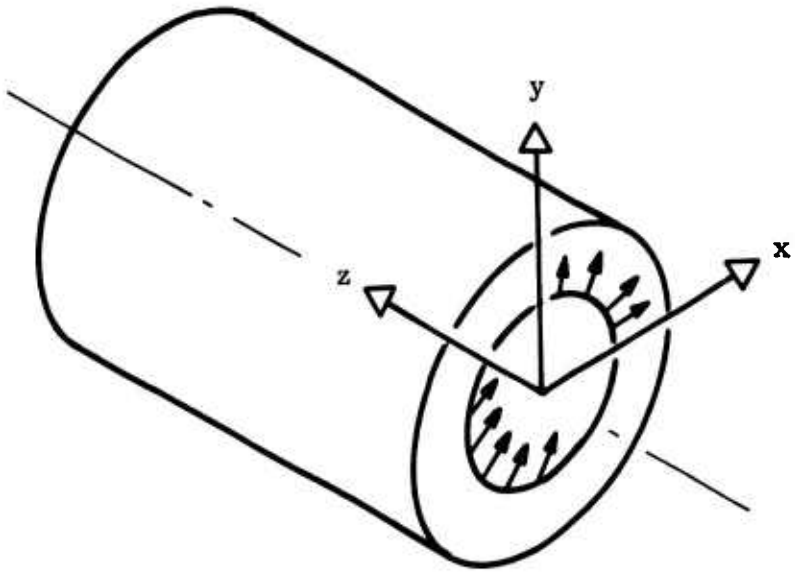

Figure 7-3. Axisymmetric geometry with asymmetric loads.

The coordinates of each node point that falls on a boundary are used in the program along with coordinates of any other node whose initial position must be specified. Not all the nodes need be used since the computer program makes use of several internal line and grid generation schemes as described in Volume III.

An element in the finite-element grid representation is designated by the number of the lowest bounding node (I, J), where I denotes the row and J denotes the column. An easy way to understand grid generation is to lay out a sketch of the bearing cross section and its I, J representation immediately below it as depicted in Figure 7-4.

Figure 7-4 shows that gridding can be thought of as a one-to-one mapping from the r-z plane to a rectangular I, J plane. An important restriction on mapping is that the r-z and I-J planes must both be either right or left handed. The method of determining right handedness is to rotate the r axis into the z axis, and this should give a vector out of the plane of the paper. Then the I-J rotation must follow the same rule as shown in Part A of Figure 7-5. A left-handed rotation is shown in Part B of Figure 7-5, and a violation of the mapping system is shown in Part C of Figure 7-5.

The procedures for grid setup are numerous. They are determined by the accuracy of solutions desired in the critical areas in the geometry. Grid density should be increased in those areas. The best test for grid adequacy is to use an even finer grid and to demonstrate that stresses and strains do not differ appreciably from those computed by the grid in question. A rule of thumb is to make the grid fineness proportional to the stress gradient in the critical area.

Some basic rules on elements shapes and sizes are given in Reference 7-1. Determination of grid fineness is generally a matter of experience in using the computer program to analyze various problems.

Typical grids for Type I, II, and III bearing geometries are shown in Figures 7-6, 7-7, and 7-8, respectively. Fine grids were used at the extreme

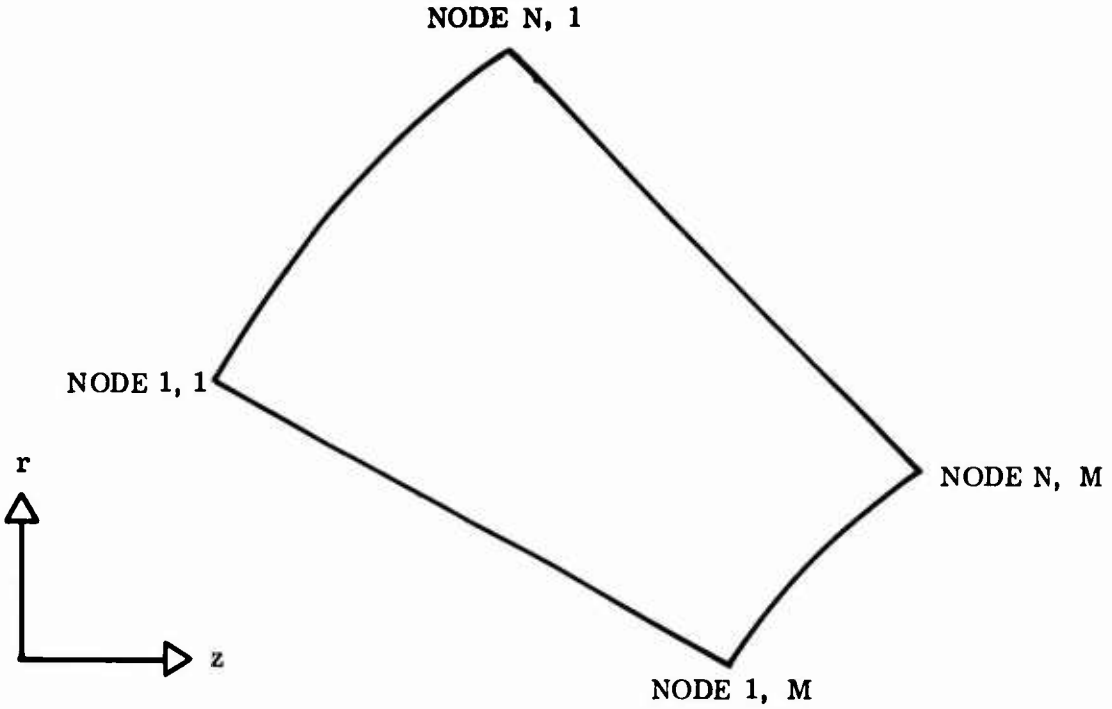

AXISYMMETRIC BEARING GEOMETRY

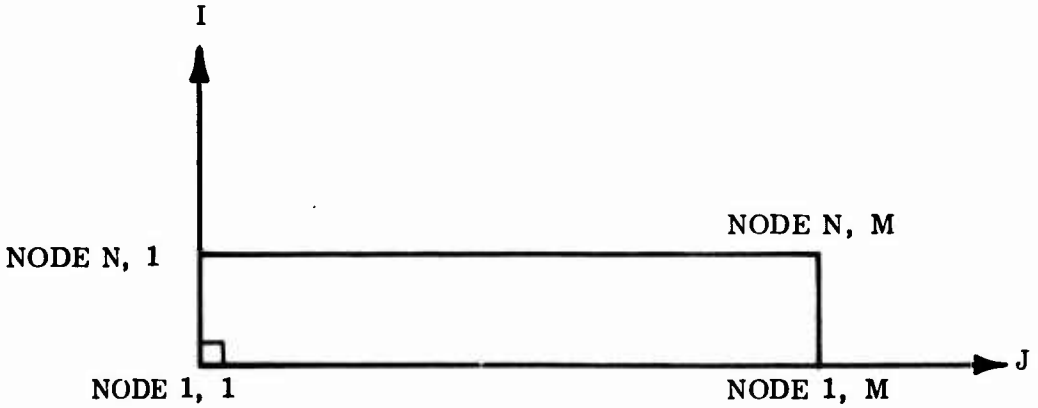

I-J REPRESENTATION OF BEARING GEOMETRY

Figure 7-4. I-J mapping of axisymmetry geometry.

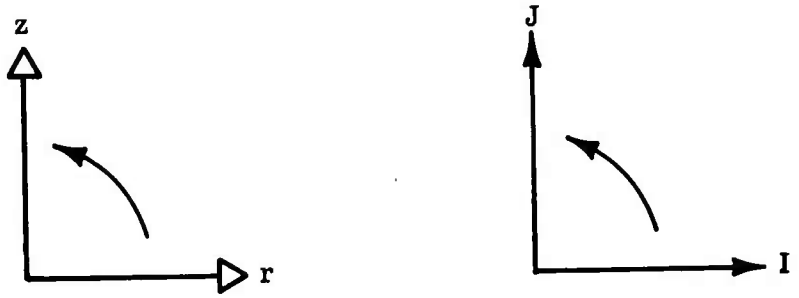

A. RIGHT HANDED

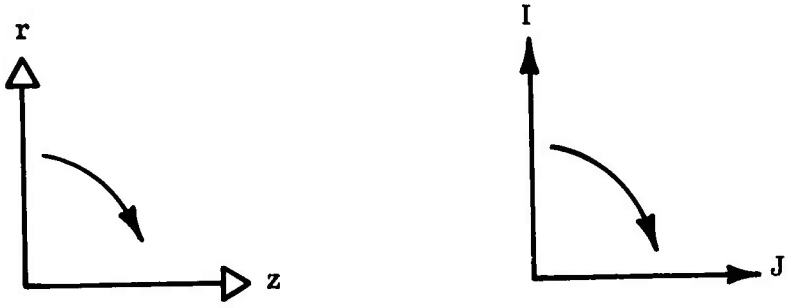

B. LEFT HANDED

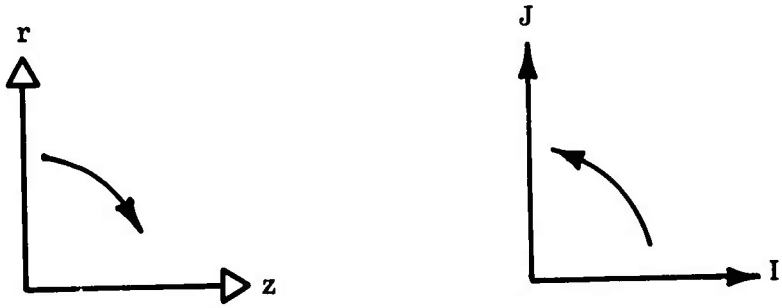

C. NOT ALLOWED

Figure 7-5. Right- and left-handed rules for mapping.

edges of the geometry because the stresses and strains are highest at these locations.

7.2.3 Boundary Conditions

The boundary conditions that can be used in the computer program are numerous. Each element within the grid can be loaded with pressure and/or shear loading on any of its four sides as well as a body force within the element, if required. The solution is very dependent on boundary conditions, and the analyst should use his very best judgment as to which conditions accurately describe the physical situation.

An important boundary condition in finite-element analysis is that rigid-body motion is eliminated. This can be achieved by fixing displacements at appropriate nodal points. Figure 7-9 shows an axisymmetric cross section under an axial body force load. The nodal point A in this case would be fixed in r and z to prevent rigid-body motion. Without this boundary condition, the model would be free to move in the axial direction and show extremely large displacements.

Another useful boundary condition provided in the computer program is the sliding boundary condition. This allows nodes to slide along a line of specified angle and is useful in simulating symmetry. Figures 7-10 to 7-12 show some of the common problems encountered in bearing design and their corresponding finite-element models.

In analyzing large problems, it may be necessary to make several finite-element model runs at different critical cross sections to obtain accurate results. Another method of obtaining accurate results is to use a coarse grid for the entire model in order to obtain boundary conditions for a critical region. A fine grid is then used for the critical region with the boundary conditions so obtained. Stresses should generally be used for the boundary conditions rather than displacements for the refined region.

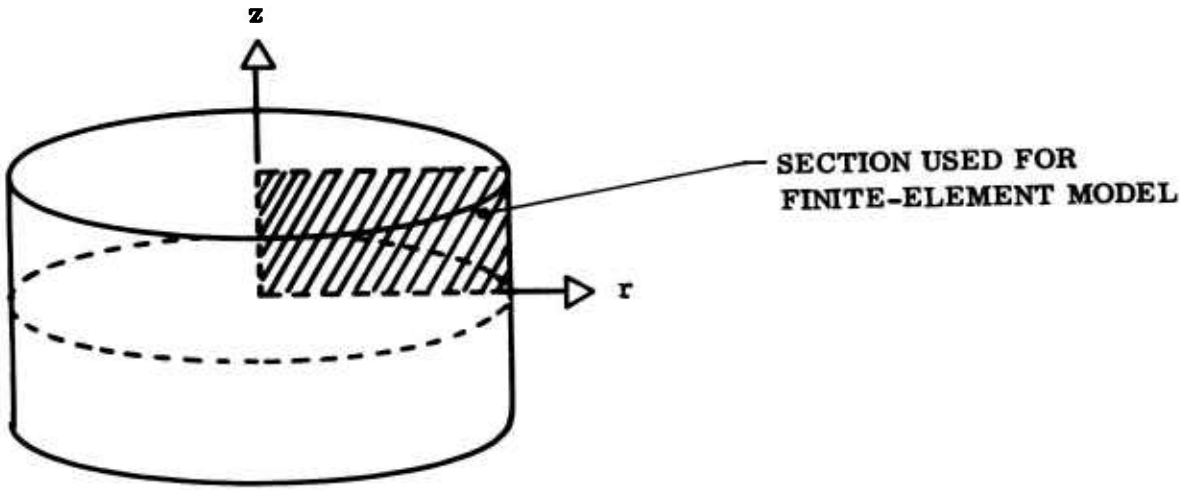

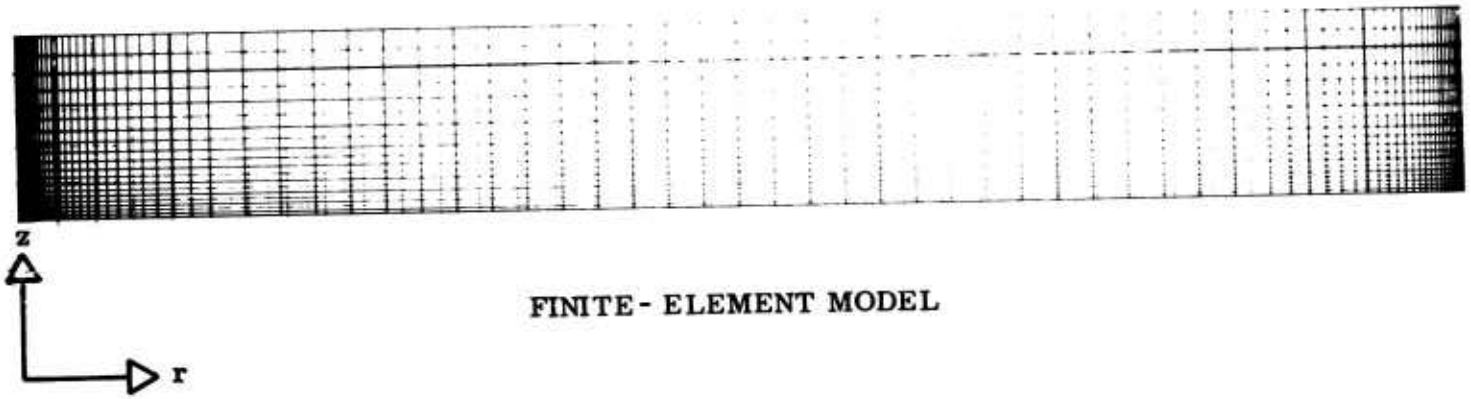

Figure 7-6. Finite-element model of Type I bearings.

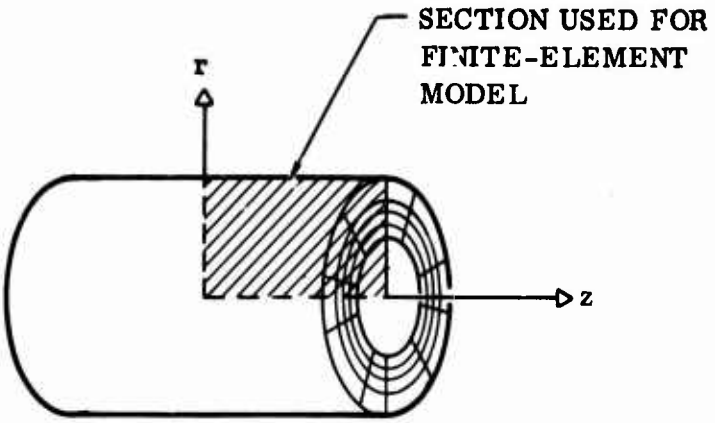

TYPE II BEARING

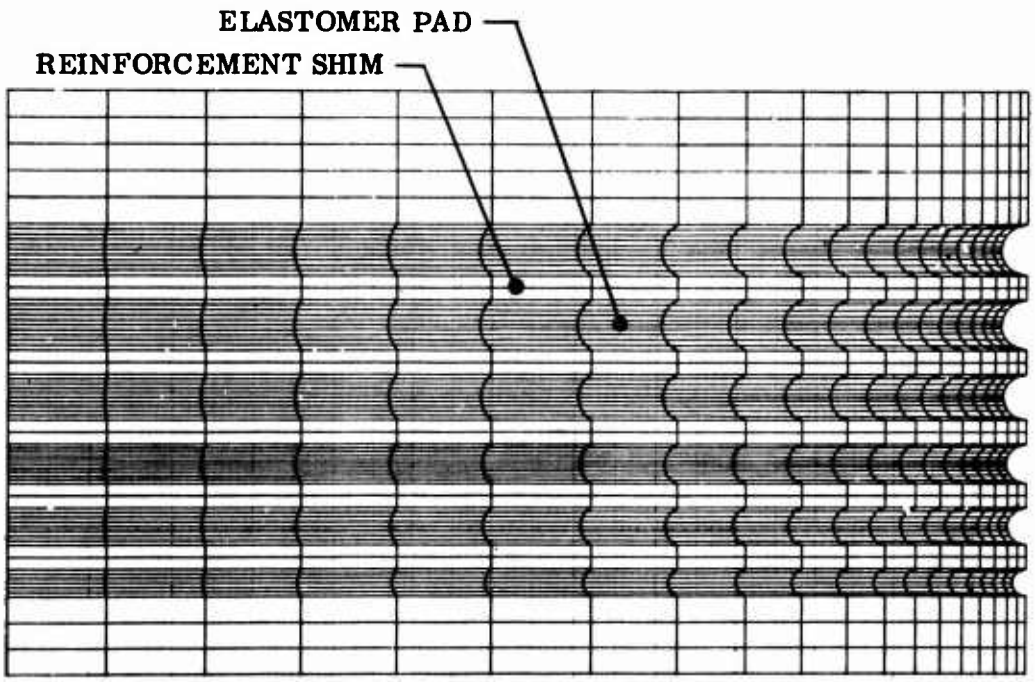

FINITE-ELEMENT MODEL

Figure 7-7. Finite-element model of Type II bearings.

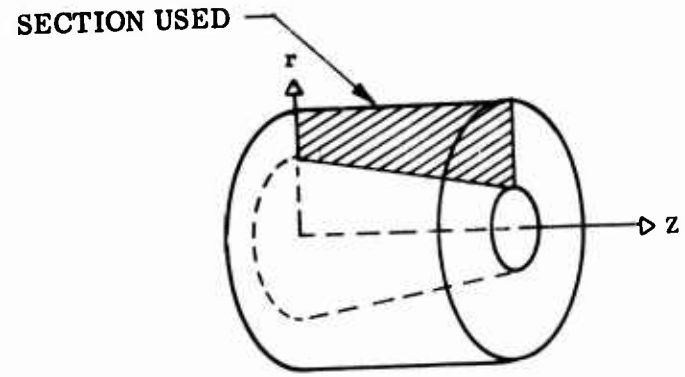

TYPE III BEARING

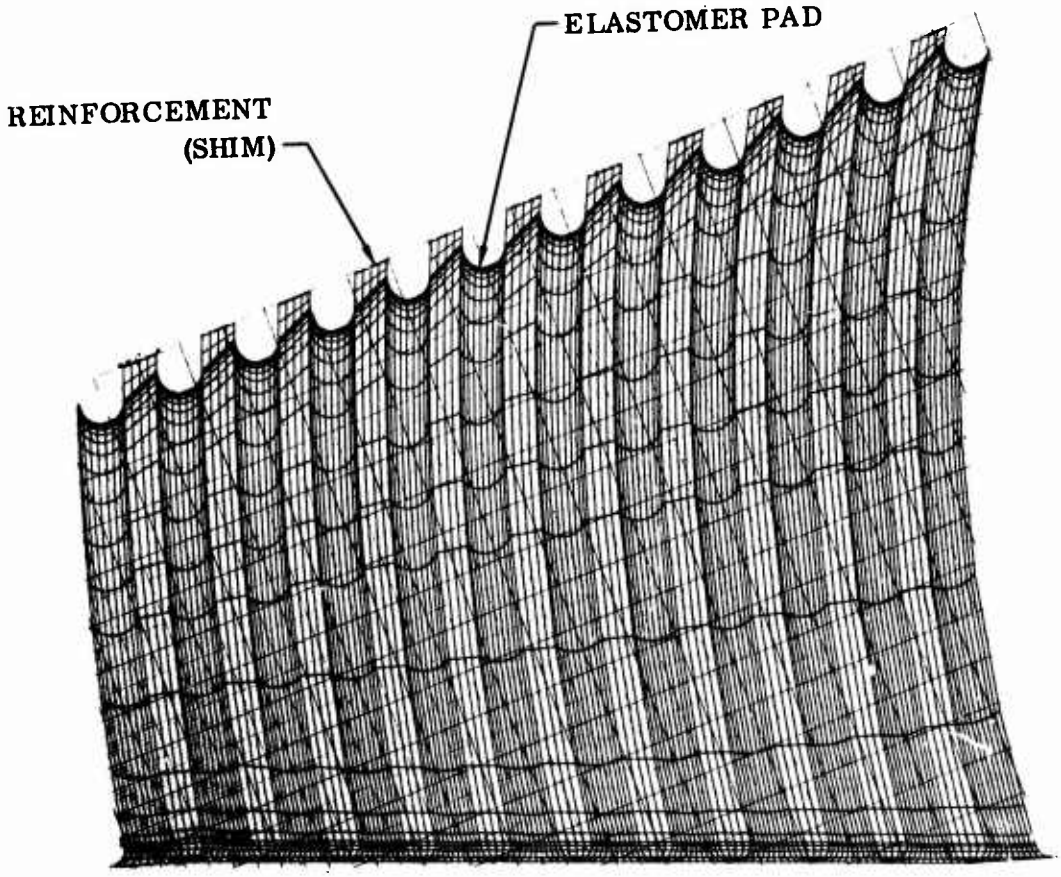

FINITE-ELEMENT MODEL

Figure 7-8. Finite-element model of Type III bearings.

7.2.4 Computer Time Considerations

It is desirable to have a large number of nodal points to closely approximate the contours of an actual problem. This will produce a fine mesh together with high accuracy of results. However, computer run times are very dependent on the fineness of the mesh used. Most efficient use of the program storage (region) is obtained by using the lowest possible integer for I. Computer run times are approximately proportional to the I^2J. This rule of thumb will usually provide a close estimate of run times and is based on experience gained in using the computer program.

The computer program user is provided with a "Mesh Only" option in running the program. It should be used to check the input and finite-element grid for any input errors. Computer time for running a "Mesh Only" program is usually about one minute.

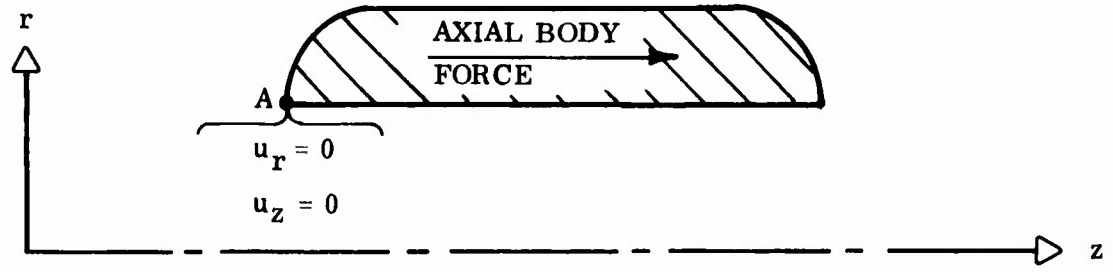

Figure 7-9. Boundary conditions for preventing rigid-body motions.

GEOMETRY

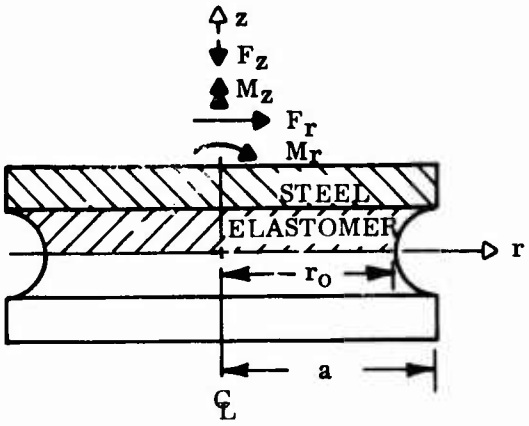

CONDITIONS AND PROCEDURE

1. MODEL SECTIONED HALF FOR FINITE-ELEMENT RUN. (NOTE: ▷ IS COORDINATE; → IS APPLIED LOAD)
2. F_z, F_r, AND M ARE APPLIED AXIAL LOAD, SHEAR AND MOMENT, RESPECTIVELY
3. AXIS OF REVOLUTION IS Z.

FINITE-ELEMENT MODEL[a]

CONDITIONS AND PROCEDURE

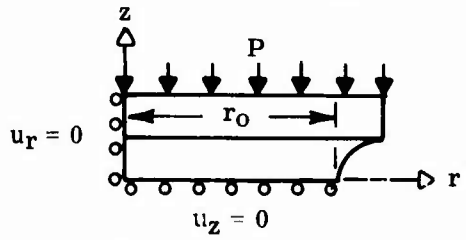

1. FOR AXIAL LOAD (F_z) USE HARMONIC = 0
2. SIMULATE AXIAL LOAD F_z AS PRESSURE P.

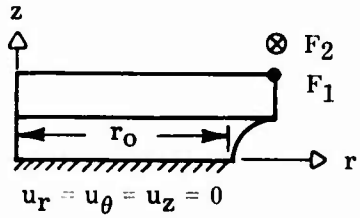

1. FOR SHEAR LOAD (F_r), USE HARMONIC = 1
2. USE $F_1 = -F_2$ = APPLIED SHEAR LOAD (F_r)
3. F_2 IS INTO PLANE OF PAPER

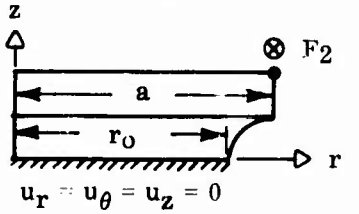

1. FOR TORQUE (M_z) USE HARMONIC = 0
2. USE $F_2 = M_z/a$

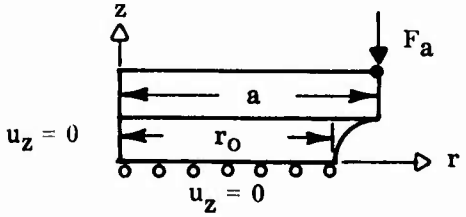

1. FOR MOMENT (M_r), USE HARMONIC = 1
2. USE $F_a = \frac{2M_r}{a}$

[a]COMPUTER WILL GIVE HALF OF TOTAL DEFLECTIONS

Figure 7-10. Finite-element representation of Type I bearing.

GEOMETRY

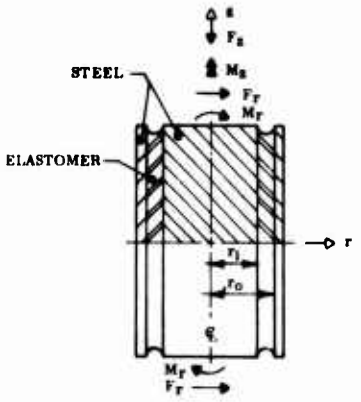

CONDITIONS AND PROCEDURE

1. MODEL SECTIONED HALF FOR FINITE-ELEMENT RUN. (NOTE: —▷ IS COORDINATE; —▶ IS APPLIED LOAD)
2. AXIS OF REVOLUTION IS Z.

FINITE-ELEMENT MODEL[a]

CONDITIONS AND PROCEDURE

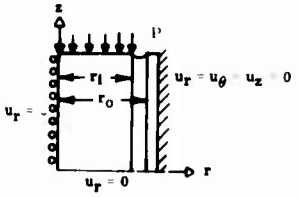

1. FOR AXIAL LOAD (F_z), USE HARMONIC = 0
2. SIMULATE AXIAL LOAD $F_z/2$ AS PRESSURE P.

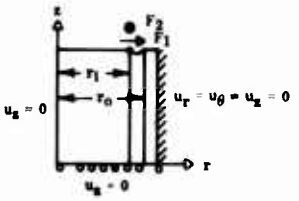

1. FOR RADIAL LOAD (F_r), USE HARMONIC = 1
2. USE $F_1 = -F_2 = \frac{F_r}{2}$
3. F_2 IS INTO PLANE OF PAPER

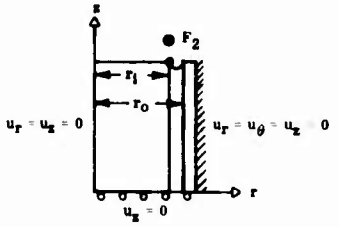

1. FOR TORQUE (M_z), USE HARMONIC = 0
2. USE $F_2 = \frac{M_z}{2r_i}$

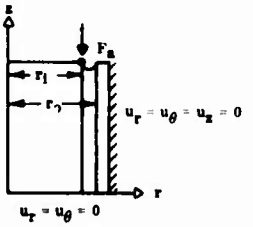

1. FOR MOMENT (M_r), USE HARMONIC = 1
2. USE $F_a = \frac{M}{r_i}$

[a]COMPUTER OUTPUT WILL GIVE TOTAL DEFLECTIONS.

Figure 7-11. Finite-element representation of Type II bearings.

CONDITIONS AND PROCEDURE

1. SIMILAR TO TYPE I EXCEPT THAT ENTIRE HALF OF BEARING MUST BE MODELED. (NOTE: —▷ IS COORDINATE; —▶ IS APPLIED LOAD)

2. COMPUTER OUTPUT WILL GIVE TOTAL DEFLECTIONS.

3. AXIS OF REVOLUTION IS Z.

GEOMETRY

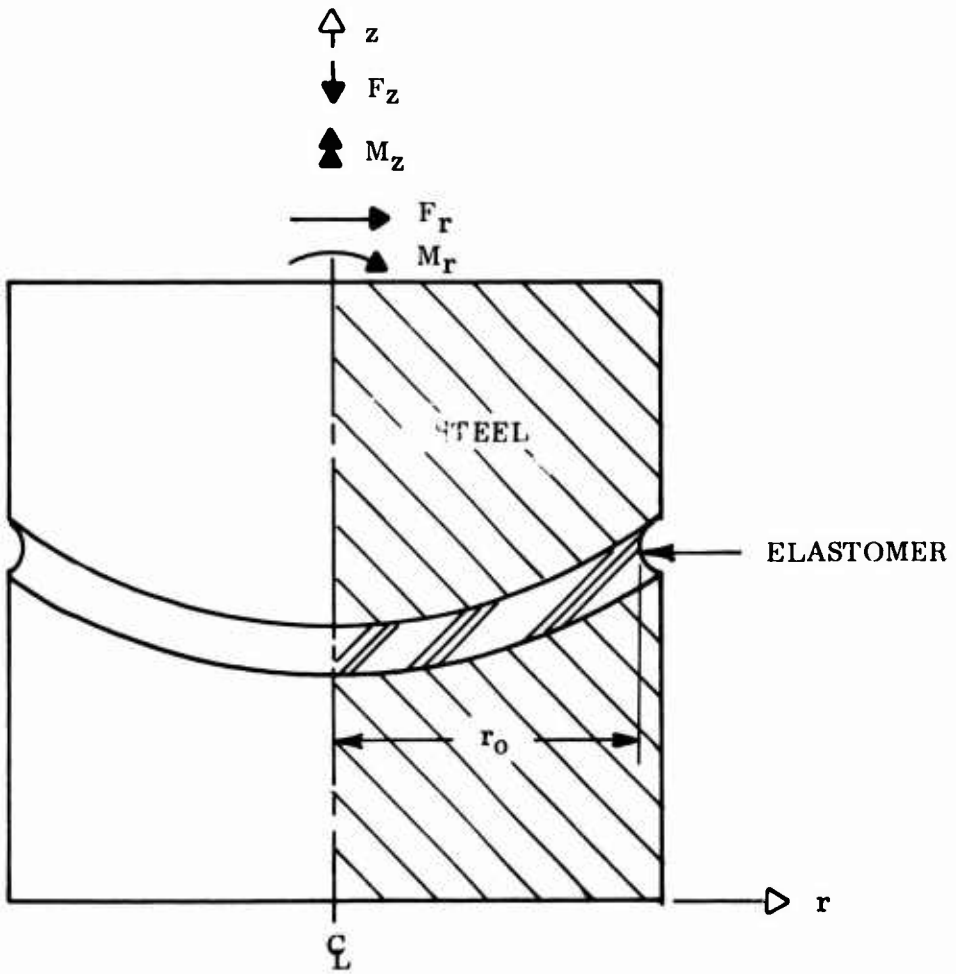

Figure 7-12. Finite-element representation of Type III bearings.

7.3 INPUT-OUTPUT FEATURES OF COMPUTER PROGRAM

7.3.1 Material Properties Input

The computer program accepts isotropic material properties as a function of temperature or strain. Each element within the grid can be assigned with a material property of its own. These properties are taken from the master material property listing. To help the user detect errors, the output lists the type of each element by its material name. Details of material property input can be found in Volume III.

7.3.2 Nonlinear Properties (k_1, k_2) Input

Linear analyses are normally sufficient for obtaining the stresses and strains in helicopter bearings with sufficient accuracy for engineering evaluations. However, the computer code includes capability to perform more accurate stress analysis for materials which have nonlinear constitutive equations as well as large deformations (the Eulerian form of nonlinear strain-displacement relations is used). The materials are assumed to behave according to the relation between principal stresses (σ_i) and large deformation principal strains (E_i) (Reference 3-20) given by

$$\sigma_i = 2k_1 [E_i + k_2 H + f/3 - e_t] \tag{7-1}$$

where

k_1 and k_2 = nonlinear material property functions

$$H = \frac{\sigma_1 + \sigma_2 + \sigma_3}{2k_1 (1 + k_2)} \tag{7-2}$$

$$e_t = \alpha \Delta T \tag{7-3}$$

$$f = -2 (E_{11} E_{22} + E_{11} E_{33} + E_{22} E_{33}) + 2 E_{12}^2 (1 - 2 E_{33}) + 4 E_{11} E_{22} E_{33} + \frac{3 (e_t)^2 \left(\frac{3}{2} + e_t\right)}{(1 + e_t)^2} \tag{7-4}$$

To gain a better insight into the constitutive equation (Equation 7-1), we note that f is proportional to (strain)^2; hence, for relatively small strains it may be neglected when compared to E_i. For linear materials under small strain (ϵ_i), the constitutive relation is normally written as

$$\sigma_i = 2\,G\,[\epsilon_i + \nu H - e_t] \tag{7-5}$$

By comparing Equations 7-1 and 7-5, it can be seen that k_1 corresponds to G while k_2 corresponds to ν for small deformations. Thus, for nonlinear materials subjected to small deformations, the shear modulus (G) and Poisson's ratio (ν) are used as functions of maximum principal strain (ϵ_i).

To determine the nonlinear material constants (k_1 and k_2) for a general material, any of a number of laboratory tests are possible. However, if pads are made from a natural-rubber vulcanizate, the material properties are dependent upon load rate, temperature, and stress field. Therefore, tests simulating these parameters over the range normally expected for the bearing application should be used. The following procedure is an outline of one possible method for k_1 and k_2 determination.

1. Determine volume change (ΔV) versus hydrostatic pressure (P) from bulk modulus (k) data using

$$\frac{\Delta V}{V_o} = -\frac{P}{k} \tag{7-6}$$

Note: The above equation is used to determine the volume change parameter (e_v) defined as

$$e_v = \frac{V^2 - V_o^2}{2V^2} = \frac{\Delta V\,(V + V_o)}{2V^2} \tag{7-7}$$

For small volume changes ($V \simeq V_o$) in compressing rubber, the volume change parameter is

$$e_v \simeq \frac{\Delta V}{V} \simeq \frac{\Delta V}{V_o} = -\frac{P}{k} \tag{7-8}$$

2. Test a square block of rubber of width (w) and thickness (h) as shown in Figure 7-13 in uniaxial compression at a constant strain rate. The rubber surfaces which contact the faces of the compression apparatus should be lubricated so that lateral stresses are negligible. Measure axial load (F_z) and axial deflection (u_z^{ave}).

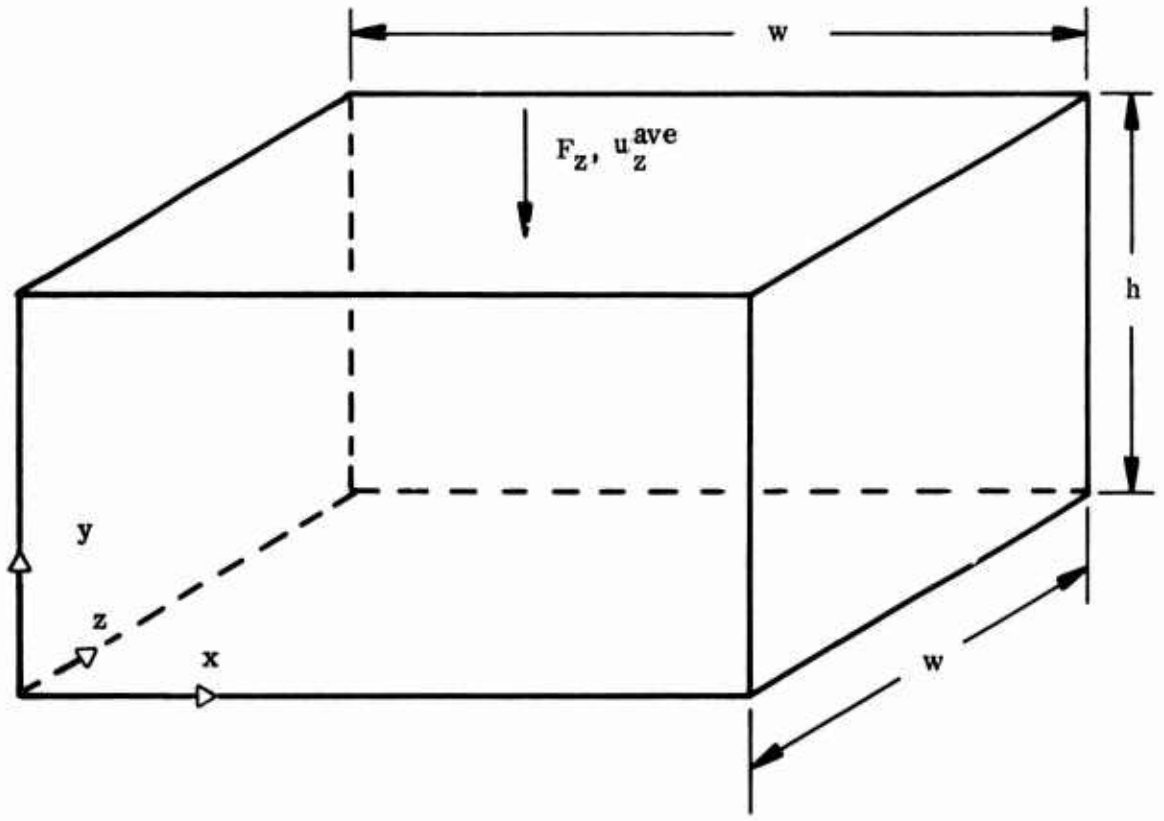

Figure 7-13. Rubber block for k_1 and k_2 determination.

3. From the test results, the following parameters can then be calculated.

Axial extension ratio (λ_1):

$$\lambda_1 = 1 + \frac{u_z^{ave}}{h} \tag{7-9}$$

Large deformation strain components (E_1, E_2 and E_3):

$$E_1 = 1/2\left[1 - \left(\frac{1}{\lambda_1}\right)^2\right] \tag{7-10}$$

$$E_2 = E_3 = \frac{E_1 - e_v}{2E_1 - 1} \tag{7-11}$$

Constant (f):

$$f = -2\left[2\,E_1\,E_2 + E_2^2\right] + 4\,E_1\,E_2^2 \tag{7-12}$$

Material properties (k_1 and k_2):

$$k_1 = \frac{F_z\,\lambda_1}{2\,w^2\,(E_1 - E_2)} \tag{7-13}$$

$$k_2 = -\frac{E_2 + f/3}{E_1 + f/3} \tag{7-14}$$

7.3.3 Output

In order to illustrate the type of data that is available from the computer run, a sample output of a typical bearing analysis is given in Volume III. It shows the type and versatility of the computer program and allows the user to obtain a clear understanding of the overall structural behavior of the problem being analyzed.

The user is also provided with plots of the grid before and after deformation.

7.4 RUNNING THE FINITE-ELEMENT PROGRAM

The standard practice for running the program is to request a "Mesh Only" run for the first time frame analysis as an aid in determining the accuracy of the input. This is achieved by carefully checking boundary conditions, loads generated by boundary conditions, material properties, and temperatures. A study of the undeformed geometry grid plot is also helpful in determining if there is any error in nodal locations or if grid spacing is acceptable. Any changes in grid fineness should be made at this time. After the user is satisfied with the input, he should request a complete program output. The output should be checked for validity and reasonableness of the solutions. After the user is satisfied that the analysis results are accurate, the bulk of the output could be suppressed by using the "Print Suppress" feature as explained in Volume III.

8.0 STABILITY

The great flexibility of an elastomeric bearing causes its size to be limited largely by stability. Much work remains to be done in the area of stability of elastomeric bearings. Because of the lack of a fully developed stability theory, analysts have used rules of thumb to maintain stability and prevent collapse of the bearing as a column. Some of these rules of thumb are given in Reference 8-1. The following analytical discussion applies to all types of bearings.

8.1 ANALYTICAL DISCUSSION

A column consisting of alternate elements of elastomer pads and shims deforms in two ways by:

1. Simple shearing in which one plate is displaced parallel to the other in its own plane, and
2. Bending in which one plate is rotated with respect to the other about an axis of symmetry in its own plane.

Consequently, the stability of a column depends on its bending and shear stiffness. Figure 8-1 shows a column with fixed ends being compressed. Following Haringx (References 8-2 thru 8-4) and Gent (Reference 8-5), the critical buckling load (F_z^c) is given by

$$\frac{F_z^c}{K'_{\theta_r}}\left(1+\frac{F_z^c}{K'_r}\right)=\left(\frac{\eta^2\pi^2}{L^2}\right) \tag{8-1}$$

where K'_{θ_r} and K'_r are the reduced bending and shear stiffness of the column, respectively.

They are related to the corresponding stiffness of a single pad by

$$K'_r = (h+t)\,K_r \tag{8-2}$$

$$K'_{\theta_r} = (h+t)\,K_{\theta_r} \tag{8-3}$$

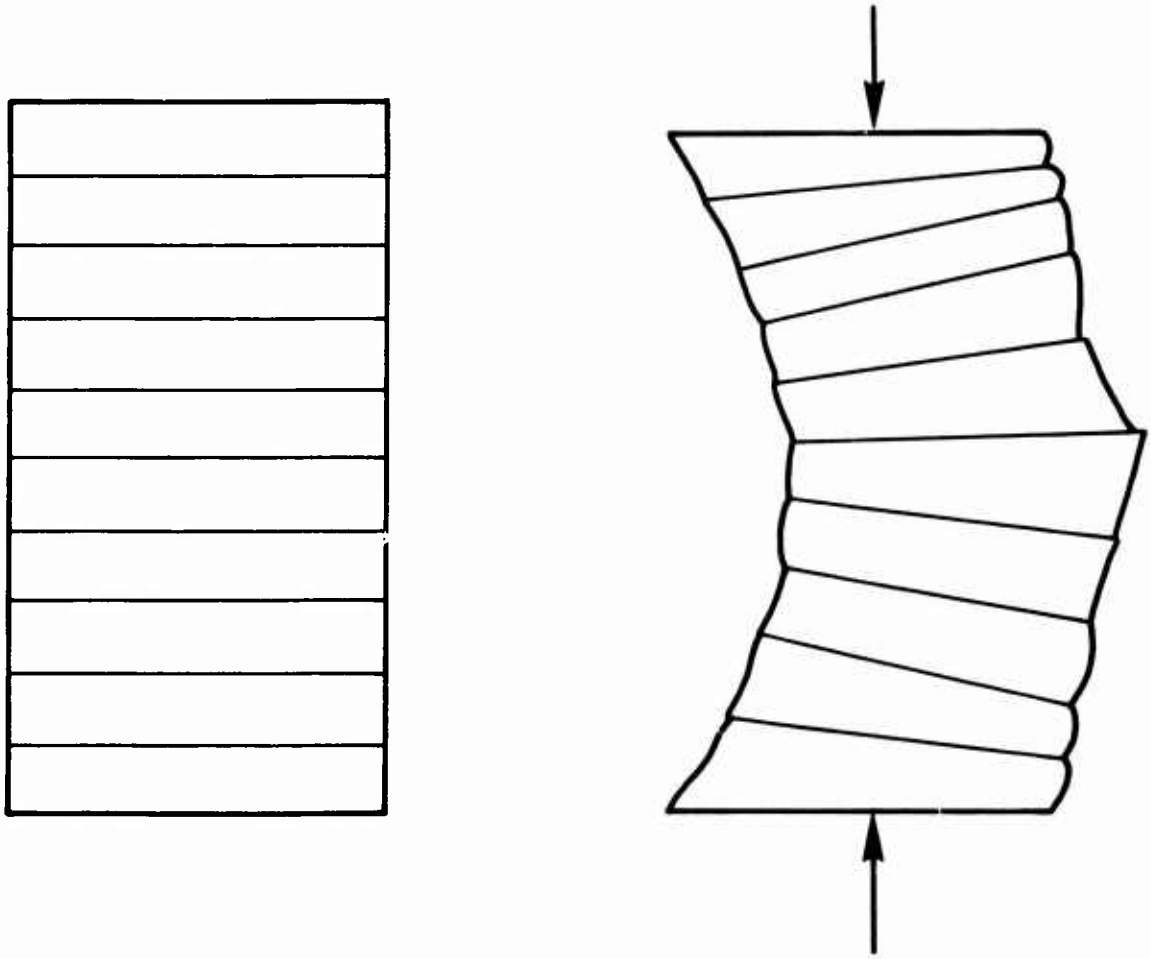

Figure 8-1. Column of bonded rubber blocks before and after compression loading.

In Equation 8-1, η is the coefficient of fixity which has the following values:

Column End Condition	Coefficient of Fixity (η)
Both fixed	2
One fixed; other free	1/2
One fixed; other pinned	$\sqrt{2}$
Both pinned	1

In normal helicopter applications, $\eta = 2$ because the end plates of the bearing are held rigid.

The critical compression in a pad (ϵ_z^c) at the buckling load is given by

$$\epsilon_z^c = \frac{F_z^c}{AE_A} \tag{8-4}$$

where A = cross-sectional area of pad

E_A = apparent modulus of elastomer in compression

Equation 8-4 assumes that all the compression is in the elastomer alone. This is a valid assumption in view of the fact that the shim material is substantially stiffer than the elastomer.

8.2 DESIGN CONSIDERATIONS

The design considerations for different types of units will now be discussed separately.

8.2.1 Type I Bearings

Type I bearings are frequently employed as thrust bearings in helicopter applications. The compressive load on the bearings is the blade centrifugal force (CF), and this load is reacted by the restricted lateral expansion of the rubber.

The bending and shear stiffness expressions for an elastomer pad in the Type I bearing have been presented earlier. Equation 8-1, therefore, gives the critical buckling load upon substitution of these stiffnesses.

In the theoretical analyses used in deriving Equation 8-1, the pads have been treated as incompressible. This assumption is satisfactory for long columns. Helicopter bearings, however, are short and undergo significant compression before buckling. Therefore, the buckling load is considerably larger than that predicted by Equation 8-1. To account for this compression, an iterative technique is used to correct for the changing geometry of the column as it is being compressed. It significantly improves correlation between theory and experiment. Details of this technique are given in Volume I. The iterative procedure has been incorporated into the stability module of the finite-element computer program that is provided for use with this manual.

Certain observations will now be made concerning Type I columns. Equation 8-1 assumes rigid shims, which implies that the buckling load will not be affected by large changes in shim thickness. The theoretical results are shown in Figure 8-2 for various columns in which the shim thickness was varied, but the total elastomer thickness was kept constant. Changing the shim thickness caused the column height to change without significantly affecting the buckling load. Therefore, the total thickness of rubber in the column is the governing factor in determining buckling load.

ELASTOMER THICKNESS: 0.125 IN.
NO. OF ELASTOMER PADS: 16
NO. OF SHIMS: 15
ELASTOMER MODULUS: 290 PSI
COLUMN HEIGHT (IN.):

A	2.6
B	3.2
C	3.8

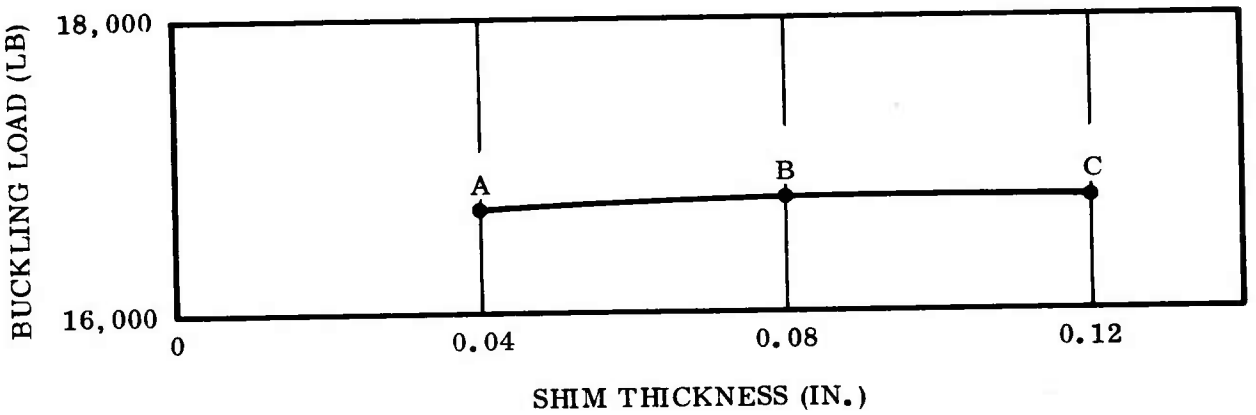

Figure 8-2. Buckling load vs shim thickness.

Elastomer thickness in helicopter applications is normally of the order of 0.03 to 0.09 inch. The critical buckling load as a function of the total height of a column is shown in Figure 8-3 for various elastomer pad thicknesses. The figure shows that--for short columns with thin elastomer pads--a slight change in the elastomer pad thickness causes a large change in the buckling load. Table 8-1 lists the buckling loads which indicate this sensitivity. Therefore, in manufacturing bearings with thin elastomer pads, a close tolerance on pad thickness is necessary.

TABLE 8-1

EFFECT OF PAD THICKNESS ON BUCKLING LOAD

Elastomer Pad Thickness (in.)	Buckling Load (lb)
0.037	134,048
0.038	127,016
0.039	120,521

Pad quantities	22
Steel shim quantities	21
Elastomer modulus	290 psi
Inner diameter	0 in.
Outer diameter	3 in.
Shim thickness	0.063 in.

The percentage of critical compression that the column undergoes at the onset of buckling is shown in Figure 8-4. It can be seen that the compression for the shorter columns can be quite significant.

The problem of designing a Type I bearing from the point of view of stability is rather complicated. It would be desirable to have a design curve that relates all the variables that affect stability, but this does not seem possible at the present time. The reason for this complication is the form of Equation 8-1. The buckling load is not directly proportional to the bending stiffness, but is also dependent on

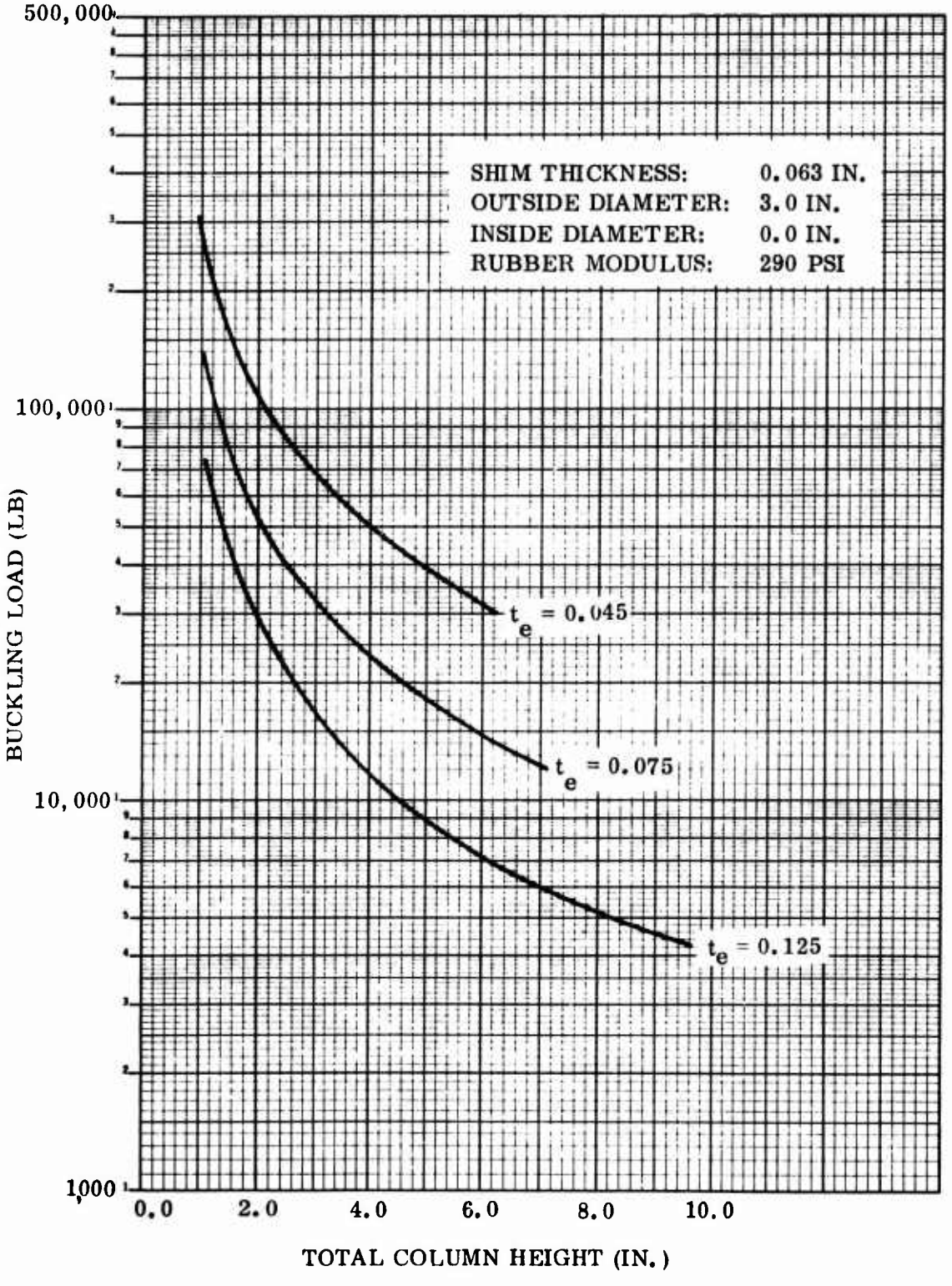

Figure 8-3. Effect of elastomer thickness on buckling load.

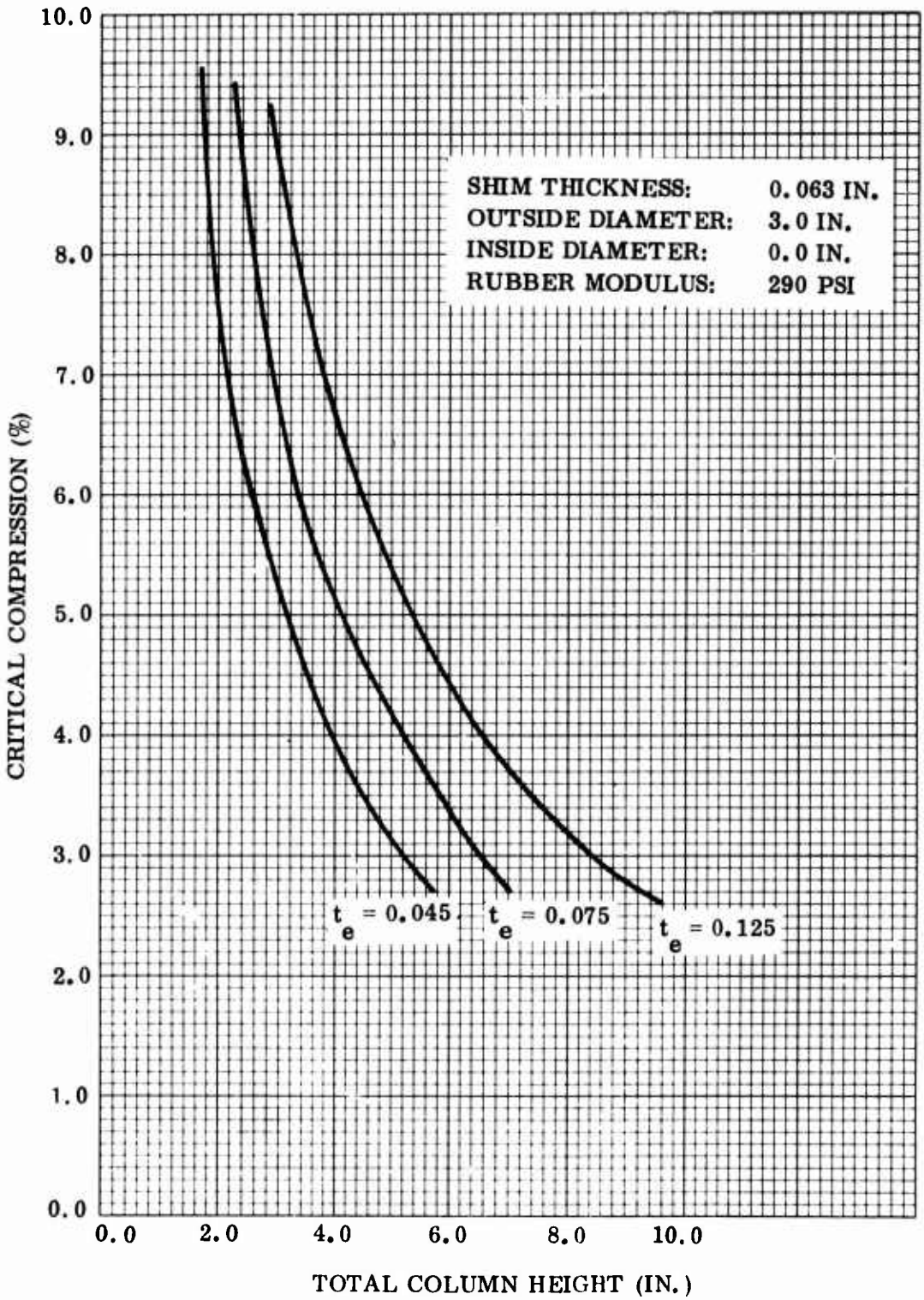

Figure 8-4. Effect of elastomer thickness on critical compression.

the shear stiffness. The dependence of the buckling load on the column variables is nonlinear. The reason for this nonlinearity is due to the use of the iterative procedure in the finite-element program. The relationship between the variables cannot be expressed by a simple multiplying factor. As a result, changing the column variables by a certain factor will not change the buckling load by a multiple of the same factor. Therefore, if an accurate estimate of the buckling load for a particular geometry is desired, a computer run using the stability module in the computer program is necessary.

For initial stability design purposes, the following equation is useful:

$$\frac{F_z^c}{\eta^2 G n r_o^2} = \frac{\pi^2}{16\sqrt{2}} \left(\frac{r_o}{h^T}\right)^2 \left(1 + \frac{r_i}{r_o}\right) \left(1 - \frac{r_i}{r_o}\right)^2 \sqrt{1+\left(\frac{r_i}{r_o}\right)^2} \quad (8\text{-}5)$$

The equation relates the critical buckling load (F_z^c) to the number of elastomer pads (n), shear modulus (G), pad outer radius-to-total thickness ratio (r_o/h^T) and pad inner radius-to-outer radius ratio (r_i/r_o). It is valid for shape factors greater than five and gives a conservative estimate of the average buckling stress (buckling load/cross-sectional area of column). For example, the buckling load predicted by the computer program for the solid circular pads is generally 10% higher than that predicted by Equation 8-5. The computer-predicted buckling loads are 25% higher for the annular pads with a r_i/r_o radius ratio of 1/3.

The following procedure for stability design is recommended:

1. Use Equation 8-5 to determine the buckling load as discussed in the section on Type I design. If the buckling load is appreciably greater than the CF load on the bearing, no stability problems exist.

2. If the buckling load given by Equation 5 is equal to or slightly less than the CF load, determine the factor of safety that exists by using the computer program. If the factor of safety is marginal, the procedure has to be repeated by considering a different pad design.

8.2.2 Type II Bearings

Buckling is generally not a problem with the Type II bearings. The geometry of the bearing is such that instability does not occur in typical helicopter configurations. However, if the diameter of the bearing is very large in comparison to its length, the bearing may become unstable under the applied radial loads.

8.2.3 Type III Bearings

Type III bearings could be manufactured with concentric shims or with equal radius shims. In the concentric configuration, the bearing would have a single pivot point. In the equal radius configuration, each elastomer pad in the bearing has a variable thickness. Figure 8-5 shows the two configurations. A Type III bearing built in the form of a cylinder (constant outer and inner diameters) with equal radius shims would have constant bending and shear stiffness per pad in the entire column. The analysis of this bearing will, therefore, be similar to that for the Type I bearing. The bending and shear stiffness expressions are given in the section on Type III bearing design.

For the bearing with concentric shims, the bending and shear stiffness would vary through the bearing. In this case, the analysis becomes more complicated. The load-carrying capacity, however, does not differ substantially from that for an equivalent bearing comprised of equal radius shims (Reference 8-7).

If the bearing is tapered, the stability analysis becomes very complicated. In such cases, energy methods have been found to be very useful. More advanced mathematical treatments by energy methods can be found in References 8-8 and 8-9.

The theoretical buckling analysis of simple Type III bearings has not been verified experimentally. Further effort is required before a complete tested analysis is available.

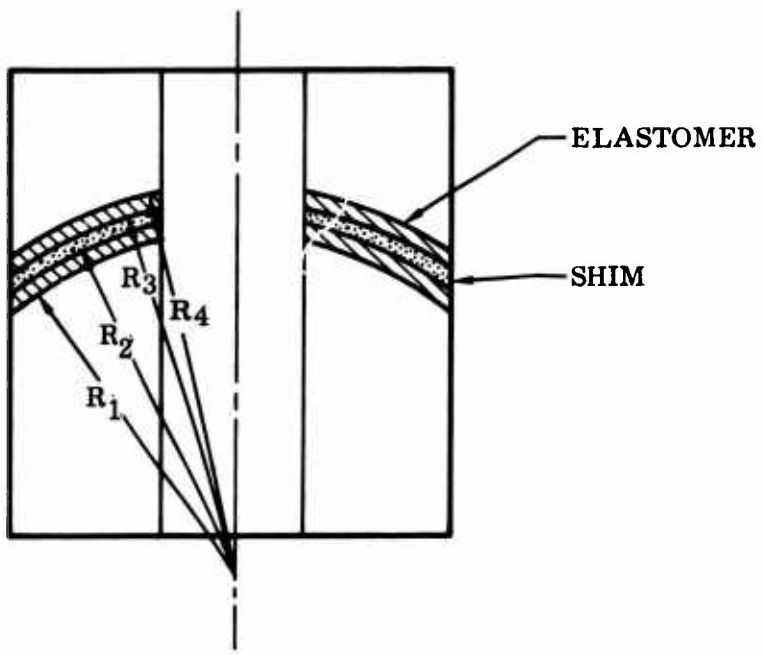

CONCENTRIC SHIM

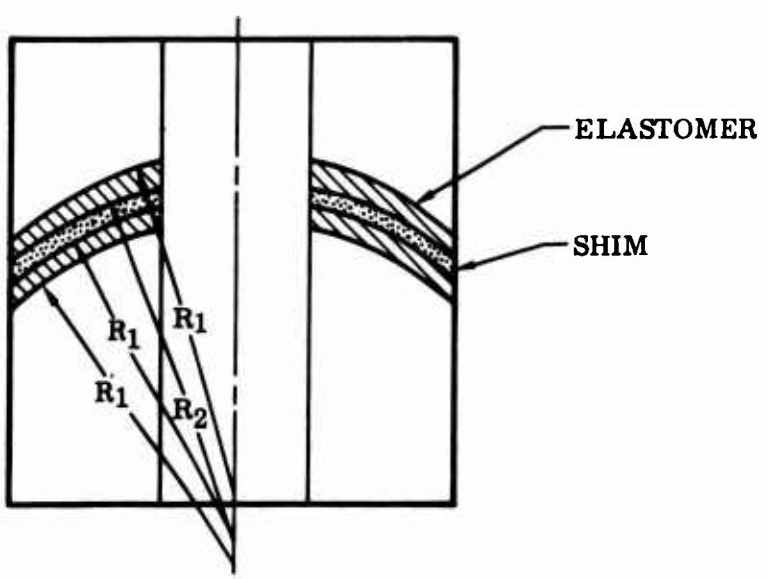

EQUAL RADIUS SHIM

Figure 8-5. Type III bearing configurations.

8.3 SUMMARY

The buckling load is characterized by the bending stiffness and the shear stiffness of a single pad in the column. This is based on the theory developed by Haringx and Gent for a beam column subjected to axial and shear loads. The theoretical buckling load is independent of the initial crookedness of the column, the magnitude of the shear (transverse) load and any eccentricities in load application. The bending and shear stiffnesses are related to pad dimensions for simple shapes. The bending stiffness for complicated shapes will have to be determined experimentally or with the aid of the finite-element computer program.

In the theoretical treatment used in deriving Equation 8-1, an axial load acting alone will always produce large deformations when it is close to the critical value. When the lateral loads are small in comparison to the critical load, their effect on the deflection is negligible. But if the lateral loads are large, a smaller axial load will be required to cause large deformations.

Equation 8-1 is derived for a perfectly straight and centrally loaded column. The experimental loads depend considerably upon these factors. With increasing accuracy in straightness and application of load, the closer will be the critical load to the theoretically predicted load. Initial imperfections in the column shape can be determined by using a Southwell plot (Reference 8-10).

Stability of a column is generally improved by using chevroned or stepped shims. Care should be exercised in choosing the chevron geometry so that high shim stresses are not set up. A careless choice of the chevron geometry may result in shim failure.

If the factor of safety for the buckling design is not adequate, the bearing will be subjected to fairly large deflections which can cause excessive tilting in a pad in the column. The tilting induces compressive and tensile loads in the two halves of the pad, and the latter loads can cause internal rupture. The critical value of the tilt has been derived by Gent (Reference 8-11) for various pad geometries.

9.0 SERVICE LIFE

The initial effort in service life prediction is to determine the most probable mode of failure for a given bearing. There are basically two types of mechanisms which lead to failure of elastomeric bearings:

1. Mechanical, in which case failure takes place by initiation and propagation of debond between pads and shims or initiation and propagation of cohesive failure within either a pad or a shim.
2. Bulk degradation of the rubber due to the reversion phenomenon, oxidation, etc.

The mechanisms leading to failure for a given bearing depend upon many factors, so each mechanism should be considered for every bearing.

9.1 MECHANICAL FAILURES

9.1.1 Eliminate Points of Stress Singularity

The initiation and propagation of flaws is an important consideration in mechanically induced failures. The point of fracture initiation depends upon the applied load as well as the bearing geometry. If the pad ends are not properly filleted (included material angle of the pad is greater than 63 degrees for plane geometries; Reference 9-1), an infinite stress is predicted by linear elastic analyses at these points (Reference 9-2). Analytical predictions of debond initiation, in such cases, requires a detailed fracture mechanics analysis and a laboratory evaluation of adhesive fracture energy (Reference 9-3). The linearity assumption is violated as stresses become large near crack (debond) tips in real materials so that the infinite stresses do not exist. However, at such points, known as singular points, the stresses in real materials generally become very large and are often the point of debond initiation. Therefore, it is recommended that the theoretical singular points be avoided by use of appropriate bond end geometries.

9.1.2 Determine Point of Failure Initiation

Once the theoretical singular points have been removed, the stresses within the pads can be determined accurately by a finite-element computer program; in some cases, analytical approximations are sufficient. For a bearing in compression, the point of fracture or debond initiation is then determined by comparing a classical failure criterion--such as maximum shear stress or strain--with the maximum shear stress or strain capability determined from laboratory testing. Tensile loads should be avoided where possible since cavitation (cohesive fracture initiation) of the pad material is experienced at very low tensile stresses. In hydrostatic tension, cavitation in rubber initiates when the stresses are about 3/4 of the elastomer tensile modulus (Reference 5-2).

Stress analyses combined with classical failure criteria are considered to be sufficient to determine the point of failure initiation in the shims.

9.1.3 Determine Flaw Growth Rate

The initiation of either debond or cohesive fracture cannot be interpreted as bearing failure since bearings have been observed to function satisfactorily for many hours after initiation of failure, as reported in Volume I. Therefore, we must also consider the growth rate of a crack. For such problems, the strain energy remains finite and an energy balance procedure as originally proposed by Griffith (Reference 9-4) is used.

9.1.4 Pads

The energy available per unit area of growth in rubber is normally termed (Reference 3-5) the tearing energy (γ_t) and is defined mathematically by

$$\gamma_t = \left| \frac{\partial U^T}{\partial A_f} \right| \qquad (9\text{-}1)$$

where U is total elastic strain energy stored in body under consideration

A_f is area of one side of fracture surface

The above definition applies to both adhesive and cohesive fracture. The terms "adhesive fracture energy" (γ_a) and "cohesive fracture energy" (γ_c) are used to denote the value of tearing energy for which cohesive and adhesive fracture propagates.

A good summary of the use of tearing energy for predicting fatigue life is contained in a paper by G. J. Lake (Reference 9-5), in which the following significant observations have been made:

1. Crack growth rate (dc/dN) and cohesive fracture energy are linearly related on a log-log plot; therefore, a power law representation should apply that is of the form

$$dc/dN = B\gamma_c^{\beta} \qquad (9\text{-}2)$$

where B is an empirically determined constant

$\beta \simeq 2$ for natural rubber vulcanizate

2. A finite fracture energy (γ_o) is required for fatigue propagation of mechanical cracks. This value is about 0.3 in.-lb/sq in. for a range of elastomers including natural rubber, SBR, polychloroprene, and butyl rubber. In addition, it has been shown that γ_o is not very sensitive to temperature over the range of 70° to 120° F.
3. Crack growth rate depends upon the minimum to maximum tearing energy ratio. At the present time, correlations between dc/dN and γ_c are comparatively poor when the cycling passes through the zero strain state. This is probably not a major limitation for helicopter bearings where a net axial force is applied.

Fatigue life can be reduced dramatically by ozone degradation (References 9-6 and 9-7). In fact, the crack growth rate due to ozone concentration can be more important than that due to mechanical fatigue in natural rubber formulations if proper ozone protection is not afforded.

Although a major portion of the fatigue effort has been applied to cohesive fracture in elastomers, Reference 9-8 shows that similar results apply to fatigue loading in adhesive fracture.

9.1.5 Reinforcements

The theory and experimental data for crack growth rate, S-N curve behavior, and fatigue limit for metal reinforcements is presently quite well documented for various metals. See References 3-24 and 9-9 thru 9-11 for detailed information on this subject.

9.2 BULK DETERIORATION OF PADS

There are at least two possibilities for bulk deterioration of pads. The first is due to attack by oxygen. It is generally possible to add antioxidants to rubber compounds; these antioxidants are very effective in preventing this failure mode. A second possibility is rubber reversion due to heat generated during cycling. Heat can be generated due to surface friction between small surface cracks (possibly caused by ozone attack) or between pads and shims if a poor bond system is present.

The major cause of bearing fatigue failure seems to be heat generated within the pads due to viscous flow. The strain energy loss per cycle due to viscous flow is converted into heat. The heat generated per cycle ($\dot{q}$) can then be calculated by Equation 3-11. Since the heat generation rate depends upon energy density, it may be different at each point in the bearing. Equation 3-11 can be used to calculate the heat generation rate at any point in the body by integrating over a small volume. Once the heat generation rate as a function of position is known, the temperature at any point in the bearing versus time can be obtained using either approximate closed-form solutions to the heat transfer equations or any of a number of numerical techniques presently in existence. A complete analysis will involve an iterative process since temperature changes cause corresponding changes in material properties and thermally induced strains.

Theoretically, one could then determine pad degradation rate by combining the temperature, strain, and time analytical results with rubber reversion rate data. Since the analytical procedure has not been verified at present and since rubber reversion rates are not generally known, the use of a failure surface is suggested.

9.2.1 Failure Surface for Pads

The testing of a series of Type I bearings was completed for a wide range of static and dynamic loads (see Volume I). The basic bearing used in these tests is

shown in Figure 9-1. Each bearing consists of only 2 pads with 3 relatively thick shims. The outer diameter of the pads was cast in the form of a circular fillet, and the inside diameter of the shims was tapered to eliminate stress singularities at pad end bondlines. A complete description of these tests is contained in Volume I, with the test results presented in Figure 9-2. The decay in torsional spring rate by 20 percent was defined as bearing failure because the spring rate decay was generally very rapid after the 20 percent decrease was noted. All bearings for which no reversion was noted survived the applied loads for 30×10^6 cycles. The form of the failure data plotted in Figure 9-2 is not suitable for direct interpretation with respect to other bearing designs. Since failures are evidently initiated in these bearings due to heat generation, parameters more directly related to heat generation rate should be used. The most directly applicable parameters are temperature, time, and some measure of load. However, additional research and heat transfer analyses are necessary before these parameters can be used directly. A simpler choice is maximum strain energy density since this parameter is proportional to heat generation rate and is also easily calculated by the finite-element computer program (see Volume III). Strain energy density (U) is defined as

$$U = \frac{1}{2E} (\sigma_r \epsilon_r + \sigma_\theta \epsilon_\theta + \sigma_z \epsilon_z + \tau_{r\theta} \gamma_{r\theta} + \tau_{\theta z} \gamma_{\theta z} + \tau_{rz} \gamma_{rz}) \tag{9-3}$$

or, in terms of stresses, it is defined as

$$U = \frac{1}{2E} (\sigma_r^2 + \sigma_\theta^2 + \sigma_z^2) - \frac{\nu}{E} (\sigma_r \sigma_\theta + \sigma_r \sigma_z + \sigma_z \sigma_\theta) \tag{9-4}$$

$$+ \frac{(1+\nu)}{E} (\tau_{r\theta}^2 + \tau_{rz}^2 + \tau_{z\theta}^2)$$

The data presented in Figure 9-2 show a fatigue life dependency upon average axial strain (ϵ_z^{avg}). This dependency is probably due to the following:

1. A closing of microflaws, which allows adjacent faces to slide over each other during cycling and thus adds to the heat generation rate (also causes the torque-rotation relationship to become nonlinear).

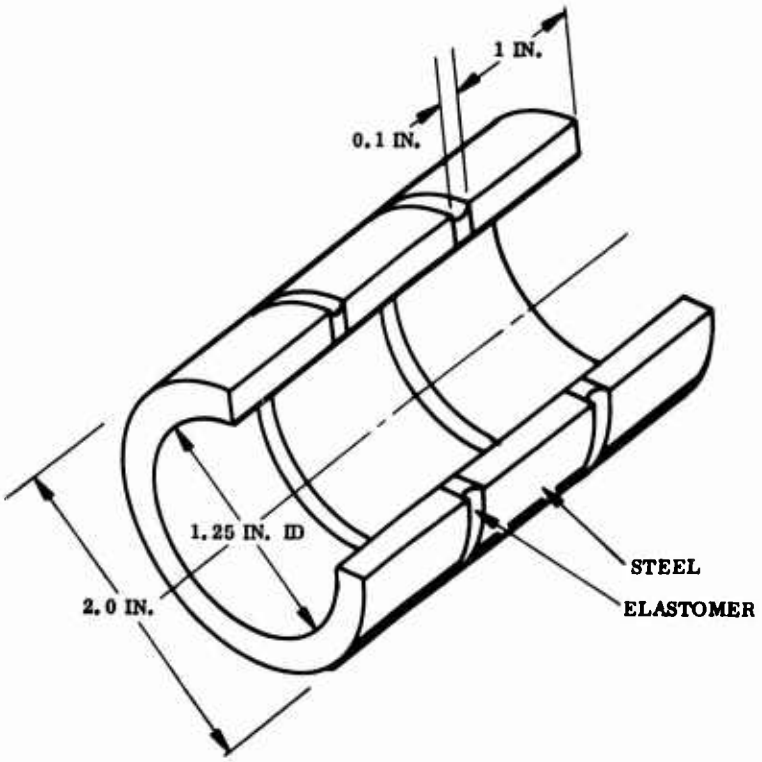

Figure 9-1. Geometry of Type I bearing specimen.

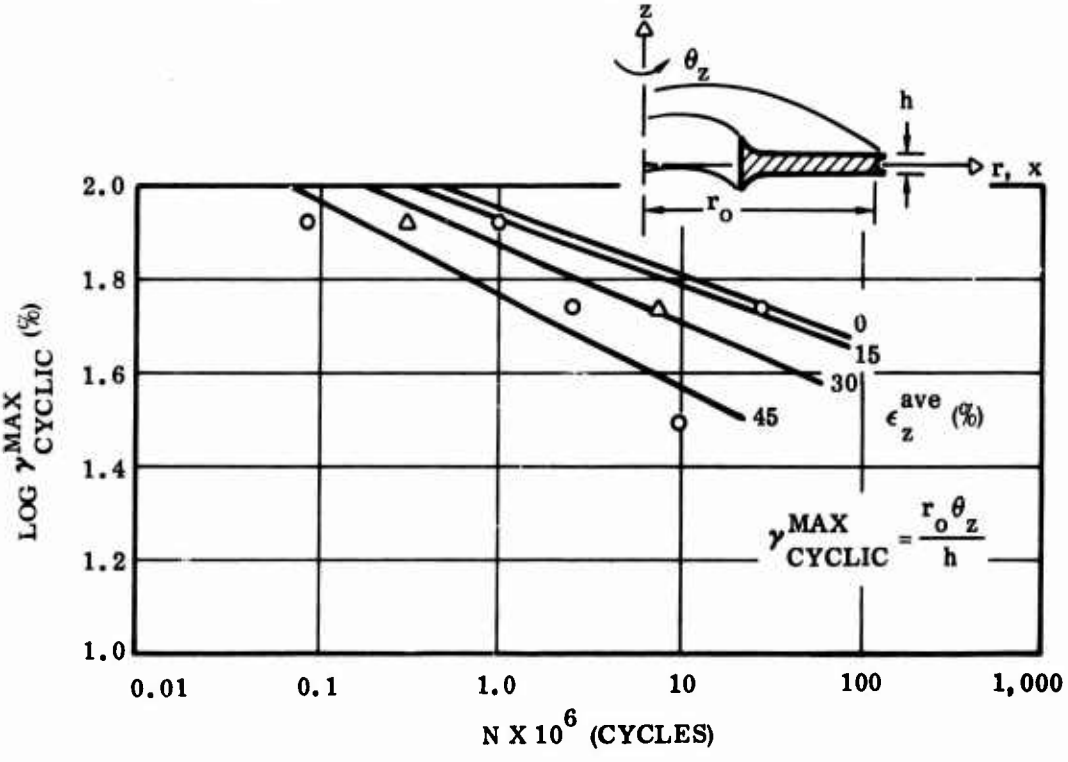

Figure 9-2. Type I bearing failure surface.

2. The adding of a steady-state shear load to the oscillatory load.

3. The changes in rubber crystallization.

To account for these effects, the maximum shear stress due to static loads (τ^{max}_{static}) and hydrostatic stress ($\bar{\sigma}$) at the point where the strain energy is maximum were determined from finite-element analysis for each ϵ^{avg}_{z} value. The hydrostatic stress ($\bar{\sigma}$) is defined as the sum of the principal stresses divided by three, viz:

$$\bar{\sigma} = \frac{\sigma_1 + \sigma_2 + \sigma_3}{3} \tag{9-5}$$

with τ^{max}_{static} defined as

$$\tau^{max}_{static} = \frac{\sigma_1 - \sigma_3}{2} \tag{9-6}$$

The strain energy density fatigue failure curve for the pad with $\bar{\sigma}$, τ^{max}_{static}, and ϵ^{avg}_{z} as parameters is given in Figure 9-3. The axial strain ϵ^{avg}_{z} value is not felt to be a valid parameter except for Type I bearings similar to those tested. At the present time, the use of either $\bar{\sigma}$ or τ^{max}_{static} is recommended.

It is emphasized that the failure curve should only be used for rough estimates of bearings with similar designs. They are conservative estimates in that they are obtained from continuous cycling as opposed to intermittent cycling and may be nonconservative in that the use of the thick shims in the tests dissipated more heat than in a typical helicopter bearing that generally uses thin shims.

Since no mechanical damage was noted for the fatigue specimens (Figure 9-1), the failure curve in Figure 9-2 is also a lower boundary for bearings which do experience mechanical damage. In this case, a more useful fatigue failure parameter is probably maximum shear stress (τ^{max}). The τ^{max} fatigue failure surface is presented in Figure 9-4. For example, in the case of a Type I bearing subjected to a cyclic pitch rotation, τ^{max} will be due to the cyclic load.

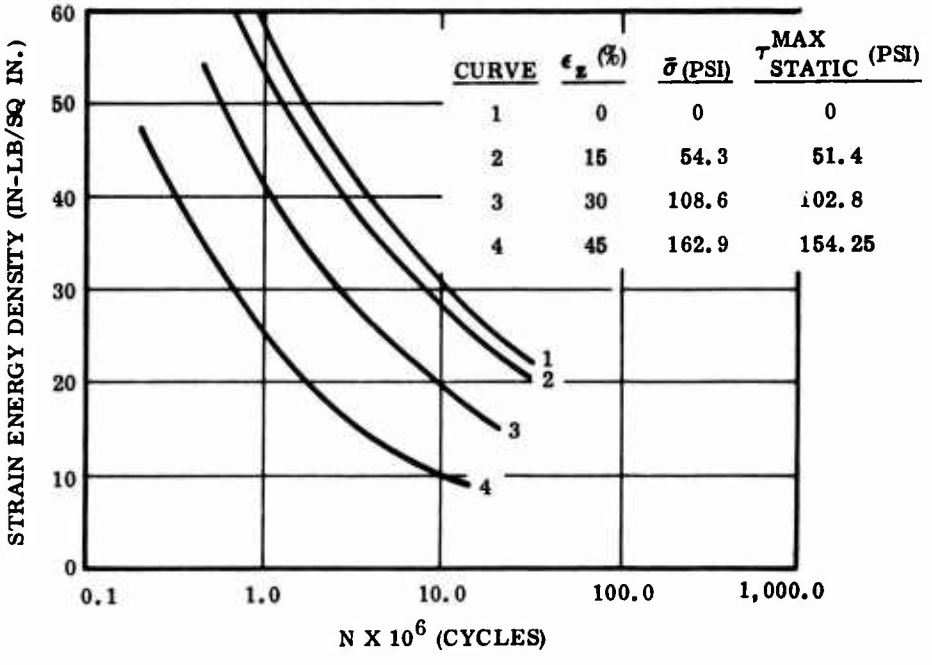

Figure 9-3. Strain energy density failure surface.

CURVE	ϵ_z (%)	$\bar{\sigma}$ (PSI)	τ^{MAX}_{STATIC} (PSI)
1	0	0	0
2	15	54.3	51.4
3	30	108.6	102.8
4	45	162.9	154.25

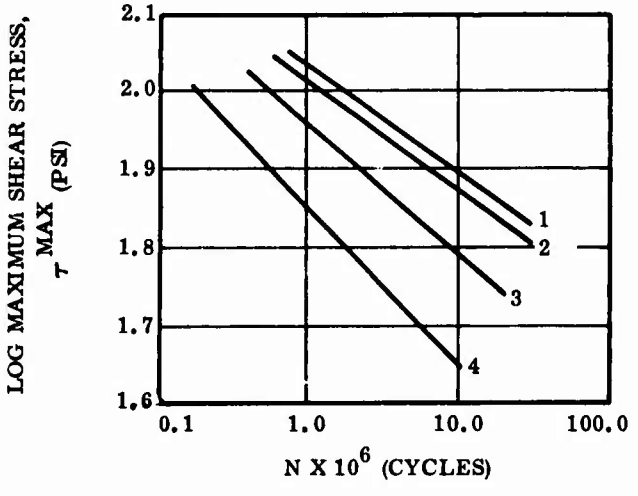

Figure 9-4. Maximum shear stress failure surface.

9.3 DESIGN PROCEDURE

It is often necessary to obtain a preliminary estimate of service life of a given bearing design without sufficient time to complete fatigue life testing in the laboratory. The failure curves generated from Type I bearings and presented in Figures 9-3 and 9-4 will provide a rough indication of service life. The energy density failure boundary will be applicable for all bearing types when failure is caused by elastomer reversion. Since this failure surface was obtained for various values of constant superimposed axial strain with a given heat dissipation mechanism, its direct use for typical helicopter bearing service life cycles is very approximate. The maximum shear stress failure boundary (Figure 9-4) can be used as a conservative estimate for mechanically induced failures since no mechanically induced failures were observed. The service life prediction procedure is therefore:

1. Obtain a load-motion spectrum for the particular bearing. A sample spectrum taken from Reference 9-12 is shown in Table 9-1.

TABLE 9-1

TYPICAL LOAD-MOTION SPECTRUM BLOCK

Cond No.	Pct Time	Axial Load (lb)	Radial Load (lb)		Pitch Motion (deg)		Dynamic Freq (cpm)
			Steady	Osc	Steady	Osc	
1	0.25	56,000	10,000	± 9,400	14	± 9.5	324
2	6.75	56,000	9,000	± 8,000	4	± 9.5	324
3	2.00	56,000	7,000	± 6,500	4	± 9.5	324
4	22.50	56,000	6,000	± 5,000	2	± 8.2	324
5	22.00	56,000	4,000	± 3,600	2	± 7.0	324
6	32.00	56,000	3,000	± 2,200	0	± 5.7	324
7	14.50	56,000	2,000	± 2,200	6	± 3.2	324

2. Select a load condition from the spectrum and obtain the stresses using the finite-element program corresponding to that load.
3. Combine the stresses to determine the applicable failure parameters. If a reversion failure mechanism is expected, the strain energy density and hydrostatic pressure may be selected. The particular loads to be included in each failure parameter are not well defined at the present time. Either of the following two methods is suggested:
   a. In any direction where oscillatory loads are applied, magnitudes of the steady-state and oscillatory components are added and the resulting maximum stresses calculated. If all oscillatory components are in phase, a direct tensor summation of stresses allows calculation of strain energy density using Equation 9-3 or 9-4 and calculation of maximum shear stress (τ^{max}) using Equation 9-6 (note that τ^{max} is due to a combination of static and oscillatory components) and allows location of the failure initiation point. If the stresses are not in phase, it may be necessary to calculate the failure parameters at several phase angles to determine the maximum value of U or τ^{max}.

      The stresses due to loads in any direction where cyclic loads are zero are then calculated at the point where U or τ^{max}_{static} is largest (failure initiation point). The stresses for each direction

of static load are then added and principal stresses calculated. The parameters $\bar{\sigma}$ and τ^{max}_{static} are then determined using Equations 9-5 and 9-6. For example, if condition 4 in Table 9-1 is selected for the basic analysis and if rubber reversion is the expected failure mechanism, one could select strain energy density and hydrostatic pressure as the fundamental failure parameters and use the failure surface of Figure 9-3. The stress components from a radial load of 11,000 lb are then added to those resulting from a pitch motion of 10.2 degrees. Strain energy density is then calculated using Equation 9-4. Then hydrostatic pressure is determined for the steady-state axial load of 56,000 lb at the point where the dynamic value of U is greatest. With the calculated values of U and $\bar{\sigma}$, the failure surface of Figure 9-3 will give the number of cycles to "failure" at condition 4 (N_{f4}).

b. A second method for combining loads is to combine only the cyclic portion of each load to obtain τ^{max}_{cyclic} or U. For condition 4 of loading spectrum Table 9-1, the stresses from the 5,000-lb radial load are combined with those from the 8.2-degree pitch motion. All steady-state loads are then combined to calculate σ or τ^{max}_{static} from Equations 9-5 or 9-6. Thus, the stresses from the 6,000-lb radial load and those from the 2-degree ptich motion would be added to those of the 56,000-lb axial load for $\bar{\sigma}$ or τ^{max}_{static} calculations. The appropriate failure surface could

then be used to estimate service life at that particular load, which is expressed as N_{fi}.

4. Calculate the stresses and service life (N_{fi}) for other loading conditions in the load spectrum. Since stresses are proportional to applied load, this step can be completed by multiplying the stresses of Step 2 by the load ratio.
5. Combine the results of Step 4 with a cumulative damage theory to predict service life.

   There are two basic methods for determining mechanically induced cumulative damage:

   a. A form of Miner's Law (References 7-1 and 9-13).
   b. The reaction-rate theory based upon the Tobolsky-Eyring work (Reference 9-14).

   Neither theory in its present form is consistently accurate even for predictions in metals. The Miner's Law approach is suggested and is usually conservative. Miner's Law is normally expressed in terms of cycles to failure under constant load and is given by

$$D = \sum_{i=1}^{m} \frac{N_i}{N_{fi}} \qquad (9\text{-}7)$$

where D = damage factor

N_i = number of cycles the specimen is exposed to i^{th} load level.

N_{fi} = number of cycles to failure if specimen experienced only the i^{th} load level.

m = number of conditions given in the loading spectrum. Failure is predicted when the damage factor is unity. Equation 9-7 can also be used to approximate the total hours of service life (SL) in terms of dynamic frequency (f_i, cpm), percentage of occurrence of each condition (p_i, %), and number of cycles to failure in the i^{th} condition (N_{fi}) by use of the equation

$$SL = \frac{1}{0.60 \sum_{i=1}^{m} \frac{f_i P_i}{N_{fi}}} \qquad (9\text{-}8)$$

where f_i = dynamic frequency, in cpm

P_i = occurrence of each condition, in percent

At the present time, the rubber reversion process is not thoroughly understood. However, it is known that a combination of strain, temperature, and time is required to initiate the reversion process. Until testing has been completed to correlate these parameters, the laboratory bearing model tests must be used directly. However, care should be taken to provide heat dissipation mechanisms in laboratory specimens which are similar to those in operational bearings so that heat buildup rate will be duplicated in the laboratory tests. In applying a failure surface such as in Figure 9-3 to a typical helicopter bearing life cycle, it is first necessary to calculate the heat buildup rate and maximum temperature in the bearing. These calculations should be completed for each load-time combination of the expected bearing life cycle (i.e., at each level for the spectrum block of Table 9-1). Those portions of the life for which the temperature-strain level is below that required for reversion should be ignored. The summation of cycles at

each load level which are sufficient to cause reversion is then used in a Miner's Law summation of the form

$$D = \sum_{i=1}^{n} \frac{N_i'}{N_{fi}} \qquad (9\text{-}9)$$

where N_i' = number of cycles at load level i after discarding number of cycles required to bring temperature to reversion level on each flight.

9.4 LIMITATIONS AND RECOMMENDATIONS

The fatigue failure curves presented in Figures 9-2 and 9-3 apply strictly to Type I bearing pads and only to those with loads, temperatures, shape factors, shim thicknesses, rubber formulation, etc., identical to those bearings tested. As bearing designs and loads are modified significantly from those used to generate the curves, the validity of their direct use decreases. In a detailed evaluation of a given bearing design, it is therefore necessary to reproduce the applicable portions of the failure curves with laboratory models of the bearing. These models should have the same shape factor, rubber formulation, bonding techniques, and heat dissipation mechanisms, and be the same in all other aspects as the bearing being analyzed. One-pad models will be sufficient for mechanical failure mechanisms. One-pad models may also be used for bearings which have heat-induced failure mechanisms if heat dissipation is properly accounted for in the evaluations. Bearings with a minimum of three pads are recommended because they more closely duplicate the heat transfer mechanism in full-scale bearings. Both steady-state and dynamic loads should be imposed with magnitudes sufficient to produce bracketing of the critical parameters determined from the bearing analysis. To determine the loads required for the laboratory tests and to interpret the test data, it is necessary to perform a detailed stress analysis of the laboratory test specimens. It will be possible to construct failure surfaces similar to those of Figures 9-3 and 9-4 once the specimens are fabricated, analyzed, and tested. The failure mechanism observed in properly constructed and tested laboratory specimens will generally be the same as for the bearing being analyzed. There is at least one exception to this rule when mechanical failures are observed in the laboratory specimens. When heavy shims are used in laboratory specimens, they will tend to dissipate more heat than thin specimens in the actual bearing. Thus, the heat buildup in the bearing pad may be more severe than in the laboratory models. In addition, the continuous cycling in laboratory tests may cause a heat-generated failure mechanism not expected in normal periodic bearing use.

10.0 FUTURE DEVELOPMENT

This section presents the more evident elements of elastomeric bearing design and analysis which, through further development, would lead to refinement of bearing design and an upgrading in the confidence of reliability for these designs. In essence, further development would emphasize more indepth understanding of the mechanism of failure and the influence or significance of secondary requirements.

The manual as developed, in conjunction with the analytic capability provided by the computer code, and when properly used, will result in bearings that meet design requirements. However, these designs could be very conservative, which reflects excess weight and cost. Conservatism is defined as the use of arbitrary limits or constraints in areas of technological deficiencies or limited knowledge.

The major anticipated influence on improvement of this manual and the associated computer code is the feedback of users and evaluators. The incorporation of case histories and data would be a significant contribution to elastomeric bearing design capability.

10.1 ELASTOMER SERVICE LIFE PREDICTION

The current approach to service life prediction relates failure to an arbitrary reduction in the torsional spring rate of the standard Type I test specimen. For Type I bearings, this can be expressed in terms of the torsional strain versus log N for various applied axial strains. This data has been generalized for application to other bearing configurations by expressing the maximum shear stress, the octahedral shear stress or the maximum strain energy density as a function of log N for various compressive strains or average compressive stress. Miner's Law is used as a conservative approach to cumulative damage.

The reduction in torsional spring rate is attributed to degradation of the elastomer, which is generally termed reversion. That is, reduction in spring rate can be correlated to the amount of reverted elastomer. Reversion is generally considered a time-temperature dependent phenomenon, but is probably also dependent on the strain or stress state. An improved service life prediction technique could be developed through acquired knowledge of the reversion process and the application of temperature prediction techniques.

A reversion boundary could be developed experimentally as a function of temperature, time, and strain. The experiment should consider testing at various temperatures, frequencies, and induced strains.

Analytic techniques for temperature prediction are available and only require adaptation to the elastomeric bearing problem. These programs are nonlinear or iterative in that they consider the change in elastic and thermal properties as a function of temperature and also allow for the change in material state such that the growth of the reverted zone can be predicted.

With a reversion failure criterion, flight and bench test conditions could be compared. This would lead to more applicable cumulative damage criteria and more realistic bench test requirements. The results could be reduced to approximate formulations or parametric presentation for the purpose of preliminary design or basic bearing sizing.

At the present time, the effect of steady-state or mean dynamic loads upon fatigue life is not fully understood. Additional research in this area would lead to more accurate service life estimates. Very little information is available concerning the effect of rubber formulation ingredients upon the reversion process and, therefore, service life. Research in this area may lead to formulations with much longer service life and possibly eliminate rubber reversion as the major service life limiting factor.

The accuracy of Miner's Law for cumulative damage as presented in the service life section should be checked when used for bearings. This criterion is normally accurate or conservative when applied to metals; however, Schapery (Reference 10-1) has pointed out that there are also instances when Miner's Law is nonconservative.

10.2 REINFORCEMENT SERVICE LIFE PREDICTION

This manual states that the conventional fatigue life and fracture mechanics techniques are applicable to the design of the metal reinforcing shims. The stress state must be predicted using the finite-element computer code and, in turn, the service life evaluated from available data for the particular material. Therefore, the development of an acceptable reinforcement design could require several design analysis iterations.

The design portion of this manual gives only arbitrary guidelines for the steel shim thickness selection. Approximation techniques for predicting critical shim stress and, thus, service life, material requirements, and thickness would be quite valuable to the designer. These approximate formulations or parametric presentations could be developed using the available computer code. The accuracy of the code in predicting shim stresses has been verified through substantial testing of rocket motor thrust vector control (TVC) bearings with instrumented shims.

The reinforcing shim material repertoire should be extended to fiber reinforced composites. Glass/epoxy shims have been successfully developed for TVC bearings, and graphite/epoxy has superb fatigue characteristics and good stiffness. Molded composite shims would have a significant and beneficial weight and cost impact on bearing design.

10.3 STABILITY

The contracted, experimental effort was limited to laminated cylindrical bearings (Type I) with and without central holes and with fixed/fixed end constraints. This manual presents reliable predictive techniques for well fabricated (minimum asymmetries) Type I bearings. Some guidelines have been provided for evaluating asymmetries and the stability of Type III (spherical) bearings.

Additional design capability could be developed using available analytic techniques, experimental data, and experimental techniques. The induced forces and changes in bearing stiffness characteristic caused by geometric asymmetries can be predicted analytically. The effect of asymmetric loads or displacements on bearing stability would be developed experimentally and theoretically.

Some of the stability test specimens and the Type III bearings were very unstable. The large deviation from predicted bulking load was presumed to be a result of fabrication-induced asymmetries or eccentricities. These bearings can be dissected and the geometric parameters measured for analysis and comparison to or development of theory. TVC bearings (Type III or spherical) have also exhibited instabilities at increasing axial loads. This is evidenced in the slope of the torque loop, which decreases and goes negative with increasing axial load. That is, at high axial load, the bearing must be held in position. This data or type of data would be applicable to the development of predictive techniques for the instability of Type III bearings.

10.4 DESIGN TOLERANCES

The sensitivity of elastomeric design to pad and shim tolerances has not been studied. Tolerance requirements are considered to be a significant design parameter, as the fabrication cost is highly related to imposed tolerances. The impact of tolerance requirements on the metal reinforcing shims is of particular concern, and pad tolerances will influence mold complexity and cost.

Tolerances can be studied in the form of sensitivity analyses using available analytical techniques. Finite-element models can be developed to account for variations in pad-to-pad thickness, shim-to-shim curvature, and shim-to shim alignment. The sensitivity of critical pad and shim stresses could then be presented in terms of tolerance and geometric parameters.

10.5 PIVOT POINT MOTION

Pivot point motion can be a significant parameter in the design of Type III bearings. TVC bearing data indicates that the difference between the actual pivot point and the geometric center of the bearing is approximately five times greater than the end ring displacement due to axial compression. This is caused by the deformation of shims to new or effective curvatures. Applicable predicted techniques have recently been developed for TVC bearings.

The impact of pivot point motion on bearing design is reflected in analysis and test procedures. The analysis requires the application of asymmetric boundary displacements which should be defined relative to the actual pivot point. Forcing displacements about any other pivot point will affect the accuracy of predicted stress or strain fields in the bearing. While this is considered to be a secondary effect, sensitivity analyses should be performed.

Most test apparatuses force motion about a prescribed pivot point. If this is not the actual pivot point, the induced stresses and strains will differ from those of the flight environment. Sensitivity analyses would indicate the significance of the effect or the accuracy to which test fixture pivot points should be defined. Experimental verification of the true pivot point is difficult in that none of the motions can be constrained. Special test fixtures would be required.

10.6 ELASTOMERIC MATERIALS

The computer program and this manual were, in essence, developed for a single elastomer formulation. Emphasis was placed on defining test methods and

data presentation and the utilization of procedures such that any formulation could--and should--be characterized for design.

The usefulness of this manual would be greatly enhanced if the material data base were expanded. In any design, a trade-off between strength or fatigue life and stiffness is generally indicated. The optimization of some designs, particularly Type III (spherical) bearings and Type II (radial) bearings, can require the use of several elastomers of various stiffnesses through the thickness of the bearing core.

The performance of an elastomer is primarily dependent on the base elastomer, fillers, curatives, protectives, and processes. A well planned program to characterize and develop design data for additional formulations would also evaluate the influence of constituents on design parameters. In turn, these influenced curves would guide the designer in selecting or developing yet additional formulations to meet particular requirements.

10.7 DESIGN MANUAL

As developed, use of this manual and computer code will provide reliable designs. However, as evidenced by the six preceding recommendations for further development, the design technology for elastomeric bearings is developing and frequent updating of this manual will be required. When available, the results of other bench and flight test programs should be critiqued and incorporated. Hopefully, positive criticisms from users and evaluators will lead to an improved presentation as well as additional applications and techniques.

10.8 COMPUTER CODE

Typically, new computer codes require considerable debugging and additional development of utilization procedures and modeling techniques. Hopefully, the present computer code will not be as exasperating to use as some, but maintenance and updating must be anticipated. New users and applications should

result in recommendations for improvements in the code. Future expansions of the code could consider:

1. Improved grid generators similar to that currently being developed for TVC bearings.
2. Pivot point motion prediction techniques also currently being developed for TVC bearings.
3. Incorporation of orthotropic capabilities for the evaluation of composite shims.
4. Development of automated design routines for particular classes of bearings from a formulation such as that presented in the design sections of this manual.
5. Improved output or graphic capability as might be indicated or required by new users and new applications.

REFERENCES

3-1 Smith, J. F., "Natural Rubber Compounds for Low Creep and Improved Dynamic Performance," Proceedings of 3rd NRPRA Rubber in Engineering Conference, 1973, pp G1-G9.

3-2 Elliot, D. J., "Natural Rubber Formulation for Engineering Applications," NR Technology Rubber Developments Supplement, N8, pp 1-6, 1972.

3-3 Knurek, T. A., and Salisbury, R. P., "Carbon Black Effect on Engine Mount Compounds," Rubber World, pp 46-57, August 1964.

3-4 Porter, M., "Improved Methods of Vulcanizing Natural Rubber," NR Technology Quarterly, V4, Part 4, pp 76-90, 1973.

3-5 Rivlin, R. S., and Thomas, A. G., J. Polymer Sci., 10 (1953) 291.

3-6 Gent, A. N., and Lindley, P. B., "The Compression of Bonded Rubber Blocks," Publication No. 324, Journal of the British Rubber Producers Association, Vol 173, pp 111-122.

3-7 Lindsey, G. H., et al., "The Triaxial Tension Failure of Viscoelastic Materials," Aerospace Research Laboratories, Report ARL 63-152, USAF Office of Aerospace Research, Sep 1963.

3-8 Levinson, M., "Variational Principles and Applications in Finite Elastic Strain Theory," Ph.D. Thesis, Calif. Inst. of Tech., 1964.

3-9 ICRPG Solid Propellant Mechanical Behavior Manual, CPIA Publication No. 21, Sep 1973.

3-10 Treloar, L. R. G., "The Physics of Rubber Elasticity," 2nd Edition, Oxford University Press, p 70, 1967.

3-11 Williams, M. L., Landel, R. F., and Ferry, J. D., "The Temperature Dependence of Relaxation Mechanisms on the Amorphous Polymers and Other Glass-Forming Liquids," J. Am. Chem. Soc., Vol 77, pp 3701-3707, 1955.

3-12 Williams, M. L., Schapery, R. A., Zak, A., and Lindsey, G. H., "The Triaxial Tensile Behavior of Viscoelastic Materials," Galcit Report SM63-6, Calif. Inst. of Tech., Feb 1963. Also in ICRPG Solid Propellant Mechanical Behavior Manual, CPIA Publications, No. 21, Sep 1963.

3-13 Farris, R. J., "Dilatation of Granular Filled Elastomers Under High Rates of Strain," Journal of Applied Polymer Science, VIII, pp 25-35, 1964.

3-14 Philyspoff, W. and Brodynayan, J., "Preliminary Results in Measuring Dynamic Compressibilities," Journal of Applied Physics, Vol 26, No. 7, p 846, 1955.

REFERENCES (Cont)

3-15 McKinney, J. E., Edelman, S., and Marvin, R. S., "Apparatus for the Direct Determination of Dynamic Bulk Modulus," Journal of Applied Physics, Vol 27, No. 5, p 425, 1956.

3-16 ASTM D696, "Measurement of Linear Thermal Expansion of Plastics."

3-17 Kingery, W. D., "Property Measurements at High Temperatures," John Wiley and Sons, Inc., 1959.

3-18 Payne, A. R. and Scott, J. R., "Engineering Design With Rubber," Interscience Publishers, Inc., New York, 1960.

3-19 Private Communication, R. A. Schapery, Texas A and M University, Austin, Texas.

3-20 Herrmann, L. R., "A Nonlinear Two-Dimensional Stress Analysis Applicable to Solid Propellant Rocket Grain," Fourth Meeting, ICRPG Mechanical Behavior Working Group, 1965.

3-21 Hofer, K. E., "Equations for Fracture Mechanics," Machine Design, Feb 1, 1968.

3-22 Osgood, C. C., "A Basic Course in Fracture Mechanics," Machine Design, Jul 22, 1971.

3-23 Hall, A. M. and Saunder, C. J., "The Metallurgy, Behavior and Application of the 18 Percent Nickel Maraging Steels," NASA Report No. SP-5051, 1968.

3-24 Aerospace Structural Metals Handbook, Air Force Materials Laboratory Report AFML-TR-68-115, 1974.

3-25 Metallic Materials and Elements for Aerospace Vehicle Structures, MIL-HDBK-5B, Sep 1971.

3-26 Marin, J., "Engineering Materials," Prentice Hall, Inc., 1952.

4-1 Messner, A. M., "Stress Distributions in Poker Chip Tensile Specimens," CPIA Bulletin of 2nd Meeting of ICRPG Mechanical Behavior Working Group, Nov 1963.

4-2 Schapery, R. A., "The Poker Chip Test," ICRPG Solid Propellant Mechanical Behavior Manual, Section 4.5.5, Jun 1963.

4-3 Lindley, P. B., "Engineering Design With Natural Rubber," NR Technical Bulletin, Natural Rubber Producers Research Association, London, 1970.

4-4 Gent, A. N. and Meinecke, E. A., "Compression, Bending and Shear of Bonded Rubber Blocks," Polymer Engineering and Science, Jan 1970, Vol 10, No. 1, pp 48-53.

REFERENCES (Cont)

4-5 Moghe, S. R. and Neff, H. F., "Elastic Deformations of Constrained Cylinders," Journal of Applied Mechanics, Jun 1971, pp 393-399.

4-6 Gent, A. N., Henry, R. L., and Roxbury, M. L., "Interfacial Stresses for Bonded Rubber Blocks in Compression and Shear," Journal of Applied Mechanics, to be published.

5-1 Sims, D. F., "Asymmetric Loading of Bonded Rubber Cylinders," Presented at 3rd AIAA Mini Symposium, Arlington, Texas, Feb 15, 1975.

5-2 Gent, A. N. and Lindley, P. B., "Internal Rupture of Bonded Rubber Cylinders in Tension," Proceedings of the Roy. Soc. A, Vol 249, pp 195-205 1958.

7-1 JANNAF Solid Propellant Structural Integrity Handbook, Chemical Propulsion Information Agency (CPIA) Publication No. 230, Sep 1972.

8-1 Naunton, W. J. S., "The Applied Science of Rubber," Edward Arnold Ltd., London, 1961.

8-2 Haringx, J. A., "On Highly Compressible Helical Springs and Rubber Rods and Their Application for Vibration Free Mountings I," Philips Res. Rep. 3, pp 401-499, 1948.

8-3 Haringx, J. A., "On Highly Compressible Helical Springs and Rubber Rods and Their Application for Vibration Free Mountings I," Philips Res. Rep. 4, pp 49-80, 1949.

8-4 Ibid, pp 401-449.

8-5 Gent, A. N., "Elastic Stability of Rubber Compression Springs," Journal of Mechanical Engineering Science, Vol 6, No. 4, pp 318-326, 1964.

8-6 Development of an Elastomeric Seal for Omniaxial Movable Nozzles (Lockseal), Technical Report No. AFRPL-TR-66-112, Lockheed Propulsion Company, Redlands, California, Apr 1966.

8-7 Hoff, N. J., "The Analysis of Structures," John Wiley and Sons, London, 1956.

8-8 Horton, W. H., Cundari, F. L. and Johnson, R. W., "The Analysis of Experimental Data Obtained From Stability Studies on Elastic Column and Plate Structures," Israel Journal of Technology, Vol 5, No. 1-2, pp 104-113 Feb 1967.

9-1 Hein, V. L., and Erdogan, F., "Stress Singularities in a Two-Material Wedge," Int. J. of Fracture, Vol 7, pp 317-330, 1973.

9-2 Williams, M. L., "Bulletin of the Seismological Society of America," Vol 49, No. 2, p 199, 1959.

REFERENCES (Cont)

9-3 Anderson, G. P., DeVries, K. L., and Williams, M. L., "Mixed Mode Stress Field Effect in Adhesive Fracture," Int. J. of Fracture, Vol 10, No. 4, 1974.

9-4 Griffith, A. A., "The Theory of Rupture," Proceedings of the 5th U.S. National Congress of Applied Mechanics, ASME, p 451, 1966.

9-5 Lake, G. J., "Mechanical Fatigue of Rubber," Rubber Chem. and Tech., Vol 45, Nos. 1-3, p 309, 1971.

9-6 Lake, G. J., "Ozone Cracking and Protection of Rubber," Rubber Chem. and Tech., Vol 31, No. 1, 2, p 1230, 1970.

9-7 Lindley, P. B., "Ozone Attack at a Rubber Metal Bond," Journal of the IRI, Vol 5, No. 6, p 243, 1971.

9-8 Gent, A. N., "Strength of Adhesive Bonds - Plastic and Viscoelastic Effects," Proceedings of the 46th Nat. Colloid Symp., Amherst, Massachusetts, 1972.

9-9 Brown, B. F. (Editor), "Stress-Corrosion Cracking in High Strength Steels and in Titanium and Aluminum Alloys," Naval Research Laboratory, Washington, D.C., 1972.

9-10 Campbell, J. E., "Plane-Strain Fracture-Toughness Data for Selected Metals and Alloys," Defense Metals Inf. Center, Report S-28, Battelle Memorial Inst., Columbus, Ohio, 43201, Jun 1969.

9-11 Liebowitz, H. (Editor), "Fracture," Academic Press, New York and London, Vol I-VII, 1971.

9-12 Fagan, C. H., "Low Temperature Tests of Elastomeric Bearing Rotors on an OH-58 Helicopter in the Climatic Laboratory at Eglin AFB," USAAMRDL TR 73-9, Bell Helicopter Company for Eustis Directorate U.S. Army Air Mobility Research and Development Laboratory, Fort Eustis, Virginia, Feb 1973.

9-13 Miner, M. A., "Cumulative Damage in Fatigue," Journal of Applied Mechanics, ASME, Vol 67, pp A159-A164, 1945.

9-14 Tobolsky, A. and Eyring, H., "Mechanical Properties of Polymeric Materials," J. Chem. Physics, Vol 11, pp 125-134, 1943.

10-1 Schapery, R. A., "A Theory of Crack Growth in Viscoelastic Media," Texas A and M University Report MM 2764-73-1, Mar 1973.

LIST OF SYMBOLS

COORDINATE SYSTEM

Rectangular (Cartesian)

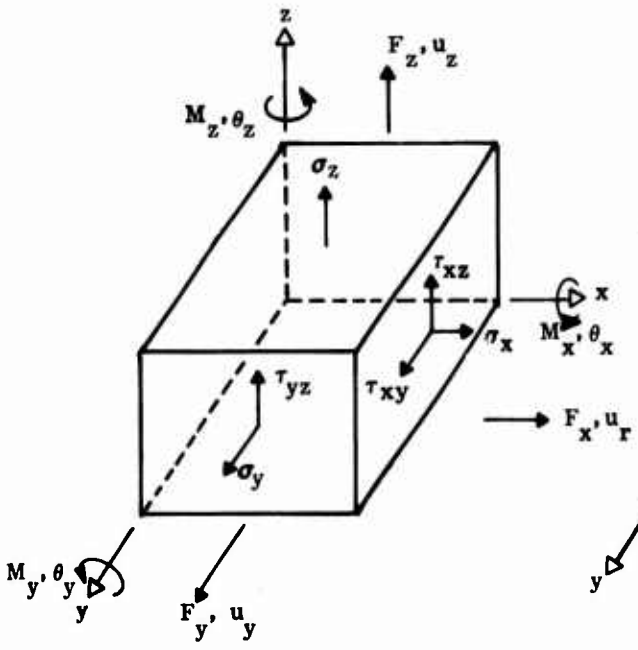

Cylindrical (Polar)

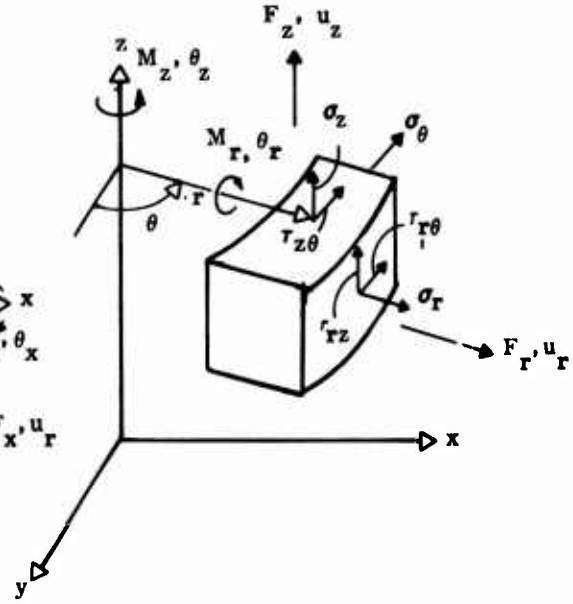

Spherical

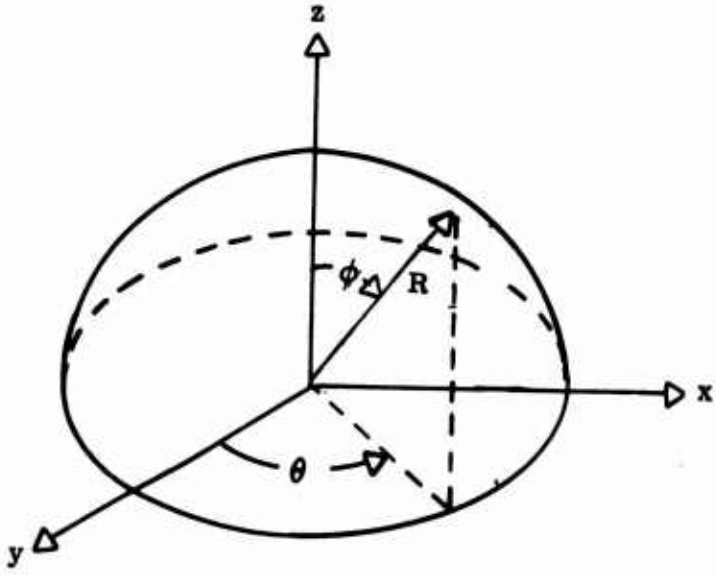

LIST OF SYMBOLS (Cont)

Loads and Displacements

Symbol	Identity	Unit of Measure
F	Force, Load	lb
M	Moment	in-lb
u	Displacement	in.
θ	Rotation	rad
σ	Normal Stress	lb/sq in.
$\bar{\sigma}$	Hydrostatic Stress	lb/sq in.
τ	Shear Stress	lb/sq in.
ϵ	Normal Strain	in/in.
γ	Shear Strain	in/in.
F^c	Critical Load	lb

Stiffnesses

K_z	Axial	$\left(= \frac{F_z}{u_z}\right)$	lb/in.
K_r	Radial	$\left(= \frac{F_r}{u_r}\right)$	lb/in.
K_{θ_x}	Flap	$\left(= \frac{M_x}{\theta_x}\right)$	in-lb/rad
K_{θ_y}	Lead-Lag	$\left(= \frac{M_y}{\theta_y}\right)$	in-lb/rad
K_{θ_z}	Torsion	$\left(= \frac{M_z}{\theta_z}\right)$	in-lb/rad
K_{θ_r}	Vector	$\left(= \frac{M_r}{\theta_r}\right)$	in-lb/rad

Note: Minimum, Maximum, Average or Allowable values are denoted by superscripts.

LIST OF SYMBOLS (Cont)

Geometric Properties

Symbol	Identity	Unit of Measure
h	Elastomer Pad Thickness	in.
t	Shim Thickness	in.
h^T	Total Elastomer Thickness	in.
t^T	Total Shim Thickness	in.
n	Number of Elastomer Pads	
r_i	Minimum Inner Pad Radius	in.
r_o	Minimum Outer Pad Radius	in.
R	Mean Spherical Radius of Pad	in.
A	Cross-Sectional Area	in.
S	Shape Factor	—
V	Volume	$in.^3$
V_o	Initial Volume	$in.^3$
J	Polar Moment of Inertia	$in.^4$
I	Moment of Inertia	$in.^4$
η	Buckling End Fixity Coefficient	
L	Bearing Length	in.

Material Properties

E	Young's Modulus	lb/sq in.
E_A	Apparent Compression Modulus	lb/sq in.
G	Shear Modulus	lb/sq in.
G_{rel}	Shear Relaxation Modulus	lb/sq in.
G^*	Complex Shear Modulus	lb/sq in.
G', G''	Real and Imaginary Parts of Complex Shear Modulus	lb/sq in.
k	Bulk Modulus	lb/sq in.
k_1, k_2	Nonlinear Material Properties	
ν	Poisson's Ratio	

LIST OF SYMBOLS (Cont)

Material Properties (Cont)

Symbol	Identity	Unit of Measure
Tan δ	Loss Tangent	
α	Coefficient of Linear Thermal Expansion	in/in/° F
	Miscellaneous	
U	Strain Energy Density	in-lb/in.^{3}
U^T	Total Strain Energy	in-lb
c	Crack or Debond Length	in.
T	Temperature	°F
ΔT	Change in Temperature ($=T_{final} - T_{initial}$)	°F
P	Pressure	psi
N	Cycles to Failure	
$\frac{dc}{dN}$	Crack Growth Rate	in/cycle
γ_t	Tearing Energy	in-lb/sq in.
γ_c	Cohesive Fracture Energy	in-lb/sq in.
γ_a	Adhesive Fracture Energy	in-lb/sq in.
A_f	Fracture Surface Area	sq in.
f	Frequency	Hz